Title

A review of thermal physics and management inside lithium-ion batteries for high energy density and fast charging

Authors

Zeng, Yuqiang
Chalise, Divya
Lubner, Sean D
et al.

Publication Date

2021-10-01

DOI

10.1016/j.ensm.2021.06.008

Peer reviewed

A review of thermal physics and management inside lithium-ion batteries for high energy density and fast charging

Yuqiang Zeng,[1,*] Divya Chalise,[1,2,*] Sean D. Lubner,[1] Sumanjeet Kaur,[1] Ravi S. Prasher[1,2,**]

[1]Lawrence Berkeley National Laboratory, Berkeley, California, USA
[2]Univeristy of California, Berkeley, California, USA

*These authors contributed equally.
**Correspondence: rsprasher@lbl.gov

Abstract

Traditionally it has been assumed that battery thermal management systems should be designed to maintain the battery temperature around room temperature. That is not always true as Lithium-ion battery (LIB) R&D is pivoting towards the development of high energy density and fast charging batteries. Therefore, it is necessary to have a comprehensive review of thermal considerations for LIBs targeted for high energy density and fast charging, *i.e.*, the optimal thermal condition, thermal physics (heat transport and generation) inside the battery, and thermal management strategies. As the energy density and charge rate increases, the optimal battery temperature can shift to be higher than room temperature. To improve the temperature uniformity and avoid excessive internal temperature rise, heat transfer inside the battery needs to be enhanced, and reducing the thermal contact resistance between the electrodes and separator can significantly increase the effective thermal conductivity of batteries. In the first part of the review various challenges and latest developments related to thermal transport and properties of LIBs are discussed. In the second part of the review various sources of heat generation inside LIBs and various approaches to minimizing battery heat generation are summarized. The importance of heat of mixing due to ion diffusion during fast charging is also highlighted. Finally, a summary of latest advancement on smart control of internal temperature of LIBs is discussed as depending on the ambient temperature and the optimal temperature; the battery heat needs to be retained or dissipated to elevate or avoid temperature rise.

Lithium-ion battery; Optimal battery temperature; High energy density; Fast charging; Battery thermal management

1. Introduction

Lithium-ion batteries (LIBs) are on the verge of revolutionizing our energy infrastructure with applications ranging from electric vehicles (EVs) to grid scale energy storage[1,2]. This revolution and widespread adoption depend on solving key problems such as safety concerns due to thermal runaway, significantly reduced battery performance in cold weather, and insufficient temperature control during extreme fast charging (XFC). Thermal management of LIBs is key to solving these problems, and it is widely believed that battery thermal management systems (BTMSs) should maintain a constant battery temperature around room temperature (RT) for optimal battery performance. However, with the development of LIBs for higher energy densities and faster charge rates [3–7], it is necessary to reevaluate the optimal thermal conditions for batteries based on recent studies. Thus, the need and design of BTMSs will change accordingly with the varied optimal thermal conditions related to the energy density and charge rate.

To regulate the internal battery temperature, it is vitally important to understand heat generation and transport inside the battery. Even with a powerful external BTMS, poor thermal transport within the battery will still cause significant internal temperature rise and a large internal temperature gradient, especially with increased battery energy density and charge rate. However, despite such great importance of internal thermal transport, the focus in the literature and the field so far has been primarily on understanding thermal behavior of the external BTMS rather than within the battery itself [5,8,9]. Now there is a growing realization that understanding and regulating thermal phenomena inside the battery is important to tackle the above-mentioned issues [10–12].

Therefore, for LIBs designed for safe high energy density and fast charging, it is necessary to provide a systematic review of the optimal thermal conditions, thermal phenomena (*i.e.*, heat transport and generation) inside the battery, and thermal management strategies. In this review we discuss recent advancements in thermal considerations for increasing energy density and charge rates of LIBs and review prior experimental and multiscale modeling efforts. This review details thermal phenomena inside the battery and provides guidance for battery thermal considerations in the development of LIBs with high energy density and fast charge capability.

2. The optimal temperature

Conventional wisdom suggests that the operation of Li-ion batteries (LIBs) should be limited in a narrow temperature range around RT (15–35 °C) to achieve the optimum performance[5,13–16]. At low temperatures, the main concern is the risk of lithium plating due to sluggish battery kinetics [6,15,17–19]. On the other hand, the accelerated side reactions at high temperatures, *e.g.*, severe solid electrolyte interphase (SEI) formation, cause fast capacity degradation [19–25]. Based on prior studies of LIBs with relatively low energy density and at slow and moderate charge rates, a balance between these two dominant aging mechanisms, *i.e.*, lithium plating and SEI formation, is typically reached around RT. For this reason, BTMSs are designed to maintain battery temperature around RT. However, the temperature dependence of different aging mechanisms can vary as battery R&D is targeting higher energy density and higher charge rate. The optimal temperature can shift accordingly with the energy density and charge rate. Fundamentally, the optimal temperature depends on the interplay between various aging mechanisms with different temperature dependences. Understanding the optimal temperature for LIBs is vital for battery performance and the design of BTMSs. A detailed review of temperature effects in relatively low-energy-density batteries at slow and moderate charge rates can be found in Refs [26–30]. However, there is a lack of systematic review on recent studies of temperature effects in LIBs with higher energy density and higher charge rate. In this section, we summarize and discuss recent research and progress on the role of temperature in LIBs towards higher energy density and faster charging. The section is organized as: 1) what determines the battery temperature; 2) the optimal temperature for LIBs with high energy density and high charge rate; 3) recent progress in battery temperature measurement.

2.1. *What determines the battery temperature?*

The temperature distribution inside the battery is governed by the Fourier's law

$$\rho C_p \frac{\partial T}{\partial t} = \frac{\partial}{\partial x}(k_x \frac{\partial T}{\partial x}) + \frac{\partial}{\partial x}(k_y \frac{\partial T}{\partial x}) + \frac{\partial}{\partial x}(k_z \frac{\partial T}{\partial x}) + \dot{q} \quad (1)$$

where ρ, C_p, k, T, and $\dot{q}$ are the density, heat capacity, thermal conductivity, temperature, and volumetric heat generation rate, respectively. The boundary condition at the surface of the battery is typically a convective boundary condition to represent the heat exchanger in the BTMS. From the governing equation and the boundary condition, the battery temperature depends on how much heat is generated inside the battery, thermal properties of the battery, convective heat transfer coefficient of the heat exchanger and the ambient temperature.

Many factors, including the battery temperature, energy density, and charge/discharge rate, impact the heat generation rate. At moderate and high charge rates, the total heat generation is typically positive and drives the battery to a higher temperature. The heat generation can be beneficial or harmful to the battery operation, depending on the ambient temperature and the optimal temperature for the battery. For example, an appropriate temperature rise of LIBs due to self-heating improves the battery performance at low temperatures [31–37], while the overheating of

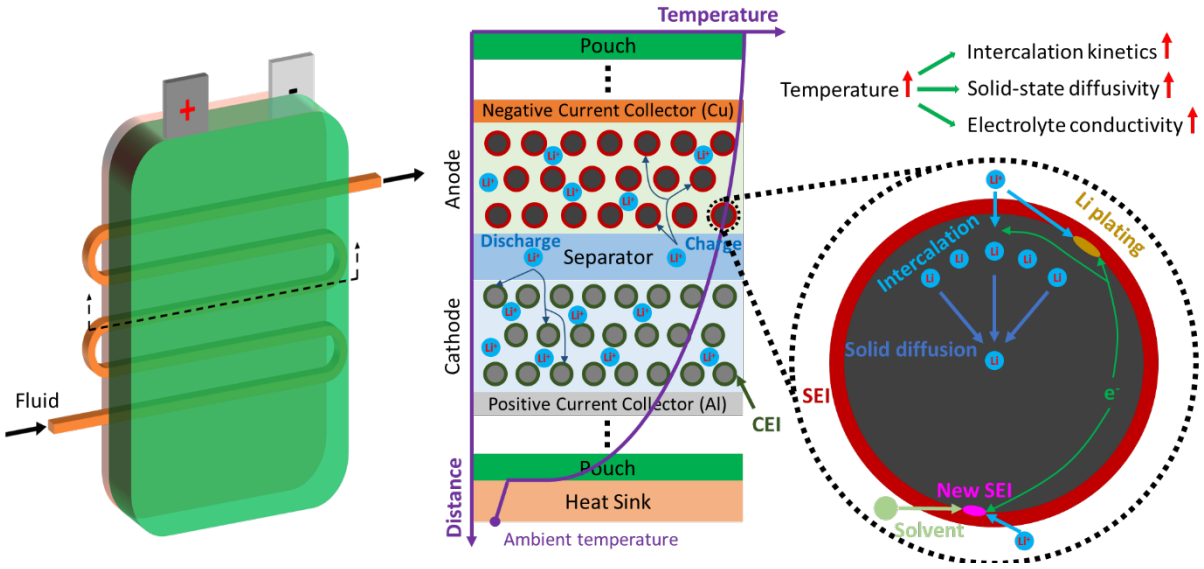

Fig. 1. Schematic of the temperature dependence of electrochemical processes in LIBs. The large cross-plane surface area enables integration of the heat exchanger, which results in a cross-plane temperature gradient across the battery. An elevation in temperature can boost battery kinetics, which accelerates SEI growth and mitigates Li plating.

LIBs hurts the life of the battery and can trigger thermal runaway in extreme cases [38–41]. A detailed review of heat generation in LIBs is discussed in Section 3.

The thermal conductivity of LIBs is highly anisotropic due to their highly anisotropic layered structure. The in-plane heat conduction is dominated by the high-k current collectors, *i.e.*, ~400 W/m-K for Cu current collector and ~235 W/m-K for Al current collector. The effective in-plane thermal conductivity ranges from 20 to 35 W/m-K in the literature [42–47], while the effective cross-plane thermal conductivity of pouch cells is approximately 0.15 – 1.40 W/m-K [44,47–50]. The effective cross-plane k is much lower due to the low k of electrodes [42,45,51–55] and the high thermal contact resistance between the layers [12,56–58]. A quick summary of the key points on thermal properties and transport inside of LIB cells shows: 1) the thermal conductivity of LIBs is highly anisotropic; 2) the poor cross-plane thermal conductivity is typically the limiting factor for battery thermal management; 3) the high thermal contact resistance between the separator and electrodes dominates the total cross-plane thermal resistance. A detailed review and discussion of thermal transport and properties inside LIB cells can be found in Section 4.

Although the in-plane k is much higher, there is less cross-sectional area available in this transport direction, and thermally interfacing with the edges of the battery layers is much harder. Therefore, heat exchangers are typically integrated onto the cross-plane direction (Fig. 1), and the thermal behavior of LIBs inside the cell is thus limited by the low cross-plane thermal conductivity. To predict the battery temperature distribution, solving Eqn. (1) can be computationally expensive. Two approximations are often used in the literature, *i.e.*, 1D heat transfer and the lumped thermal capacitance model. The first approximation considers only 1D heat conduction across the cell (typically along the cross-plane direction), and Eqn. (1) is simplified as

$$\rho C_p \frac{\partial T}{\partial t} = \frac{\partial}{\partial x}(k_z \frac{\partial T}{\partial x}) + \dot{q} \quad (2)$$

This approximation neglects in-plane temperature variation, which is valid only when the in-plane heat fluxes are negligible. Further, the second approximation assumes negligible temperature gradients inside the battery compared to the temperature change across the BTMS. This lumped-capacitance model is a common approximation in modeling battery temperature [59–63]. By assuming a uniform temperature distribution, the battery temperature can be simply calculated as

$$mC_p \frac{\partial T}{\partial t} = hA(T - T_a) + \dot{Q} \quad (3)$$

where m, h, A, and $\dot{Q}$ are the mass of battery, BTMS heat transfer coefficient, convective surface area, and heat generation rate, respectively. However, the lumped capacitance model is valid only when the heat conduction inside the battery is much faster than the heat convection at the surface. For a battery of thickness L, that requires the Biot number (Bi), defined as hL/k, to be much smaller than 0.1. Given the poor thermal conductivity of LIBs, Bi < 0.1 is typically not fulfilled for high-capacity cells, *e.g.*, the Biot number is smaller than 0.1 only for cells thinner than 5 mm assuming k = 0.5 W/mK and natural heat convection coefficient h = 10 W/m^{2}K. For active cooling with h > 100 W/m^{2}K, the Biot number can easily be larger than 0.1 if the cell is thicker than 0.5 mm. Therefore, it is apparent that the lumped capacitance model is not a reasonable approximation for high-capacity cells with multilayer electrodes and thickness > 5 mm. It is worth noting that the lumped-capacitance model has been used for thermal analysis of high-capacity cells in the literature [64–66]. For Bi > 0.1, the temperature gradient inside the battery is nonnegligible and the temperature distribution should be calculated by solving Eqn. (1) [64,67,68].

2.2. *The optimal temperature for LIBs*

In the past, studies of cells with relatively thin electrodes, low areal density, and at slow and moderate charge rates supported the notion that the optimal temperature for LIBs is around room temperature. Temperature effects in LIBs with low energy density and at slow/moderate charge rates have been discussed and reviewed in Refs [26–29]. In those cases, battery operation at room temperature avoids both the risk of lithium plating at low temperatures and sever SEI formation at high temperatures. Fundamentally, the optimal temperature depends on the interplay between these two main aging mechanisms, *i.e.*, lithium plating and SEI formation, which is a function of energy density and charge rate for a certain electrochemical system. As battery R&D is targeting higher energy density and faster charge rate, the optimal temperature can change based on a new balance between the aging mechanisms. Here, we first review the temperature dependence of the two main aging mechanisms in LIBs. Then, we summarize and discuss literatures on the optimal temperature for LIBs with focus on high energy density and fast charging.

2.2.1. Temperature dependence of aging mechanisms

The growth of SEI with time (t) follows a $\sqrt{Dt}$ dependence based on simple analytical models [69–73], where D is the diffusivity through the SEI of the electrolyte solvent that forms SEI. High

temperature accelerates SEI growth as the diffusivity follows the typical Arrhenius-type temperature dependence. Thus, batteries need to be operated or stored at low temperatures to minimize the capacity loss due to SEI formation. However, Li plating has an opposite temperature dependence. The parameters influencing Li plating can be known from the charging process: 1) Li^+ ions, deintercalated from the cathode, move to the anode through the electrolyte; 2) Li^+ ions in the electrolyte are intercalated into graphite particles; 3) Li^+ ions diffuse through the graphite particle. From the Arrhenius relation, all these steps during charging slow down as the temperature decreases (see Fig. 1). That means Li plating is prone to occur at low temperatures. Therefore, the optimal battery temperature is a result of the opposite temperature dependence of Li plating and SEI growth. As one aging mechanism becomes dominant, the optimal temperature may shift accordingly to mitigate the corresponding capacity loss [74,75].

2.2.2. Energy density

Typically, thin electrodes (< 50 μm) have a relatively low areal density (< 2 mAh/cm^2)[74]. To increase the energy density of LIBs, an effective method is to use thicker electrodes to increase the areal loading of active materials. The impact of electrode structure and thickness on electrochemical dynamics can be modeled using commercial finite element tools such as COMSOL, *e.g.*, vertically aligned electrodes were known to have a lower tortuosity [76–78]. While these novel designs showed good promise in reducing the tortuosity, this review focuses on commercial electrodes which have a relatively high tortuosity. The thicker electrodes have higher tortuosity and larger liquid-phase polarization due to the porous structure and the increased thickness [79,80]. Lithium plating has a higher tendency to occur in thicker electrodes due to the higher tortuosity and larger polarization. Malifarge *et al.* performed rate capability experiments of graphite electrodes with various areal loadings (2 - 6 mAh/cm^2) and porosities (0.1 - 0.45) [80]. Their analysis revealed different lithium plating mechanisms in electrodes with various areal loadings. Lithium plating may occur in low-loading electrodes due to the relatively larger pore-wall flux associated with the smaller active surface area per geometric area, compared to that in thick electrodes. With the increased electrode thickness, the pore-wall flux reduces, and the liquid-phase limitation becomes the key factor for lithium plating in high-loading electrodes. As a result of the long diffusion paths in high-loading electrodes, a large salt concentration and liquid-phase potential gradient develops across the cell, and thus a large liquid-phase overpotential forms accordingly. Further, the large liquid-phase potential gradient causes non-uniform local state of charge (SOC) across the electrode. Both the large overpotential and non-uniform SOC increases the propensity of lithium plating. The large cell polarization and underutilization of active materials can even offset the advantage of high areal loading in thick electrodes [80,81].

This agrees with the prior observation by Gallagher *et al.* that the rate performance of LIBs drops as the areal loading increases (see Fig. 2a) [82]. They tested the performance of cells with areal loading from 2.2 to 6.6 mAh/cm^2 at C/3 – 1.5C charge rates. For 1C charge at 30 °C, a large amount of lithium was observed in the aged cell with 4.4 mAh/cm^2, while the cell with 3.3 mAh/cm^2 had a stable 1C charge performance. Their study suggested that graphite cells should be charged below 4 mA/cm^2 to avoid lithium plating in the graphite anode, which means a slow or moderate charge rate for high areal-loading cells. Similarly, Spingler *et al.* observed serious

lithium plating in LIBs with high areal loading anodes at moderate charge rates (1.5C and 2C) [83].

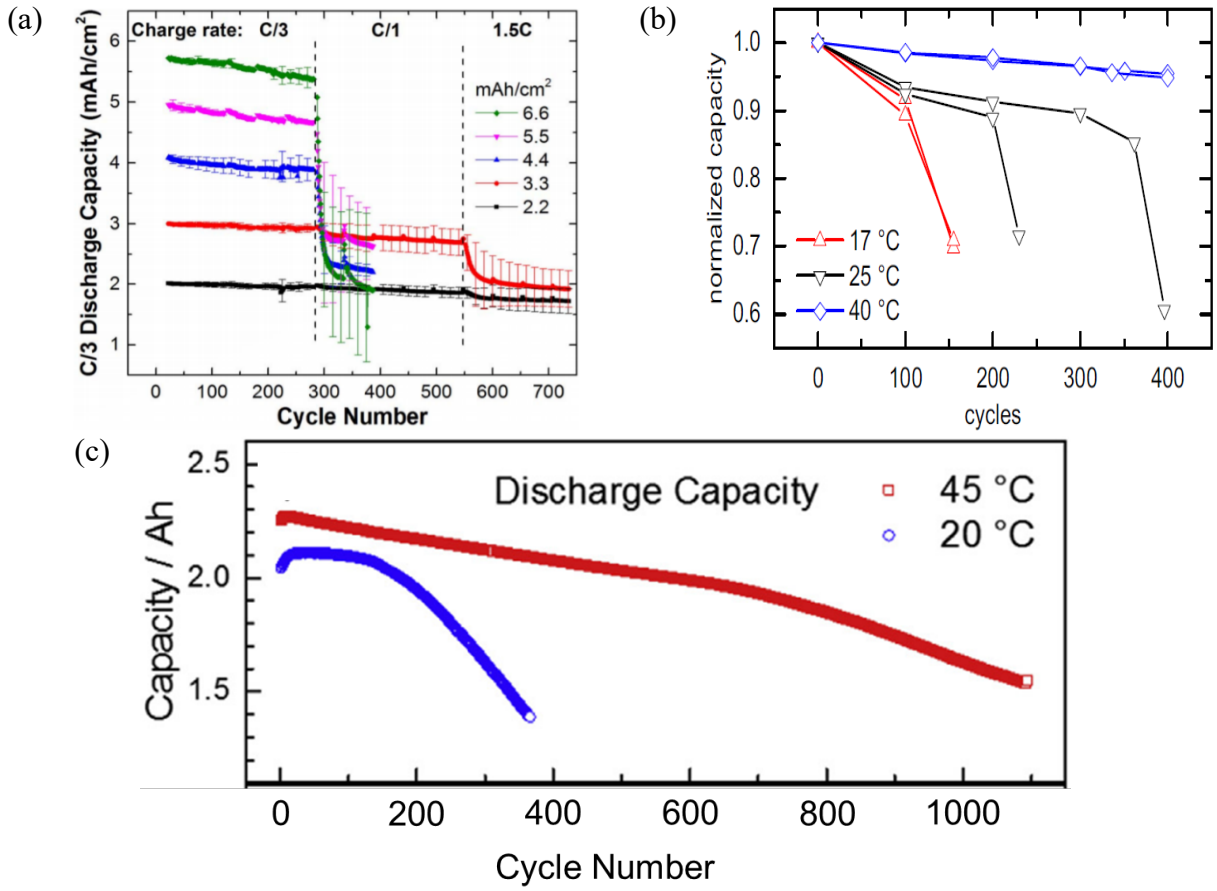

Fig. 2. (a) Cycle life tests for NMC/Gr pouch cells with various areal loadings by Gallagher *et al.* [82]; (b) Cycle life of high energy cells charged at 1C and at temperatures 17 °C, 25 °C, and 40 °C by Rieger *et al.* [17]; (c) Cycle life of high energy cells charged at 20 °C and 45 °C by Friesen *et al.* [84]. Panels reproduced from: (a) Ref [82], the Electrochemical Society; (b) Ref [17], Elsevier; (c) Ref [84], Elsevier.

As the areal loading and the electrode thickness increases, lithium plating becomes the dominant aging mechanism for LIBs operated around RT due to the higher tortuosity and larger polarization in thicker electrodes. Considering the opposite temperature dependence of SEI growth and lithium plating, the optimized temperature for high-energy cells should be higher than RT to mitigate the dominant aging mechanism, *i.e.*, lithium plating. In the literature, some cycling tests of high-energy-density cells at various temperatures support the increase of the optimal temperature with the energy density. Rieger *et al.* tested high-areal-loading cells with 77 um thick anode at 1C charge and discharge rate (see Fig. 2b) [17]. Their cycling tests at different temperatures (17 °C, 25 °C, and 40 °C) revealed the best 1C cycling performance at 40 °C. Specifically, their cells lost ~5% capacity in 400 cycles when operated at 40 °C, while the cells cycled at 17 °C and 25 °C lost more than 30% capacity in 150 and 400 cycles, respectively. They observed a thick surface layer of SEI on the anode in the aged cells in a post-mortem study and lithium plating was estimated to

be the failure mechanism for the operation around or below RT. Further, Sturm *et al.* cycled cells with similar areal loadings and found that the cycle life at 25 °C was greatly improved when the charge rate was reduced from 1C to 0.5C [24]. That indicated lithium plating as the dominant aging mechanism in high areal-loading cells even at a moderate charge rate (1C). Similarly, Friesen *et al.* tested 18650-type lithium ion cells based on NMC532/graphite with 1C rate at 20 °C and 45 °C and observed a better cycle life in the cells cycled at 45 °C (see Fig. 2c) [84].

2.2.3. Fast charge

Extreme fast charge has been identified by the US Department of Energy (DOE) as a critical challenge to the widespread adoption of battery electric vehicles (BEVs)[3,4]. A detailed review of challenges in fast charging can be found in Refs [4,5,85,86]. Specifically, Keyser *et al.* reviewed battery thermal barriers in XFC and highlighted the requirement of an oversized BTMS due to the increased cooling need [5]. The optimal temperature is a key parameter in the proper design of BTMSs for XFC conditions. Previously, the rule of thumb was to minimize the temperature rise and maintain batteries around RT. It is true that high temperatures accelerate side reactions and an extremely high temperature can trigger thermal runaway. However, a reasonably high temperature can mitigate lithium plating, which is the dominant aging mechanism for battery operation at RT as the charge rate increases to > 1C [74,75].

As for the battery thermal safety, an increase of the charge temperature, *e.g.*, from 20 °C to 50 °C, does not degrade the thermal safety if the peak temperature is below the thermal runway triggering temperature [18,39,41,84,87–89]. Contrary to expectation, a thicker SEI layer in cells operated at a reasonably higher temperature does not decrease the battery thermal safety[18,84,87], while the lithium plating in cells tested at low temperatures or fast charge rates can lead to an early thermal runaway [18,88]. The particular behavior depends on the chemical reactivity of the SEI layer and plated lithium. The SEI layer formed at high temperatures is electrochemically stable and an increase of the thickness of SEI at higher temperatures does not fundamentally change the thermal safety. In contrast, plated lithium can react with electrolyte, which can lead to an earlier thermal runaway of cells compared to those under moderate charge rates, *e.g.*, a decrease of the thermal runaway triggering temperature from 215.5 °C for cells charged at C/3 to 103.9 °C for cells charged at 3C [88].

Indeed, recent studies have shown that the cycle life at XFC can be significantly improved by operating cells at temperatures above RT. Matsuda *et al.* performed cycle life tests of commercial 18650 cells (Fig. 3a) at various temperatures (0 °C, 25 °C, and 45 °C) and charge rates (1C and 2C) [90]. In their study, the cycle life was better at 45 °C than at 25 °C for a 2C charge rate, while for 1C charge tests the 25 °C cell had much longer cycle life than the 45 °C cell. Yang *et al.* developed a battery aging model and systematically studied how charge rate and energy density affect SEI growth and lithium plating at various temperatures [74]. Their simulations demonstrated that lithium plating became the primary aging mechanism around RT for LIBs with an increase of charge rate and energy density. To rebalance the capacity degradation due to SEI growth and lithium plating, they suggested that elevating the charge temperature would reduce lithium plating and extend the cycle life (Fig. 3b). Similarly, reduced-order electrochemical models by Yin and Choe revealed that the optimal temperature for cycle life increased with the charge rate (Fig. 3c)

[75]. Active control of the battery operating temperature by varying the charge current can extend the cycle life.

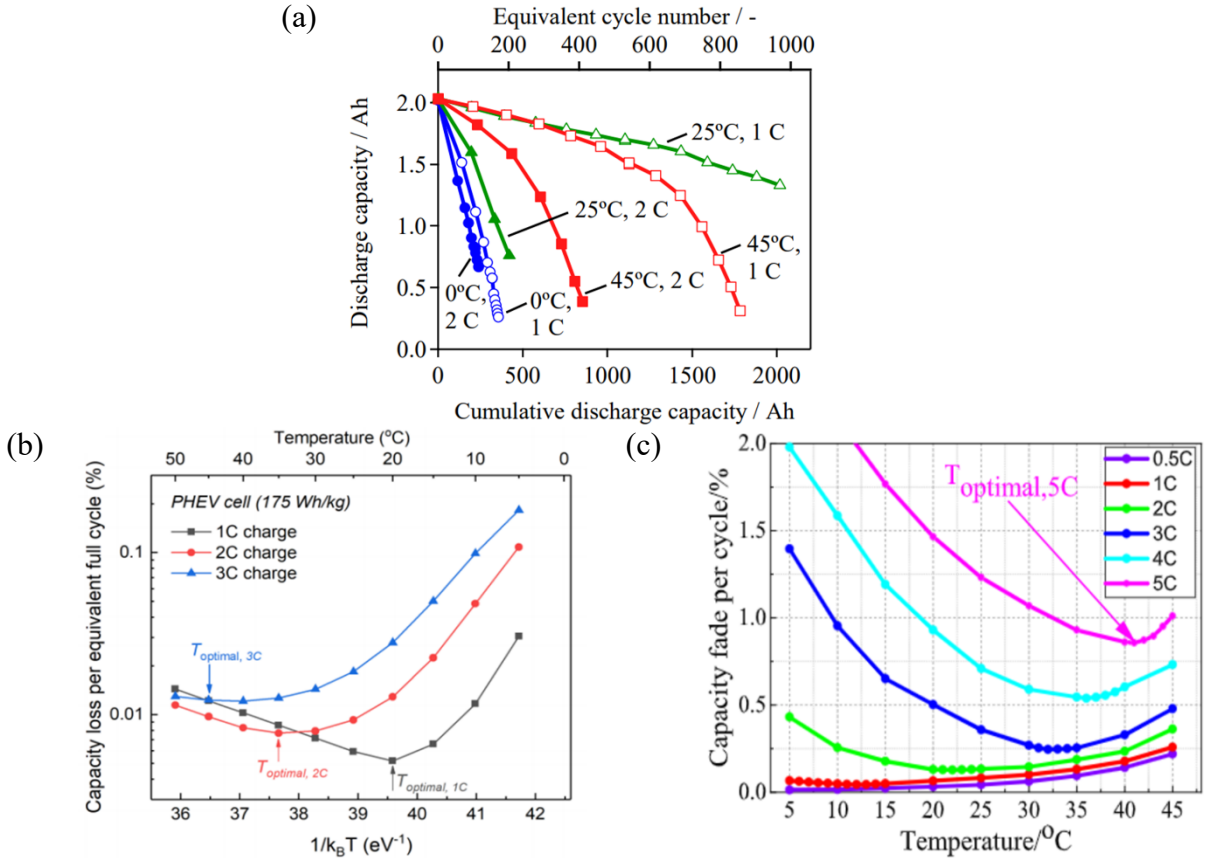

Fig. 3. (a) Cycle life tests at different rates and temperatures by Matsuda *et al.* [90]; (b) Aging rate *vs.* temperature of LIBs with different rates by Yang *et al.* [74]; (c) Comparison of capacity fade *vs.* temperature at different rates by Yin and Choe [75]. Panels reproduced from: (a) Ref [90], the Electrochemical Society; (b) Ref [74], Elsevier; (c) Ref [75], Elsevier.

In addition to modulating the battery temperature using heat generated by itself, extra heat sources inside or outside the cell have been applied to control the temperature. An example of heating outside the battery for fast charging is the "On-route Battery Warmup" strategy adopted by Tesla. That is to preheat the battery to a temperature above RT when BEVs are on the way to a fast-charging station. On the other hand, Wang *et al.* innovated a self-heating battery with embedded heaters inside the battery for a fast heating [91]. Further, Yang *et al.* proposed an asymmetric temperature modulation (ATM) method, *i.e.*, charging batteries at ~60 °C and discharging at lower temperatures, for improving the cycle life during XFC [92]. Embedded thin nickel (Ni) foil heaters enabled a rapid preheating of the cell from 20 °C to 60 °C before charge, which minimized its exposure to high temperatures. However, it is worth noting that a detailed analysis of the BTMS and cost is required before the adoption of the ATM method for XFC in BEVs. More discussions can be found in Section 5.

2.2.4. Temperature uniformity

Besides the temperature rise, the temperature uniformity inside a battery becomes an important issue. As the volumetric heat generation rate increases with the energy density and charge rate, there is more battery heat to be dissipated, requiring more cooling power. Stronger surface cooling then causes a larger temperature gradient within the cell based on Eqn. (2). According to the Arrhenius law, the high temperatures locally accelerate the electrochemical reactions and increases the current, and thus results in a local high SOC. The non-uniform SOCs in electrodes due to the uneven temperature distribution accelerates the aging of the electrodes at high SOCs and the aging of the cell. Thus, both the undesirable temperature rise and temperature non-uniformity accelerate the aging of LIBs. Note that a rapid change of the battery temperature by a large external heating or cooling power leads to a large temperature gradient. That indicates the optimal battery temperature depends on a balance between the temperature rise and the temperature uniformity [9,93–97].

2.3. *Temperature measurement methods*

The temperature rise and temperature non-uniformity accompanied with the increase of energy density and charge rate necessitates the development of advanced temperature measurement techniques for BTMSs. Refs [98–100] have explained in detail various temperature sensing techniques in LIBs. To probe the spatial temperature in a battery, especially the internal battery temperature, contact temperature sensors need to be embedded in LIBs and non-invasive techniques need to be developed. Towards obtaining the spatial temperature information, we summarize and discuss the techniques based on the acquired spatial temperature information, *i.e.*, point (see Table 1), surface, and integrated (entire cell) temperature measurement techniques. Specifically, we review new techniques, the techniques not detailed in prior works, and the assumptions and limitations of these techniques.

2.3.1. Point temperature measurement techniques

2.3.1.1. Thermocouples

Thermocouples, based on Seebeck effect, are one of the most common temperature measurement devices [101]. Thermocouples can be easily attached on the outer surface of the battery and monitor the surface temperature [102–106]. Thermocouples embedded inside the cells have also been used for internal temperature sensing [104,107–111]. Heubner *et al.* [110,112] reported an internal temperature measurement with up to 5mK resolution using K-type thermocouples embedded in a cell (see Fig. 4a). They observed a resolved temperature difference among different cell components and attributed the temperature difference to the heat generation in these components. However, a detailed analysis of the signal-to-noise ratio and the uncertainty needs to be conducted as the measurement resolution and the noise due to ambient temperature fluctuations can be of a similar magnitude as the measured temperature rise. Nevertheless, this work demonstrated the possibility of experimentally probing the internal temperature and resolving the heat generation in different components with thermocouples embedded in a battery.

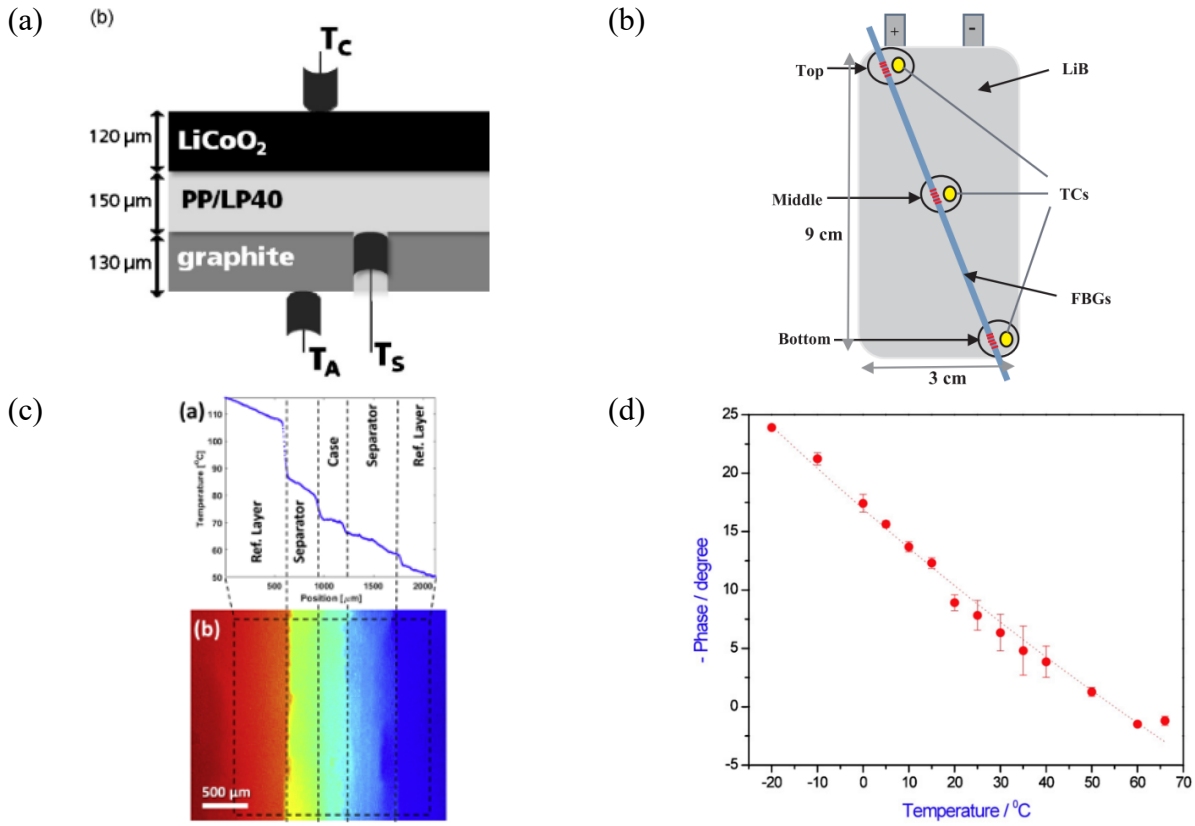

Fig. 4. (a) Thermocouples embedded in different components of a cell [112]; (b) Multiple FBG sensors embedded in the same optical fibers for multi-location temperature measurements [113]; (c) Temperature jump at separator-case interface measured by infrared thermometry with a spatial resolution of 1.7 µm [56]; (d) Phase-Temperature relationship for impedance measured at 40 Hz for a 53-Ah GS Yuasa LSE50- 002 Li-ion cell [114]. Panels adapted from: (a) Ref [112], (b) Ref [113], (c) Ref [56], and (d) Ref [114], Elsevier.

2.3.1.2. Resistance based techniques - RTDs and thermistors

Resistance Temperature Detectors (RTDs) and Thermistors both rely on a calibrated relationship between the electrical resistance of a conductor (or semiconductor) and its temperature [90]. RTDs have a typical temperature resolution and sensitivity of 0.01-0.2 K and 0.38%/K, respectively [98]. RTDs are easy to fabricate, and can be easily embedded in a live battery [58]. On the other hand, thermistors are more sensitive to temperature change (-4.3 %/K), but their stability in harsh chemical environments still needs to be improved [98].

2.3.1.3. Optical fiber-based techniques

Optical fibers with embedded bragg-gratings can be used for temperature detection as the wavelength of the reflected signal (Bragg Wavelength, λ_b) shifts with the temperature. The Bragg wavelength is given by [90]

$$\lambda_b = 2\eta_{eff}\Lambda \tag{4}$$

where η_{eff} is the effective refractive index of the fiber core and Λ is the grating spacing. The temperature dependence of Bragg wavelength comes from the temperature dependence of the core refractive index and the grating spacing change due to thermal expansion/contraction [98]. Fiber Bragg Grating (FBG) sensors are minimally invasive while being robust and able to work in the chemical environment inside a battery [98,115] . Moreover, the same fiber can have gratings in multiple locations, which allows multi-point measurement with the same sensor (see Fig. 4b) [113]. One disadvantage with this technique is that the wavelength shift can be caused by either a temperature change or a mechanical strain in the sensor, which need to be decoupled with additional calibrations [116].

Table 1
Comparison of different point temperature measurement techniques.

Technique	**Temperature Resolution**	**Sensitivity**	**Advantages**	**Disadvantages**
Thermocouples [102,104–108]	1 K [98]	1-70 μV/K [98]	Widely available, fairly sensitive	Difficult to modify and embed in cells
RTDs [117–119]	0.01-0.2 K [98]	0.38 %/K [98]	Small size, stable in electrolyte	Low temperature sensitivity
Thermistors [120–122]	1 K [98]	-4.3 %/K [98]	Easy to fabricate, high temperature sensitivity, 2-point probe	Non-linear temperature response, insufficient stability in harsh chemical environments
FBG sensors [113,115]	0.2-0.4 K [98]	10pm/K [98]	Minimally invasive, stable in electrolyte	Additional calibrations needed to decouple temperature rise and strain

2.3.2. Surface temperature measurement techniques

2.3.2.1. Infrared (IR) thermometry

Infrared (IR) thermometry has been widely used in measuring surface temperature of batteries [56,121,123–127] and has been reviewed in Ref. [100]. Typically, this technique requires a special sample preparation such as deposition or coating of high emissivity material like graphite [128] and has a temperature resolution of ~2K [98]. In batteries, IR thermometry has been especially useful in determining the in-plane temperature profile due to non-homogeneous current distribution, mainly near the electrical tabs connected to the current collectors [121,124,125,127]. Additionally, IR thermometry has been used to study the thermal interface resistance and the internal temperature of the cells. Gaitonde *et al.* [56,129] used an infrared microscope with a spatial resolution of 1.7 μm to visualize the temperature jump at the separator-case interface in a cylindrical Li-ion battery (see Fig. 4c), which indicated the high thermal interface resistance. By measuring the surface temperature measured by IR thermometry and assuming a constant heat generation rate, Anthony *et al.* [128] were able to reconstruct the transient temperature distribution inside a cell by solving the thermal diffusion equation. However, the assumption of a constant heat generation in the reconstruction is an oversimplification because of the dynamic [130,131] and temperature dependent [132] nature of heat generation.

2.3.2.2. Thermochromic liquid crystals (TLC)

Liquid crystals that change their color with temperature have been used for surface temperature measurement in batteries [133]. With TLC coated strips on the surface of a battery, Giuliano *et al.* [133] obtained a 2D TLC color map and translated it into a temperature map based on a calibrated color-temperature relationship. This technique typically has a temperature resolution of ~1K [98].

2.3.3. Integrated temperature measurement techniques

Electrochemical Impedance Spectroscopy (EIS) is a widely used technique to determine the SOC, SOH (State of Health) and other electrochemical parameters of a battery [134–136]. Recently, EIS based methods have been investigated for measuring the battery temperature [105][137–142]. For a sinusoidal voltage $V(\omega)$ or current $I(\omega)$ applied at a frequency ω and the corresponding current or voltage measured at the same frequency, the impedance is defined as

$$Z(\omega) = \frac{V(\omega)}{I(\omega)} \tag{5}$$

The measured impedance, $Z = Z(\omega, SOC, T)$, is a function of the SOC, temperature and the applied frequency [138]. The real part [105,138,142], the imaginary part [143], and the phase [114,144] of the impedance have been used to determine the battery temperature. Fig. 4d shows a linear phase-temperature relationship for the impedance measured at 40Hz [114]. Besides, Raijmakers *et al.* [140] evaluated the effectiveness of the frequency with zero imaginary value as a parameter for temperature measurement. Generally, the temperature resolution of these impedance based measurements is 0.17 K to 2.5 K and depends on the battery type and the method used [98][138,142].

Although non-invasive and easy to experimentally implement, impedance-based methods have certain limitations. Firstly, the impedance based methods [138,141] require a knowledge of the SOC to predict the temperature. In XFC conditions, the local state-of-charge varies within the electrode and a single SOC cannot represent the entire cell. Additionally, crosstalk signals [138,145] from different cells in the pack might influence the impedance signal from a cell and affect the result, although it can be resolved somewhat by methods such those proposed by by Beelen *et al.* [138]. However, the biggest limitation of impedance-based methods is the lack of spatial temperature information. As the impedance is measured for the whole cell, this technique is agnostic to the temperature non-homogeneity inside the cell and can only give an average temperature information. To get the spatial temperature, Richardson *et al.* [105] developed a method to determine the internal temperature of a battery by combining impedance measurements with the surface temperature measurement. Various other works [139,141,142] followed a similar approach of impedance and surface temperature measurements to determine the internal temperature. Some limitations of these works include the use of a single SOC for the entire battery and the use of constant thermal properties over multiple cycles in addition to common inaccuracies in modeling temperature rise as described in Section 2.1.

3. Heat generation

Volumetric heat generation can increase significantly with the increase of energy density and charge rate. A comprehensive understanding of battery heat generation can be instructive for the design of BTMSs and the safe operation of LIBs. In this section, the different sources of heat generation inside the battery are reviewed in detail. The contribution by various sources can vary with the energy density and charge rate, *e.g.*, the heat of mixing, assumed to be negligible in prior works, contributes ~23% to the total heat generation at a charge rate of 6C [146]. We also review and evaluate existing models to calculate battery heat generation. Lastly, from the understanding of heat generation by various sources, different methods to minimize heat generation sources are summarized and proposed.

3.1. *Sources of heat generation*

In this section we discuss the four main sources of heat generation in batteries: irreversible heat due to ohmic and kinetic losses, reversible heat due to entropy change of the reaction, heat due to side reactions and heat of mixing. Readers should refer to Fig. 5 for the schematic of the cell described by the equations presented in this section.

3.1.1. Irreversible heat related to losses

Irreversible heat generation occurs due to transport losses or kinetic overpotentials related to the charge transfer reaction. The Ohmic heat generation is caused by the potential drop due to the transport related losses in the electrolyte, electrodes, and the current collector. In the electrodes and the current collectors, the potential drop occurs due to electron transport resistance, while in the electrolyte, the potential drop occurs due to concentration overpotential and ion transport resistance [130,147].

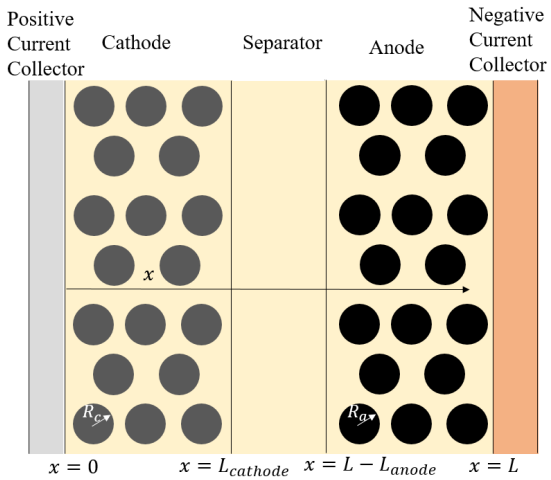

Fig. 5. Schematic of a porous electrode. The concentration of the electrolyte and the local current ($I(x)$) can vary in the x-direction. Concentration of Lithium in the particles can vary radially (along R_a or R_c).

The local current distribution is governed by the interplay between the transport of the species and the kinetics of the reaction in the cell and can be described by a set of coupled equations discussed in [131,147–149]. The Joule heating per unit nominal cross-sectional area (W/m^2) in the different components can be written as

$$q_{ohmic,CC/Electrodes} = \int_0^{L_{electrode}} \sigma_e^{eff} \left(\frac{\partial \Phi_s}{\partial x}\right)^2 dx \quad (6)$$

$$q_{ohmic,Electrolyte} = \int_0^{L} \left(\kappa^{eff} \left(\frac{\partial \Phi_e}{\partial x}\right)^2 + \kappa_D^{eff} \frac{\partial ln c_e}{\partial x} \frac{\partial \Phi_e}{\partial x}\right) dx \quad (7)$$

The effective transport properties such as the electronic conductivity (σ_e^{eff}), ionic conductivity (κ^{eff}) and the ionic diffusional conductivity (κ_D^{eff}) are functions of the material transport property as well as the porosity (volume fraction) and tortuosity. ϕ_s and ϕ_e are the solid- and electrolyte-phase electrochemical potential and c_e is the electrolyte concentration. It is observed that transport losses typically contribute ~50% of the overall heat generated [5,150]. As the ionic conductivity in the electrolyte is in general much smaller than the electronic conductivity in the electrodes [151,152], most of the potential drop related to transport occurs in the electrolyte.

Additionally, there can be irreversible losses related to the overpotentials associated with the charge transfer reactions. Without an application of a driving force, an electrochemical reactions at an electrode is at equilibrium [147]. Application of a potential away from the equilibrium potential (U) can drive an electrochemical reaction towards a certain direction, and current can flow [136,147]. The difference between the applied potential and the equilibrium potential is known as the kinetic or surface overpotential (η_s).

For an electron transfer reaction with a single elementary step, the relationship between the current density (i) and the surface overpotential is given by a kinetic relation known as the Butler-Volmer (BV) relation [147].

$$i = i_0 \left(\exp\left(\frac{(1-\beta)nF}{RT}\eta_s\right) - \exp\left(-\frac{\beta nF}{RT}\eta_s\right)\right) \quad (8)$$

where, β, known as the symmetry factor, describes the change in the activation energy as a fraction of the applied voltage and i_o, known as the exchange current density, describes the kinetics of the reaction and is a function of the rate constants for the forward and the backward reaction, symmetry factor, and concentration of the reacting species [136,147]. For a Li-ion battery, the reactions at the porous electrodes are generally considered to be a one-step process and are therefore usually modeled with BV kinetics [130,148,149]. The surface overpotential (η_s) is the voltage consumed in driving the reaction away from the equilibrium. Therefore, the energy associated with it cannot be used as work and is instead dissipated as heat.

For the entire electrode, the heat generated per unit cross sectional area is given by [153]:

$$q_{rxn} = \int_0^{L_{electrode}} a i(x) \eta_s(x) dx \quad (9)$$

where $a = \frac{3\varepsilon_{ins}}{R}$ is the total surface area per unit volume of the porous electrode and ε_{ins} is the active material volume fraction. In general, the reaction heat associated with the kinetic loss contributes ~30-40% of the total heat generated [5,150].

3.1.2. Reversible Heat Related to Entropy Change

The heat released or absorbed due to the entropy change of the system is known as the reversible heat because the same amount of entropic heat absorbed (or released) in the forward reaction is released (or absorbed) in the backward reaction. From thermodynamics, the entropy change (ΔS) in an electrochemical system at constant temperature and pressure can be related to the open circuit potential (U) with the following relation [147]

$$\frac{\Delta S}{nF} = \frac{\partial U}{\partial T} \tag{10}$$

The term $\frac{\partial U}{\partial T}$ is also known as the entropic coefficient. For a lithium insertion compound, the open circuit potential (U) is a function of the lithium concentration or the lithium stoichiometry (SOC) in the compound. Therefore, the entropic coefficient is also a function of the lithium concentration or SOC.

For the entire porous electrode with a local current density $i(x)$, the entropic heat per unit cross sectional area is

$$q_{entropic,rxn} = -\int_0^{L_{electrode}} ai(x)T\frac{\partial U_{surf}}{\partial T}(SOC(x))dx \tag{11}$$

However, the reaction is not the only source for the entropy change. Entropy of the electrochemical system can also change due to diffusion within electrode particles to form uniform concentration, and in such a case, the heat released or absorbed due to entropy change contributes to the total heat of mixing [146]. The entropic coefficient $\left(\frac{\partial U}{\partial T}\right)$ can generally be measured by two methods. One is by measuring the open circuit potential (U) as a function of temperature for different SOC's [164]. The other, much quicker, method is using isothermal calorimetry [146,154,155]. At lower charge/discharge rates, the entropic heat can be comparable in magnitude to the irreversible heat [156,157]. However, as the charge/discharge rate increases, the percentage contribution of the entropic heat in the overall heat generated decreases significantly [150].

3.1.3. Heat generation due to side reactions

In addition to the primary reactions at the electrodes, there are other reactions in the cell such as gas evolution [158,159], SEI formation [70,73], electrolyte-anode and electrolyte-cathode reactions [70,160–162] and electrolyte-lithium metal reaction in the presence of lithium plating [163]. At elevated temperatures, due to increased kinetics, there can be a series of reactions that generate a significant amount of heat and can possibly lead to thermal runaway [85,164]. In general, the heat generated due to side reactions can be modeled as

$$Q_{rxn} = \sum_{i=1}^{n} r_i \Delta H_i \tag{12}$$

where i is the index of a particular side reaction, and there are n side reactions that occur. r_i is the rate of the reaction (mol/s) and ΔH_i is the reaction enthalpy (J/mol).

At lower temperatures, the reaction rates for the side reactions are generally low [85,132]. Therefore, in most heat generation models for normal operating temperatures, the heat due to side

reaction is neglected [150,165]. However, at high temperatures, due to Arrhenius type kinetics, the reaction rate increases exponentially, and these reactions become the dominant source of heat generation. The increased temperature promotes the side reactions which generate more heat and in turn elevate the temperature further. If heat cannot be efficiently dissipated, the battery enters a self-reinforcing temperature rise stage known as thermal runaway [164,166].

There are many causes that trigger thermal runaway such as mechanical abuse (crash or puncture), electrical abuse (short circuit [167] and overcharge [168]), lack of adequate thermal management [169–172], and chemical cross-talk [173,174]. Additionally, the risk of thermal runaway increases with increased energy density of the cells [175,176]. LIB safety evaluation consists of electrochemical (*e.g.*, overcharge [177]), mechanical (*e.g.*, nail penetration and impact tests [178]), and thermal tests, and a detailed summary can be found in Ref [179]. The series of dominant reactions that occur during thermal runaway are extensively covered in literature dedicated to thermal runaway [39,40,169]. At the anode, the reactions that lead to thermal runaway include SEI decomposition and regeneration [39,180] as well as the reaction between the lithiated graphite anode and the electrolyte [160,161,181]. In the presence of lithium plating, the metallic lithium can react with the electrolyte [88,163] to release heat. In solid-state batteries with lithium metal anode and oxide electrolyte, the reaction between the oxygen released from the electrolyte and the lithium metal has been identified as a possible cause of thermal runaway [162]. Additionally, the decomposition of cathode and subsequently the oxygen released from the decomposed cathodes can react with the electrolyte, the lithiated graphite anode or plated lithium to release a significant amount of heat [160,161,181].

Feng *et al.* [39] summarized the process in a temperature *vs.* time plot (see Fig. 6a). Further, Feng *et al.* provided a visual summary of energy released by different reactions in a thermal runaway (see Fig. 6b), where the width of the reaction indicates the temperature range of the occurrence of the reaction, the y-location indicates the enthalpy (ΔH) of the reaction and the height represents the heat generation rate.

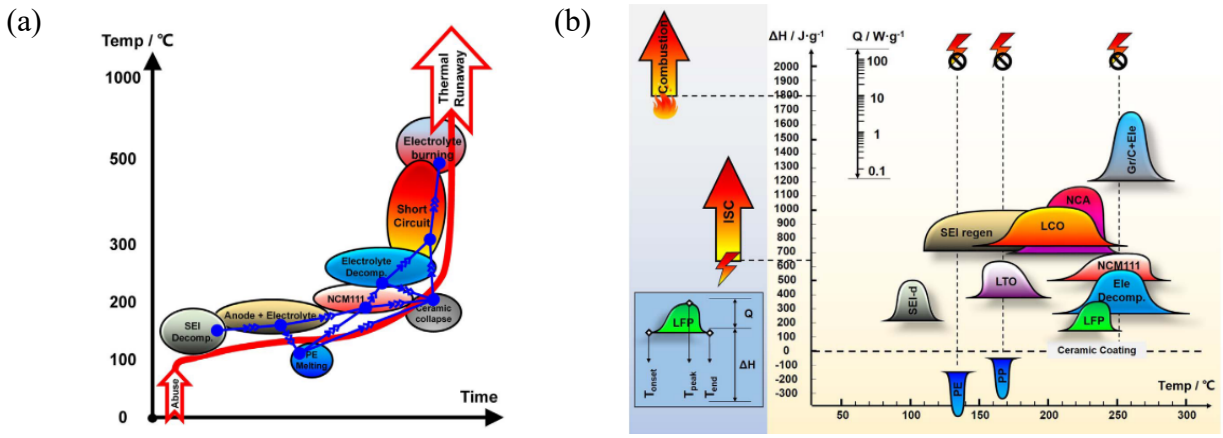

Fig. 6. (a) The chain reactions in a thermal runaway in a Li-ion cell. As the reactions initiate, the temperature rises further that enables other exothermic side reactions. (b) Energy release diagram for side reactions involving cathode materials (LFP, NCM111, LTO, LCO), Separator (PE, PP), anode material (Gr/C), SEI and electrolyte. Panels adapted from Ref [39], Elsevier.

3.1.4. Heat of mixing

After a charge transfer reaction at the surface of an electrode particle, the solid lithium diffuses in an intercalation compound. The composition of the intercalation compound determines its energy [156]. As illustrated in Fig. 7a, when lithium diffuses inside an electrode particle in the presence of a concentration gradient of lithium within the particle, the local composition and hence the energy of the active material experienced by the particle changes with time. This change in the energy is manifested as heat and is known as the heat of mixing in the particles [146]. At low charge/discharge rates, the rate of diffusion is comparable to the lithium flux in or out of the particle and strong concentration gradients do not develop within the particle. For a lithium ion diffusing inside a particle with weak concentration gradients, the local composition does not change rapidly as it diffuses. Because of this, the rate of change of its enthalpy due to the change in local composition is low compared to the change in enthalpy due to the electron transfer reaction at the surface. This is why the heat of mixing due to enthalpy change during the diffusion process inside the electrode particle is often neglected while modeling heat generation in batteries [131,150]. However, at higher charge/discharge rates, the net lithium-ion flux in or out of the particle is high compared to the diffusion rate. As a result, the surface concentration of lithium ions differs significantly from the concentration inside the particle, and a strong concentration gradient develops within the particle. When lithium diffuses through this strong concentration gradient the local composition and therefore energy changes rapidly and is manifested as heat [146]. Therefore, at high charge/discharge rates, heat of mixing cannot be neglected. Recently, Chalise *et al.*[146] demonstrated that during a 6C discharge of an NMC cathode, ~23% of the total heat released is because of heat of mixing. Fig. 7b shows the average contribution of heat of mixing during the discharge of an NMC cathode at different C-rates. The heat of mixing is non-negligible even at 1C, and its contribution increases as the charge/discharge rate increases.

It is generally seen that the enthalpy or the enthalpy potential $\left(U_H = U - T\frac{\partial U}{\partial T}\right)$ of the typical cathode materials is a strong function of the composition (SOC) [146,155]. On the other hand, the enthalpy potential of a typical anode such as graphite does not change much with the composition [155]. Therefore, it is expected that heat of mixing, which originates from enthalpy change due to composition change, is much more significant in cathode materials than in anode materials.

In lithium insertion compounds used in the cathode, the enthalpy potential and therefore the energy typically decreases monotonically with the lithium content in the composition (SOC) [146,155]. The diffusion process, the driving force for mixing, always makes lithium move from a higher concentration to a lower concentration and therefore from a state with a higher energy to a state with a lower energy. Hence, this movement of lithium (mixing) in typical cathode materials is always exothermic regardless of whether the battery is charging or discharging. Therefore, heat of mixing in typical cathode materials is exothermic during both charge and discharge [146].

(a)

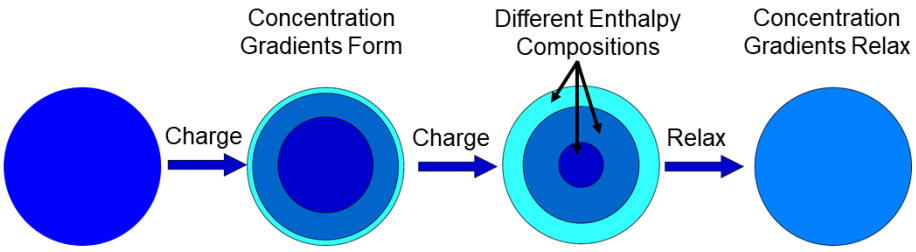

(b)

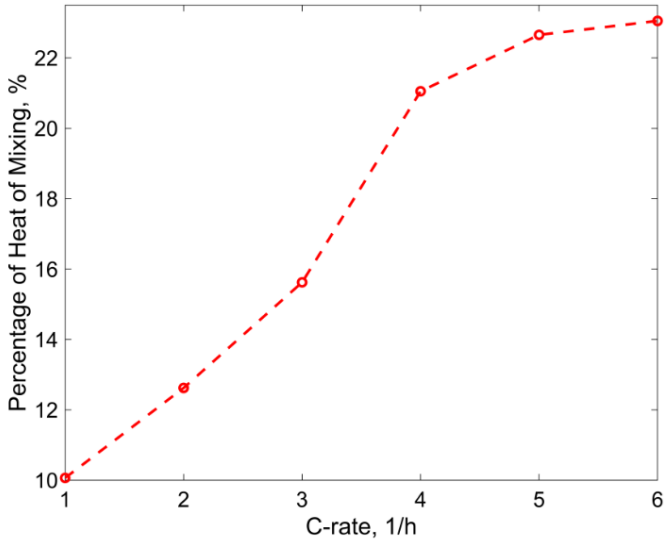

Fig. 7. (a) Formation and relaxation of concentration gradients in an active material particle during charge or discharge. The enthalpy change due to the change in the local composition during the formation or relaxation of the concentration gradients leads to heat of mixing. (b) Percentage contribution of heat of mixing in the overall heat generated at various C-rates. At 6C, the heat of mixing can contribute to 23% of the total heat generated in the cell. Panel adapted from Ref [146], the Electrochemical Society.

3.2. *Modeling heat generation*

3.2.1. Isothermal heat generation models

Isothermal heat generation models assume that the battery operates isothermally and do not account for temperature changes and its impact on heat generation. Broadly, these isothermal models can be divided into two categories: uniform current/reduced-order models and distributed current/full-order models.

3.2.1.1. Uniform current (reduced-order) heat generation models

Uniform current models assume that each particle in a porous electrode sees the same amount of current regardless of its position in the electrode. Doing so, one does not need to account for current distribution within the electrode that arises from multiple coupled effects of transport and kinetics. Because of the increased simplicity in modeling, these constant current or so called reduced-order

models have been extensively used to model the charge/discharge behavior as well as heat generation in batteries [65,153,182–185]. The commonly used form of the heat generation equation in these models is

$$\dot{Q} = I(U_{avg} - V) - IT\frac{\partial U_{avg}}{\partial T} + \sum_{l} \Delta H_l^{avg} r_l + \int \sum_{j} \sum_{i} (\overline{H_{ij}} - \overline{H_{ij}^{avg}})(\frac{\partial c_{ij}}{\partial t})dv \quad (13)$$

Here, the first term is the irreversible heat associated with the kinetic and transport losses, the second term is the entropic heat, the third term is the heat due to side reactions and the last term is for heat of mixing.

These models work well at low charge/discharge rates, where mass transport is not limiting and the current distribution is fairly uniform [146,186]. However, as the charge/discharge rate increases, mass transport limitations become dominant and the current distribution is largely non-uniform [130,186][127,189]. In such a case, a single SOC cannot describe the entire cell since different particles in the cell are at different SOC's as they receive different amounts of current. Then, in order to model the heat generation at higher charge/discharge rates, it becomes essential to account for the non-uniform current distribution.

3.2.1.2. Non-uniform current (full-order) heat generation models

Before focusing on distributed current heat generation models, we should discuss how the current distribution itself is modeled for a porous electrode battery. The current distribution in porous electrodes is usually modeled using the Doyle, Fuller and Newman Model, generally known as the Pseudo-2D (P2D) model [130,148,149]. The P2D model describes the transport and kinetics, mass and charge transport in the battery with a set of coupled partial differential equations. The equations allow a 1D variation in the current distribution along the length of the electrode (x) while also allowing a radial variation in the lithium concentration in the particles at a fixed position inside the electrode.

Once the local current density (i) is known, the overall heat generated by the cell can be obtained by [131,150]:

$$q = \sum_{\substack{particle,\\ electrodes}} ai(\phi_s - \phi_e - U) + \sum_{\substack{particle,\\ electrodes}} aiT\frac{\partial U_{surf}}{\partial T} \quad (14)$$
$$+\sigma^{eff}\nabla\phi_s \cdot \nabla\phi_s + k^{eff}\nabla\phi_e \cdot \nabla\phi_e + k_D^{eff}\nabla \ln c_e \cdot \nabla\phi_e$$

Eqn. (14), which accounts for heat generation due to apparent loss mechanisms as well as entropy change, has been used extensively for heat generation modeling at high charge/discharge rates [130,131,151,165,187,188]. However, it is evident that this equation does not account for heat generation due to side reactions. Since the isothermal modeling is usually done for room temperature, where the rate of the side reactions is not significantly high [132,169,172], it is reasonable to omit the heat generation due to the side reactions. Nevertheless, if the modeling is done for high temperatures, it is necessary to account for the side reactions. In such conditions however, the temperature becomes crucial in determining the heat generation rate, and an

isothermal heat generation model cannot be used. Therefore, a coupled electrochemical-thermal model that includes temperature rise and its effect on heat generation becomes essential [132,166].

Further, Eqn. (14) does not include heat of mixing. However, at high charge/discharge rates, the enthalpy within a particle changes rapidly as strong concentration gradients develop [146]. Therefore, at high charge/discharge rates, it is essential to model heat of mixing within the particles. Thus, authors [64,189–191] have tried to incorporate heat of mixing in a distributed current model. Usually, the expression used to calculate heat of mixing in the particles is [189,191]

$$Q_{mixing} = \int \sum_{j,electrode} \sum_{i,particle} (\overline{H_{ij}} - \overline{H_{ij}^{avg}})(\frac{\partial c_{ij}}{\partial t})dv = \frac{\partial}{\partial t}\left[\sum_{j,electrode} \sum_{i,particle} \frac{1}{2} \frac{\partial \overline{H_s}}{\partial c_s} \int (c_s - c_{s,\infty})^2 dv \right] \quad (15)$$

This expression comes from the simplified expression of enthalpy of mixing derived by Thomas and Newman [156,157] based on second order Taylor expansion of the enthalpy about H_∞ (the enthalpy at the average concentration $c_{s,\infty}$). The simplified Taylor expanded expression for heat mixing derived by Thomas allows further simplification by not having to numerically solve for the concentration profile within the particles by using a pseudo-steady state assumption for the purpose of estimating the magnitude of heat of mixing. However, in a distributed current model, the concentration profiles within the particles are already solved for. Therefore, using the Taylor expanded expression for enthalpy of mixing [64,189,191] as opposed to a non-simplified expression [146] does not reduce any computational burden. In our recent work [146], we have shown that using the Taylor expanded expression, which implicitly assumes small concentration gradients, can instead incorrectly predict the enthalpy change due to mixing at high charge/discharge rates, where the concentration gradients within the particles are significant. We have presented an alternative expression for heat of mixing without assuming small concentration gradients. The expression for heat of mixing within one electrode particle is

$$Q_{mixing,particle} = (\frac{dH}{dt}) - 4\pi R^2 i U_{H,surface} \quad (16)$$

where $U_H = U - T\left(\frac{dU}{dT}\right)$ is the enthalpy potential [156] and $\frac{dH}{dt}$ is the rate of enthalpy change of the particle given by

$$\frac{dH}{dt} = -4\pi F \int_0^R r^2 (\frac{dc_s(r,t)}{dt}) U_H(SOC(r,t))dr \quad (17)$$

Since the local state of charge $SOC(r,t)$ and the concentration profile $c_s(r,t)$ is determined while solving the P2D model itself, calculating the heat of mixing using this expression does not increase any computational burden than what the Taylor expanded expression already requires. In fact, this expression (Eqn. (17)) requires only one volumetric integral while the Taylor expanded form requires two: one volumetric integral over the particle volume to calculate the average concentration $c_{s,\infty}$ and another volumetric integral given in Eqn. (15). Therefore, this method of calculating heat of mixing is more accurate and therefore appropriate at high charge/discharge rates while being computationally more efficient. Using this method, the total heat of mixing for all the particles in an electrode per unit nominal electrode area (W/m^2) can then be calculated as [146]:

$$q_{mixing,electrode} = \frac{3\varepsilon_{ins}}{4\pi R^3}\int_0^{L_{electrode}} \left(\left(\frac{dH}{dt}\right) - 4\pi R^2 i U_{H,surface}\right) dx \tag{18}$$

3.2.2. Coupled electrochemical-thermal heat generation models

Factors that contribute to the heat generation, namely the transport properties [64,165,188], exchange current density [136,147], the open circuit potential [165,192], the entropic coefficient [193]and rates of the side reactions [132], depend on the local temperature. For a single cell with external cooling, where the temperature rise is small, the isothermal assumption and therefore isothermal heat generation modeling is reasonable. However, for a cell stack, especially undergoing fast charge or discharge, the temperature varies within the stack, and the temperature of the cells near the center can be significantly higher than the ones near the surface [43]. Additionally, when the heat generation rate is high, for instance during the initiation of a thermal runaway or during fast charge/discharge, the temperature rise can be substantial and it can in turn affect the heat generation [132]. Moreover, heat generation rate in general itself is a strong function of temperature [194,195].Therefore, for large cells undergoing fast charge or discharge, a coupled electro-thermal model that simultaneously simulates the current distribution, heat generation and temperature rise with a coupling among one another is required.

There are many coupled electrochemical-thermal models proposed in the recent past [64,65,67,103,132,165,184,188,196]. In general, as illustrated in Fig. 8, for a set of given initial conditions, these models simulate the current distribution (or assume uniform current distribution) and the isothermal heat generation for a particular time-step. Then, from the heat generation and the thermal properties of the cell, these models simulate the local temperature and according to the local temperature update the transport and kinetic parameters and the potentials for the next time-step. The specific dependence of parameters on the temperature however varies model to model. Various authors [165,188] have used Arrhenius type temperature dependence on the transport properties and the exchange current density while others [64] have used experimental data on the temperature dependent transport properties. The temperature dependence of the OCV (U) is usually obtained from the entropic coefficient $\left(\frac{dU}{dT}\right)$ using the first order Taylor expansion of U about the OCV (U_{ref}) measured at the reference temperature (T_{ref}) [165,192], *i.e.*,

$$U(T, SOC) = U_{ref}(SOC) + (T - T_{ref})\frac{\partial U}{\partial T}(SOC) \tag{19}$$

Note that the entropic coefficient $\left(\frac{dU}{dT}\right)$ might itself be a function of temperature (*i.e.*, $\frac{\partial^2 U}{\partial T^2} \neq 0$) [193]. In that case, the first order Taylor expansion would be inadequate and an additional second order term might be needed. Also, if that is the case, the entropic coefficient used in calculating the reversible heat needs to be evaluated at different temperatures.

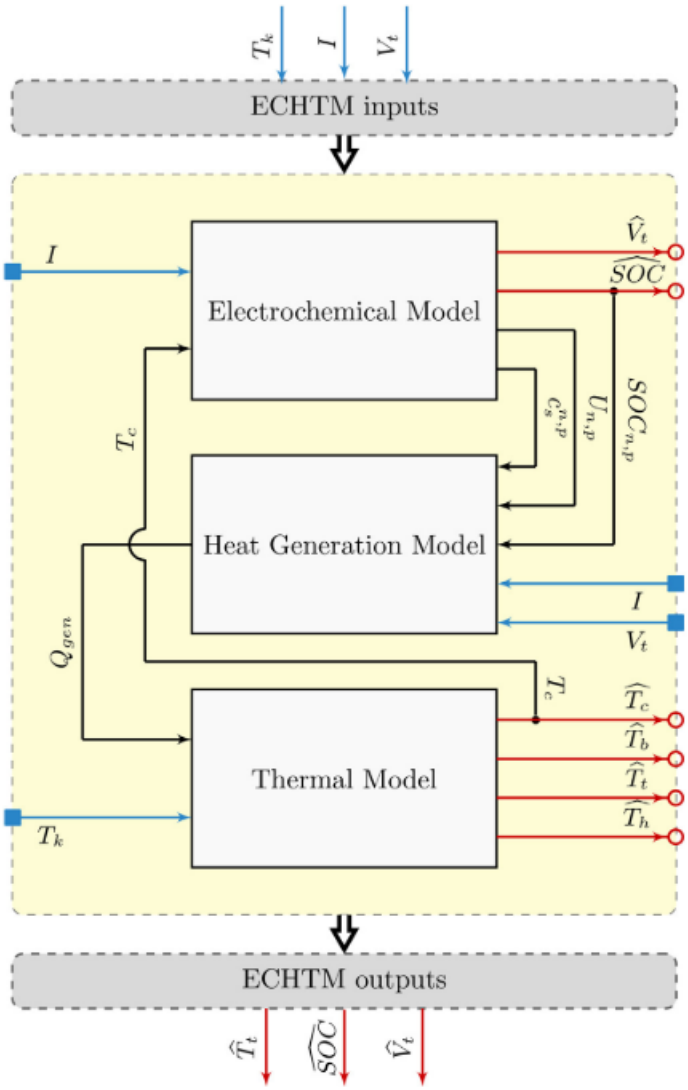

Fig. 8. A typical data flow diagram for a coupled Electrochemical-Thermal Model. According to the notation of Farag *et al.* [64], T_c, T_b, T_t, T_h and T_k represent the temperature of the core, base, terminals, housing and the cooler respectively. Other acronyms are consistent with the nomenclature for this paper. Panel adapted from [64], Elsevier.

Although most coupled electro-thermal models have been shown to agree reasonably well with the experiments [64–67], some common inconsistencies with these models are frequently encountered in the literature. The most common mistakes related to the thermal modeling include the omission of anisotropic thermal conductivity [66,197], the omission of thermal interface resistance [67,165,196], and the use of lumped thermal analysis [64–66]. From the electrochemical perspective, the common inconsistencies include the use of uniform current distribution [65,196] or the omission of heat of mixing at high C-rates [188,198]. These inconsistencies need to be eliminated in order to develop a robust electrochemical-thermal model that can work for a wide range of temperature and a variety of external conditions such as different charge/discharge rates, ambient temperatures and external cooling rates.

3.3. *Material level modifications for minimizing heat generation*

A significant portion of the literature on battery thermal management has focused on facilitating heat dissipation, whether by enhancing external cooling [151,199–202] or by improving thermal transport properties [5,12,203][3,8,206]. However, possible modifications to minimize the heat generation itself has not been discussed extensively. Minimizing the heat generation, especially that arising from irreversible sources, not only helps in reducing the temperature rise but also increases the overall energy utilization of the battery. Thus, it is essential to understand how heat generation in the cell itself can be decreased. In order to do so, we need to understand the material dependence of heat generation and the possible improvements at the material level. Therefore, this section is dedicated towards explaining how material properties affect heat generation and what improvements at the material level can mitigate heat generation.

3.3.1. Irreversible heat generation

3.3.1.1. Transport Losses

Minimizing transport losses essentially means decreasing the potential drop across the electrodes and the electrolyte. The potential drop across the electrode is given by Ohm's law and is inversely related to the electrode's electrical conductivity. Hence, to decrease the potential drop at the electrode, the electrical conductivity must be increased. This is typically done by increasing the volume fraction of carbon black in the electrode [204]. However, there is a limit to doing so as it also decreases the active material volume fraction and hence adversely affects the energy density. Additionally, the typical electronic conductivity of electrodes (40-1000 mS/cm,[151]) is much greater than the typical ionic conductivity of electrolytes (1-10 mS/cm, [152]), and hence the potential drop in the electrode is comparatively minimal. Therefore, more attention should be given to decreasing the potential drop across the electrolyte.

The potential drop across the electrolyte is described by the modified version of Ohm's law [130] which additionally accounts for the concentration overpotential [147]. The potential drop $\frac{\partial \emptyset_e}{\partial x}$ is inversely proportional to the effective ionic conductivity (κ^{eff}) and directly proportional to the ionic diffusional conductivity (κ_D^{eff}) and the concentration gradient. Therefore, measures to decrease the concentration gradient or the ionic diffusional conductivity or increase the effective ionic conductivity helps in decreasing the potential drop (transport loss) across the electrolyte. Additionally, decreasing the transport length by limiting the thickness of the separator is also essential in decreasing the potential drop across the electrolyte in the separator region.

The effective ionic conductivity of the solution can be increased either by increasing the bulk solution ionic conductivity or by increasing the porosity (volume fraction of electrolyte) of the separator or electrodes. A simple relation using the Bruggeman tortuosity correlation for the effective ionic conductivity is [130]

$$\kappa^{eff} = \kappa \varepsilon_e^p \tag{20}$$

where κ^{eff} is the effective ionic conductivity, κ is the bulk solution ionic conductivity, ε_e is the electrolyte volume fraction (porosity) and p is the Bruggeman factor related to the tortuosity.

The bulk ionic conductivity κ of liquid electrolytes depends on the salt concentration [130,205] and is typically 1-10 mS/cm [152] for commercial liquid electrolytes that typically contain Lithium salts (*e.g.*, $LiPF_6$) in mixtures of organic solvents such as ethylene carbonate (EC) and diethyl carbonate (DEC) [206]. Kufian *et al.* [206] have shown that adding ethyl propionate (EP) additive in the electrolyte with 28.6% volume fraction of EP in 1M $LiPF_6$ in 1:2 EC:DEC increases the ionic conductivity by nearly 60% at room temperature. Guerfi *et al.* [207] have examined mixed electrolytes with ionic liquids in organic solvents. They have shown that the organic electrolyte with 40% ionic liquid (TFSI as the anion and EMI as the cation) optimizes the ionic conductivity while restricting the viscosity from increasing [207]. Additionally, Das *et al.* [208] have shown that dispersed oxide particles additives in electrolytes can increase the effective ionic conductivity to 14 mS/cm and Tominaga *et al.* [209] have shown that TiO2 nanoparticles can increase the ionic conductivity of polyethylene carbonate based electrolytes by a factor of 2. However, it should be noted that any efforts to change the electrolyte composition to increase the bulk solution conductivity might adversely affect the voltage stability window of the electrolyte and promote side reactions with the electrodes [152]. Alternatively, the effective ionic conductivity can be increased by increasing the volume fraction of the electrolyte (porosity) according to Eqn. (20). This is not preferable for electrodes as it would decrease the active material volume fraction and thus decrease the energy density. However, the ionic conductivity in electrodes can be effectively increased by decreasing the tortuosity [210,211] without compromising the volume fraction of active material. Additionally, a separator with an increased porosity and reduced thickness could minimize the potential drop in the electrolyte by both increasing the effective ionic conductivity and decreasing the transport distance. However, the requirement for a high mechanical strength has restricted the porosity and thickness for a typical separator to be about 0.6 and 25μm respectively [146]. Separators with a high mechanical strength such as the one demonstrated by Zhai *et al.* [212] can potentially overcome this limitation. Additionally, researchers have also shown that modifying the separator-electrolyte interaction through surface modification of the separators can increase the effective ionic conductivity and cation transference number [213–215][216–218].

The concentration gradient in the electrolyte depends on the effective diffusivity and the transference number [130]. As the effective diffusivity and the conductivity are related by the Nernst-Einstein relation [147], the same strategies of decreasing tortuosity and increasing porosity work for increasing the effective diffusivity. The bulk diffusivity of Lithium ions in a typical organic electrolyte is concentration dependent and is typically between 10^{-9} to 10^{-11} m^2/s [216,217]. In comparison, ionic liquid electrolytes generally have a lower lithium ion diffusivity [218]. However, various authors have shown an improvement in the bulk diffusivity of ionic liquids with the addition of organic solvents [218,219]. As shown by Diederichsen *et al.* [152], a high cation transference number results in decreased concentration gradient within the electrolyte (Fig. 9). This decreases the concentration overpotential and hence the potential drop across the electrolyte.

In the literature, considerable attention has been given to increasing the cation transference number

and getting it close to unity [152,220,221]. Diederichsen *et al.* [152] have presented a comprehensive review on achieving high transference number in electrolytes, and the readers are directed to the article for further information on this topic. However, it is important to note that, as Diederichsen *et al.* point out, there can be an inherent trade-off between the transference number and ionic conductivity. This is generally true because traditionally, a higher cation transference number has been achieved by restricting the anion mobility, which effectively decreases the ionic conductivity [222]. However, McCloskey *et al.* have recently shown that using Nonaqueous Polyelectrolyte Solutions, both high conductivity and transference number can be achieved simultaneously [223,224].

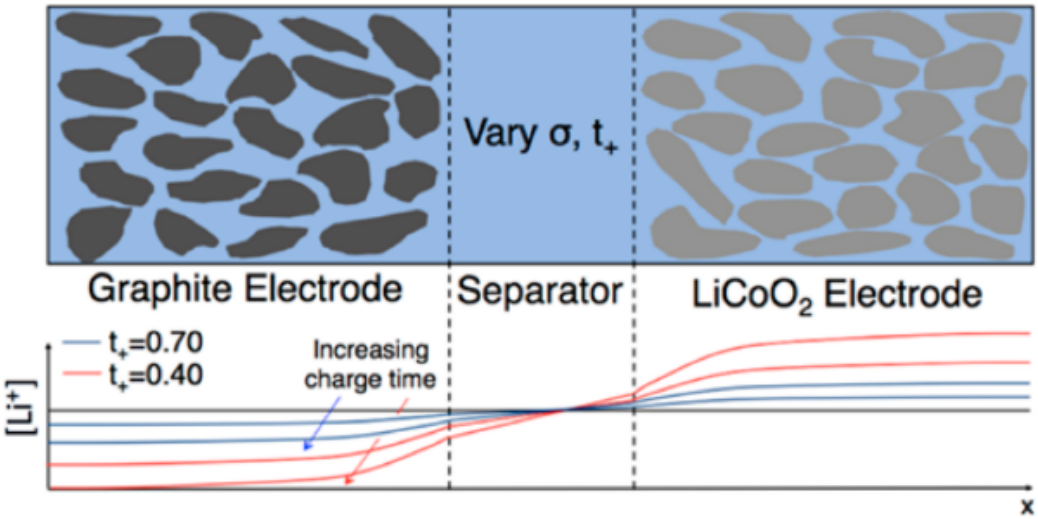

Fig. 9. Electrolyte concentration gradient decreases with the increase in the cation transference number. Transport loss due to the concentration overpotential caused by the concentration gradient can thus be minimized by increasing the cation transference number. Panel adapted from Ref [152], American Chemical Society.

3.3.1.2. Kinetic Losses

It was mentioned in Section 3.1.1 that the kinetic overpotential leads to irreversible heat generation of the type

$$q_{reaction} = i\eta_s \tag{21}$$

where η_s is the surface overpotential for the reaction at the electrode surface and i is the local current density.

The kinetic overpotential can be described by the Butler-Volmer (BV) equation (Eqn. (8)) or an equivalent kinetic expression [147,225][165,228]. At high currents, we can simplify the BV equation into the Tafel equation [165], in which case the local heat generation due to kinetic overpotential can be rewritten as

$$q_{rxn} = i\eta_s = i\frac{RT}{\alpha_a F}\log(\frac{i}{i_0}) \tag{22}$$

Thus, the heat generated and the surface overpotential scales up with the local current density (i) and scales down with the exchange current density (i_o). From this, one strategy to reduce the kinetic loss can be decreasing the local current density. This can be achieved by increasing the reaction surface area or, in other words, making the particles smaller. However, large surface area (small particle size) also increases the surface area for parasitic side reactions between the electrodes and the electrolyte and thus impacts long term capacity retention [226]. Therefore, there is a limit to how small the particle size can be. Alternatively, the kinetic losses can be minimized by having a high exchange current density, *i.e.*, achieving fast charge transfer kinetics.

The exchange current density is a measure of charge transfer kinetics at the electrode and is determined by the rate constant K of the reaction and the concentration of the species. The rate constant depends on the activation energy (E_a) for the reaction and the temperature [147]. With other factors constant, the charge transfer resistance, which can be directly related to the exchange current density with linearized BV equation for a small current density, can be related to the activation energy and the temperature as [227]

$$\frac{1}{R_{ct}} = A\exp(-\frac{E_a}{RT}) \tag{23}$$

The slope of the semilog plot between the charge transfer resistance and $1/T$ gives the activation energy, which can directly be used as a measure of the kinetics of the reaction [227–229]. Note that the charge transfer resistance (R_{ct}) can be obtained experimentally from electrochemical impedance spectroscopy (EIS) [227,230].

The charge transfer (oxidation) at an electrode usually involves 3 steps [227,230]: (1) desolvation of Li ion at the electrolyte-solid electrolyte interphase (SEI) or electrolyte-cathode electrolyte interphase (CEI) interface, (2) Li ion transport through SEI/CEI, and (3) charge transfer and intercalation at the electrode-SEI/CEI interface. Similarly, reduction charge transfer reaction includes de-intercalation, transport, and solvation. Many studies have shown that depending on the nature of the electrolyte and the SEI/CEI formed, both the desolvation process [231,232] and the transport through the SEI [230]can be rate limiting. Ogumi [227] has shown that the activation energy related to desolvation is directly related to the solvation number (number of molecules bound to the solvated ion). For instance, the activation energy for 1:1 EC:DEC solution with a solvation number 2.5 is 51 kJ/mol while it is 32 kJ/mol for pure DEC solution with a solvation number of 0 (no desolvation process involved). This result suggests that the choice of electrolyte affects the charge transfer kinetics when the desolvation process is rate limiting.

The activation energy related to the transport through the SEI/CEI layer can be studied by modifying the SEI/CEI using additives in the electrolyte [230]. These additives are added in low concentrations so that they do not change the property of the electrolyte but change the type of the SEI/CEI formed thereby altering the activation energy for transport. Abe *et al.* [228]showed that in two types of preformed SEI at the interface of HOPG-Electrolyte (1M $LiClO_4$ in 1:1 EC:DEC), the activation energy for the charge transfer through the SEI formed with Pentafluorostyrene (PFS) additive was 40 kJ/mol compared to 52 kJ/mol for SEI formed without the additive. Various other experiments [228,233] supported that changing SEI/CEI composition through electrolyte additives

changed the activation energy for charge transfer. Therefore, SEI/CEI modification can be a feasible method to enhance the kinetics of charge transfer.

In addition to the electrolyte and SEI modification, electrode surface modification has also been shown to improve the charge transfer kinetics. Ogumi [227] has shown that in the same electrolyte (1M $LiClO_4$ in propylene carbonate), the activation energy for charge transfer in $LiCoO_2$ cathode is reduced from 60 kJ/mol to 47 kJ/mol by coating $LiCoO_2$ with MgO. Additionally, Goodenough *et al.* [234] have shown that surface modification of $LiFePO_4$ with Nitrogen (using NH_3) or Sulfur (using Sulfur vapor) decreases the energy barrier for the charge transfer reaction by promoting strong binding of Li on the surface electrode and thereby increases the rate constant for the charge transfer reaction. As shown in Fig. 10, the rate constant was enhanced by up to a factor of 1.4 with Sulfur and 1.1 with Nitrogen.

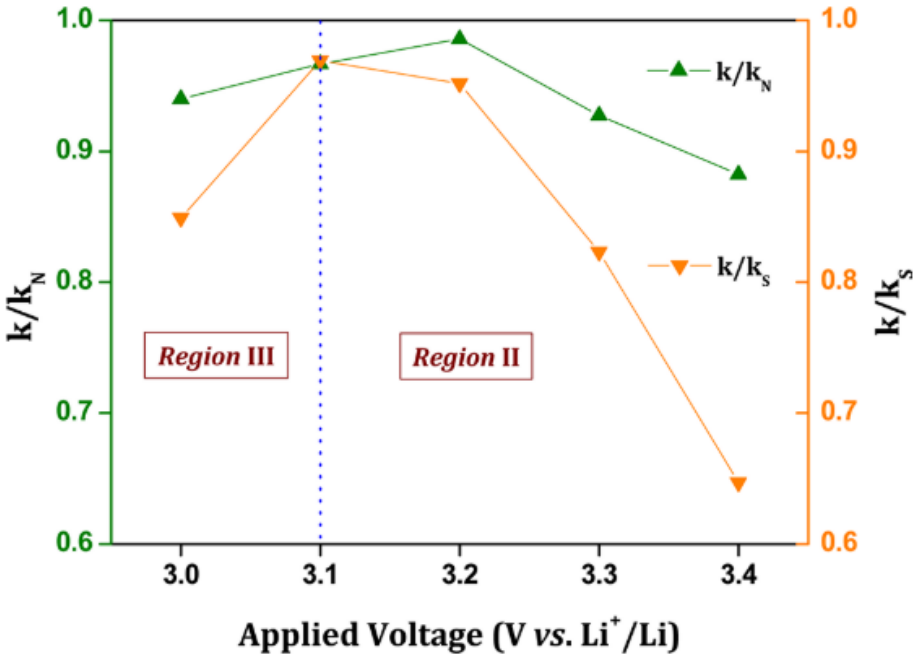

Fig. 10. Ratios of the rate constants for the charge transfer reaction in $LiFePO_4$ for different applied voltages. At all voltages, the rate constant for surface modified $LiFePO_4$ with nitrogen (κ_N) or sulfur (κ_S) is greater than that for bare $LiFePO_4$ (κ). Panel reproduced from Ref [234], American Chemical Society.

3.3.2. Side reactions and thermal runaway

The best way to prevent thermal runaway is avoiding the conditions that lead to it, namely mechanical, electrical and thermal abuse conditions [41,169]. However, provided that these conditions do occur, there are several material level improvements that can avoid the propagation of thermal runaway reactions. Shah *et al.* [172] derived a non-dimensional number called the 'Thermal Runaway Number (TRN)' based on the heat transfer analysis of a battery to determine whether or not the battery is likely to undergo thermal runaway. According to Shah,

$$TRN = \frac{\beta R^2}{k_r \mu_1^2} \tag{24}$$

where, R is the radius of the cylindrical cell, β is a constant associated with the reaction and describes the propensity of the reaction to generate more heat as the temperature rises [132,172], μ_1 is the first eigenvalue related to the series solution of the thermal diffusion equation and increases with the wall heat transfer coefficient (h), and k_r is the radial thermal conductivity of the cell. As stated by Shah *et al.* and shown in Fig. 11, if the TRN is less than 1, the cell can prevent thermal runaway even in the case of an initial abnormal temperature rise. Therefore, this formula tells us that the thermal property (k_r), external cooling rate (h) and the cell geometry (R) play a significant role in determining whether thermal runaway occurs. Thus, material level improvements to the thermal conductivity, as suggested in Section 4.4, can be key to avoiding thermal runaway.

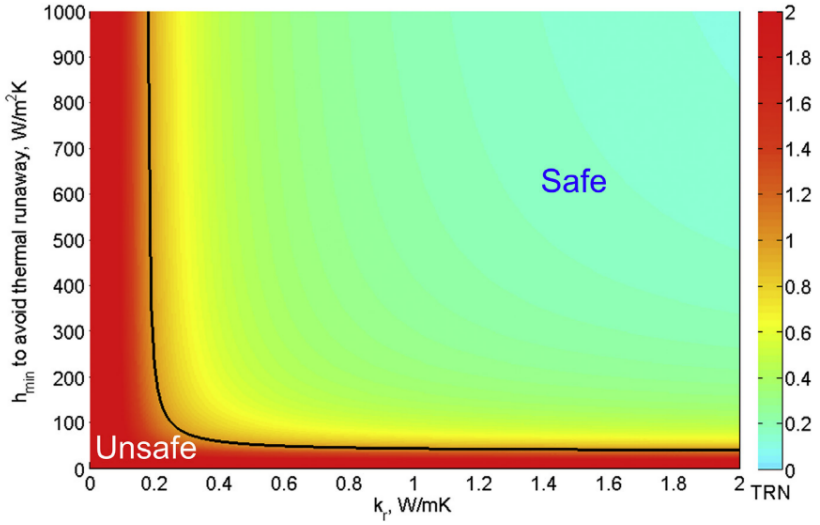

Fig. 11. Plot of the minimum convection coefficient (black line) required to prevent the thermal runaway for a given value of the cross-plane thermal conductivity. Simultaneously plotted as a color map is the thermal runaway number (TRN). For a cell operating with TRN > 1, the convection coefficient is less than the minimum required convection coefficient to prevent the thermal runaway. Panel reproduced from Ref [172], Elsevier.

In addition to improving the thermal properties of the cell, there can be several steps taken to prevent individual reactions that lead to thermal runaway. These steps are covered in detail in [39]and here we only summarize some of them. Surface modification of cathodes with oxides (Al_2O_3, MgO) [235] and element substitution with Al [236] have been shown to improve the thermal stability of cathodes and prevent decomposition at high temperatures. Similarly, Al_2O_3 coating [237] and modification of SEI [238] has been shown to improve the thermal stability of anodes. Additionally, for separators, ceramic coating [239] and changing the base material [240]can be beneficial to reduce the shrinkage and increase the critical temperature for shrinkage [169]. Most importantly however, as organic based electrolytes are prone to ignition and lead to serious safety issues such as fire and explosion [164], modification or replacement of organic based

electrolytes with ionic liquid electrolytes [134,241] or solid state electrolytes [242] will be crucial in minimizing the effects of thermal runaway.

3.3.3. Heat of Mixing

As heat of mixing has largely been unexplored until recently [146], there has not been much work in understanding or mitigating heat of mixing. Here, we propose some potential methods for minimizing heat of mixing. As the heat of mixing is related to the diffusion limitation and the formation of concentration gradients [146,156], decreasing the concentration gradients within the particles can minimize the heat of mixing. This can essentially be achieved either by having small particles or by increasing the lithium diffusivity in the intercalation compound. Decreasing the particle size has a limitation due to increased surface area for side reactions as discussed in Section 3.3.1.2. Enhancing the diffusivity on the other hand can be beneficial both in minimizing heat of mixing and in improving electrochemical performance through enhanced kinetics [170,243]. Because of the electrochemical aspect of enhancing the kinetics, numerous works have already been done in increasing the lithium diffusivity in the electrode materials [170,243–245]. Therefore, the same strategies can be suggested to reduce the heat of mixing. From the perspective of minimizing the heat of mixing however, enhancing the diffusivity in the cathode materials is more important than doing so in the anode materials since the cathode materials generally generate more heat from mixing because of the strong concentration dependence of enthalpy and a lower lithium diffusivity.

4. Thermal transport

Thermal management of LIBs with high energy density and charge rate is challenging partly due to the poor thermal transport properties. With a low *k*, the thermal resistance of a battery increases appreciably as it is made thicker for higher capacities. With a significant amount of heat generation, the poor thermal transport impedes efficient heat dissipation and results in battery temperature rise and a large temperature difference across the cell. The large temperature difference can cause different utilization levels of electrodes and thus different aging levels, which finally accelerates the aging of LIBs. In an extreme case, the undesirable temperature rise can trigger decomposition of SEI and thermal runaway. Improving thermal transport properties inside LIBs can mitigate the battery thermal safety concerns. In this section, we review prior thermal transport studies of LIBs and analyze the dominant thermal resistance component in batteries. From the analysis, we discuss the improvement of battery thermal transport properties by thermal engineering of each component.

4.1. *Components*

A unit cell of a battery comprises five layers, *i.e.*, the positive current collector, cathode, separator, anode, and negative current collector (see Fig. 1). The current collectors are metal foils with high *k*, *i.e.*, 237 W/m-K for Al and 401 W/m-K for Cu. The separator is typically a poor thermal conductor due to its porous polymer nature. As for the electrodes, the thermal conductivity mainly depends on the thermal conductivity of active particles, electrolyte, and the contact between particles. The thermal conductivity of battery components has been measured using various measurement techniques in prior works. Here, we summarize the thermal conductivity data of the electrodes and separator and discuss the factors affecting the thermal conductivity.

4.1.1. Electrodes

Table 2 summarizes the thermal conductivity data of various electrodes with and without electrolyte in previous experimental works. Many factors affecting the electrode thermal conductivity have been investigated including the intrinsic particle thermal conductivity, particle size, polymer binder, porosity, electrolyte, temperature, and pressure. Maleki *et al.* performed thermal conductivity measurements of dry graphite anodes with various particle sizes and polymer binder and carbon black contents at different temperatures and compression pressures (see Fig. 12) [51]. They observed a decrease of the *k* with temperature, which was attributed to the relaxed contact pressure among the particles due to the softening and/or melting of polymer binder at higher temperatures. The contact among the particles can be improved by increasing the compression pressure, which explained the increase of the *k* with pressure. This effect was weakened at higher temperatures due to the relaxation of contact pressure among the particles. Increasing the content of polymer binder can enhance the contact between the particles and slightly increase the *k*, *e.g.*, an increase of *k* by 11-13% with the content from 10 to 15 wt.%. From their study, a high-*k* anode should have small carbon-black content (5 wt.%) and large graphite particle sizes (75 μm diameter). Increasing the carbon-black content caused an increase of surface area in the graphite anode, *e.g.*, a 18-20% increase of the surface area because of increasing the

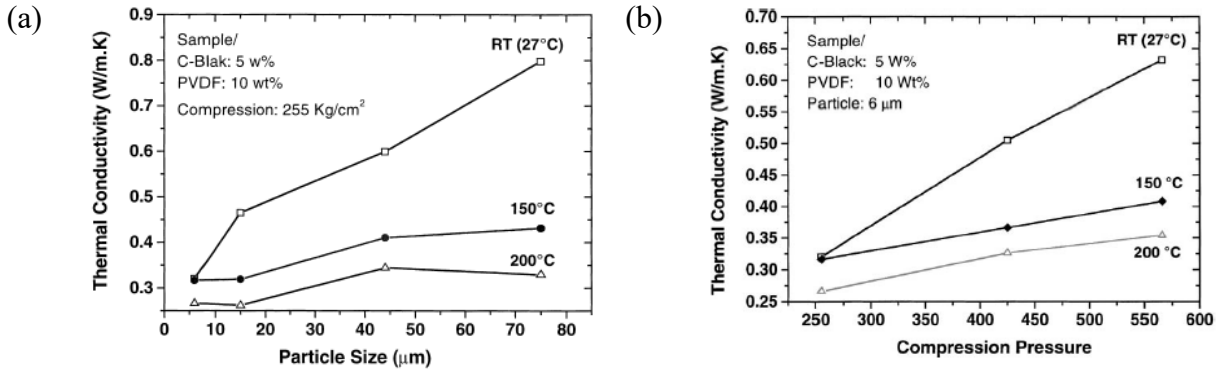

Fig. 12. Thermal conductivity of dry graphite anode *vs.* (a) particle size and (b) compression pressure at RT, 150 and 200 °C. Panels adapted from Ref [51], Elsevier.

carbon-black content from 5 to 10 wt.%. That led to more interface areas in the electrode per volume and can explain the decrease of the *k* with the increasing C-black content, *e.g.*, 0.320 W/m-K at 5 wt.% and 0.191 W/m-K at 10 wt.%. The same logic can qualitatively explain the increasing *k* with the graphite particle size. However, the porosity of graphite anodes with various particle sizes was missing in this study. In addition, it is worth noting that the effect of electrolyte was not considered, which can affect the impact of these factors on *k*.

As SEI or CEI (cathode electrolyte interphase) layers are formed in the electrodes due to side reactions during cycling, it is vital to know the evolution of thermal transport properties in the battery life. Richter *et al*. cycled 17.5 Ah LIBs with $LiNiMnCoO_2$|graphite chemistry and reported the thermal conductivity of fresh and aged electrodes in wet (with electrolyte) and dry (dry from the wet) conditions [54]. The *k* of dry electrodes was found to increase in the aging process, while the *k* of electrolyte-soaked electrodes decreased with aging. For the dry electrodes, the increase of *k* was attributed to the SEI or CEI layers formed during cycling. Though there is no thermal conductivity data of SEI and CEI layers, it is reasonable to assume the *k* is higher than that of air (0.024 W/m-K). Thus, the *k* of the dry electrodes increased with aging as the gap among the particles was gradually filled with higher-*k* materials. This agrees well with the decrease of porosity in aged graphite anodes observed in other works [73,246–253]. Similarly, the decrease of *k* in aged electrolyte-soaked electrodes can be explained if the *k* of electrolyte is higher than that of SEI and CEI layers. Note that those post-mortem studies cannot represent the *k* of electrodes during operation as the aged electrode was dried and then refilled with electrolyte. That excluded the effects such as electrolyte distribution and gas produced during cycling, which may largely affect the thermal transport properties. Additionally, Richter *et al*. reported that wet LCO cathodes had a higher *k* (1.03 W/m-K) than that of wet NMC (0.82 W/m-K) and LFP (0.32 W/m-K) cathodes [55]. That may indicate a *k* dependence of cathode materials, but other parameters like particle sizes and porosity were missing for a conclusive study. Note that in their thermal measurements the *k* was an effective number extracted from a stack of many cathode layers and the thermal contact resistance between layers in the measurement stack was neglected in the analysis, which implied the extracted *k* of electrodes can be much lower than the intrinsic *k*.

Recently, Lubner *et al.* measured the thermal conductivity of dry and wet electrodes and explained the thermal conductivity using Bruggemann's model [58]. The model describes a quantitative

relationship between the effective *k* and the *k* of the medium and particles. With the known thermal conductivity of the medium, *i.e.*, 0.024 W/m-K for air and 0.2 W/m-K for the electrolyte, the *k* of electrode particles can be determined with Bruggemann's model from the measured *k* of electrodes with and without electrolyte. Though the model characterizes the impact of the *k* of medium on the *k* of electrodes, the effective medium theory cannot capture the microscopic mechanism of thermal transport in electrodes, *e.g.*, the impact of compression pressure on the intercontact among the particles. In other words, the *k* of electrode particles by this method represents the effective thermal conductivity of idealized homogeneous particles under a specific condition.

Table 2

A summary of *k* of fresh and aged electrodes with and without electrolyte.

Authors	Electrodes	Particle size(μm)	Porosity (%)	k_{fresh}(W/m-K)		k_{aged}(W/m-K)	
				Dry	Wet	Dry	Wet
Maleki *et al.*[51]	C	6-75	-	0.320-0.798	-	-	-
Richter *et al.* [54]	C	-	-	0.31±0.05	0.66±0.06	0.33±0.01	0.60±0.02
	NMC	-	-	0.14±0.02	0.54±0.02	0.18±0.01	0.52±0.06
Richter *et al.* [55]	C		-	0.32±0.03	0.89±0.01	-	-
	LCO	-	-	0.17±0.02	1.03 ±0.09	-	-
	NMC	-	-	0.30±0.05	0.82±0.04	-	-
	LFP	-	-	0.13±0.02	0.32±0.01	-	-
Lubner *et al.* [58]	C	~20	~50%	1.05	1.44	-	-
	NMC	~10	~50%	0.548	0.828	-	-

In addition, the state of charge or the degree of lithiation affects the thermal conductivity of electrodes. An early work by Maleki *et al.* observed an increase of *k* with OCV (open-circuit voltage) for both the graphite anode and LCO cathode without electrolyte [42]. As the OCV increased from 2.75 to 3.75 V, *i.e.*, lithiation for the graphite anode and delithiation for the LCO cathode, the *k* of the graphite anode and LCO cathode increased by 26% and 5-6%, respectively. The dependence was attributed to the impact of lithiation or delithiation on the electron's contribution to the *k*. However, that is contradictory to the current understanding that phonons dominate the heat conduction in these materials. In contrast, Cho *et al.* performed an *in-situ* measurement of the *k* of a deposited $LiCoO_2$ film during cycling and demonstrated a ~31.5% decrease of the *k* with the delithiation from $Li_{1.0}CoO_2$ to $Li_{0.6}CoO_2$ (see Fig. 13a) [254]. The variation of the *k* may be attributed to the phase change related to the degree of lithiation (see Fig. 13b). Later, the *k* of lithium ion intercalated graphite was investigated by molecular dynamics simulations (see Fig. 13c) [255,256]. The in-plane *k* decreased rapidly with the lithium-ion concentration, while the cross-plane *k* initially decreased with the degree of lithiation and then increased with further lithiation. At low lithium-ion concentrations, the phonon scattering rate increased due to the interaction between the lattice and the intercalated lithium ions. As the lithium-ion concentration crossed a specific threshold, the anisotropic variation of the elastic constants played a different role in the in-plane and cross-plane thermal transport, *i.e.*, the increasing cross-plane elastic constants enhanced the cross-plane thermal transport and decreased

the in-plane *k* by weakening the in-plane phonon focusing effects. Though there is a lack of *k* measurements of lithium ions intercalated in graphite, these simulation results agree reasonably well with the concentration-dependent *k* of other types of graphite intercalation compounds (see Fig. 13d) [257].

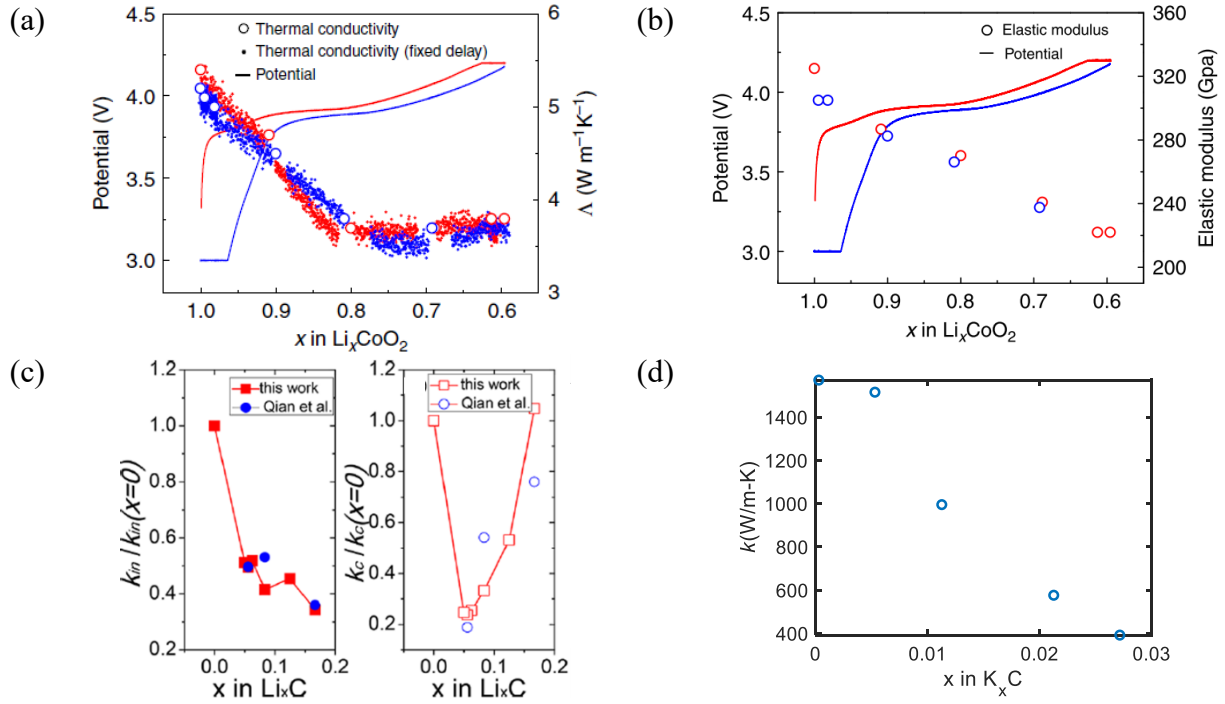

Fig. 13. The variation of (a) *k* and (b) elastic modulus in Li_xCoO_2 with the degree of lithiation [254]; (c) The in- and cross-plane *k* in lithiated graphite by molecular dynamics simulations [255]; (d) The in-plane *k* of K intercalated graphite [257]. Panels reproded from: (a) and (b) Ref [254], Springer Nature Ltd; (c) Ref [255], Elsevier; (d) Ref [257], American Chemical Society.

4.1.2. Separators

The *k* of separators is typically low given their microporous polymer nature. Moreover, the *k* is anisotropic due to the extruding and stretching steps in production. Vishwakarma *et al.* reported that the in-plane *k* of dry separators was 0.5 W/m-K at room temperature and remained relatively constant at temperatures below 50 °C [258]. In contrast, the cross-plane *k* ranged from 0.07 W/m-K to 0.18 W/m-K for dry separators and from 0.10 W/m-K to 0.40 W/m-K for wet separators [55]. Note that the *k* of separators is typically lower than that of electrodes.

4.2. *Interfaces*

Besides the thermal resistance of each layer, the thermal contact resistance (TCR) between layers impedes heat transfer across the cell. Although the TCR can be dominant in the total thermal resistance of the cell, relatively few TCR measurements exist in the literature. Vishwakarma *et al.* investigated the thermal resistance of the cathode-side half-cell and found that the TCR between the cathode and separator contributed ~88% to the total thermal resistance of the half-cell [12].

The high TCR (420 μm^{2}K/W) was attributed to the weak van der Waals adhesion and large acoustic mismatch between the separator and cathode. An amine-based chemical treatment at the interface improved the thermal adhesion and reduced the TCR to 90 μm^{2}K/W. The TCR between the anode and separator was not measured as their theoretical model predicted a low anode-side TCR. Note that this work neglected the thermal transport contribution of electrolyte and measured the thermal resistance using the stack of dry electrodes and separators. Further, Gaitonde *et al.* reported the TCR between the dry separator and metallic case in a range of 1058 - 2532 μm^{2}K/W [56], which was >2 times higher than the TCR between the dry separator and cathode in the prior work. No clear dependence of temperature in the range of 35-120 °C and pressure of 0.1-0.25 MPa was observed for the TCR given the large sample-to-sample variations and the relatively large measurement uncertainty. A physical explanation was not given for such a high TCR. Although the TCR between the dry stack is high, adding electrolyte can improve the contact and significantly decrease the TCR. That necessitates an experimental investigation of the TCR in wet conditions.

In addition to the effect of electrolyte, it is vital to know how the TCR varies as the interface properties change with cycling, *e.g.*, the SEI or CEI formed on electrode particles and gas produced in electrochemical reactions. Lubner *et al.* developed an embedded thermal sensor in live batteries, which enabled *operando* detection of thermal transport properties inside the battery [58] . The thermal sensor known as 3-omega sensors are based on the use of thermal waves where the penetration depth of the signal can be changed by changing the frequency of the thermal wave [259–262]. They measured the combined TCR between the separator and electrodes (*i.e.*, a sum of the TCR between the separator and anode and the TCR between the separator and cathode) in two cells during formation cycling. With the embedded thermal sensor, the *operando* TCR measurements revealed the effect of electrolyte on the TCR and the evolution of TCR in formation cycles. Adding electrolyte decreased the combined TCR from 538±107 μm^{2}K/W to 173±38 μm^{2}K/W in battery 1 and from 445±85 μm^{2}K/W to 115±32 μm^{2}K/W in battery 2. A model based on prior work by Prasher [263]was developed to explain the TCR between the electrode and separator. The TCR was comprised of the thermal constriction resistance (R_c) due to the variation of cross-sectional areas in particles, the thermal boundary resistance (R_b) due to the phonon mismatch, and the thermal resistance (R_f) of the fluid (or medium) filling the gaps between particles (see Fig. 14). It was found that the thermal constriction resistance was typically 10–1000 times higher than the thermal boundary resistance. Based on this calculation, it is unlikely to see the significant enhancement of TCR by the surface treatment improving R_b in Ref [12]. Adding electrolyte decreased the TCR by reducing the thermal resistance of the medium as the k of electrolyte (0.2 W/m-K) is >8 times higher than that of air (0.024 W/m-K). Further, the TCR increased with formation cycling and contributed ~65% to the total thermal resistance after formation cycles. The increase was likely due to morphology change of the electrode particles or gas bubbles formed at the electrode-separator interface. The first *operando* measurement of thermal transport properties in live batteries highlighted the increases of thermal resistance during cycling, from which more characterizations of thermal resistance *vs.* cycle (or retention capacity) are necessary for the whole-life battery thermal management. For example, a rapid increase of thermal resistance due to electrolyte drying or gas formation may lead to a local hot spot or a surprisingly high internal temperature rise, which is underestimated without considering the change of thermal resistance.

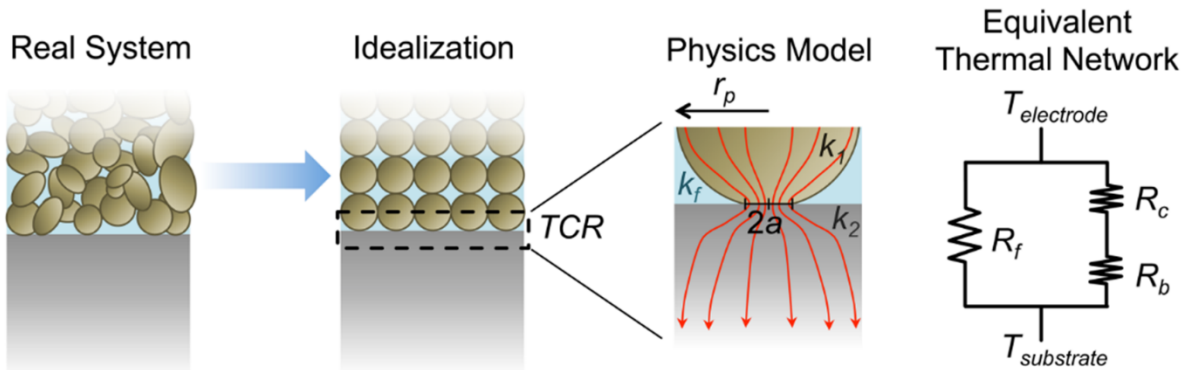

Fig. 14. Idealized thermal model for the thermal conduct resistance between the electrode and separator. Panel adapted from Ref [58], the American Institute of Physics.

4.3. *Cell level*

Cross-plane thermal transport in LIBs is poor given the low cross-plane thermal conductivity ($k_{\perp}$) ranging from 0.15 W/m-K to 1.63 W/m-K (see Table 3). Existing data for the $k_{\perp}$ of cells show large variations, which possibly results from cell-to-cell variations and discrepancies between various measurement methods. The effective $k_{\perp}$ is typically much lower than the calculated k of the five layers due to the high thermal contact resistance between the separator and electrodes. Similar to the k dependence of cathode materials reported by Richter *et al*., the k data of assembled cells (*i.e.*, pouch and cylindrical cells) demonstrated that cells based on LCO (1.19-1.63 W/m-K) cathodes had a higher k than those of NMC (0.48-0.88 W/m-K) and LFP (0.15-0.53 W/m-K) cathodes. Although graphite anode was used in all the cells for these measurements, it is insufficient to conclude that the cells of LCO cathodes have the highest k among the commercial cells given the complexity of thermal transport in LIBs and limited information provided in the measurements.

The in-plane thermal conductivity ($k_{||}$) is much higher than the low $k_{\perp}$ as the in-plane thermal transport is dominated by the high-k metal layers. From the literature, $k_{||}$ can be as high as 20 – 36.96 W/m-K [42–44,46–51,264,265]. However, the surface related to the cross-plane heat conduction is commonly used for heat dissipation due to its large area (see Fig. 1), which means $k_{\perp}$ largely impacts the temperature rise of LIBs. Non-negligible in-plane heat fluxes can affect the in-plane temperature uniformity of the cell, *e.g.*, the temperature difference between the center and edge [121,124,125,127]. In recent works by Offer *et al.*[9][93–97], large tabs were used to dissipate most heat along the in-plane direction, which reduced the cross-plane temperature difference by reducing the heat flow across the cell.

Table 3

A summary of the thermal conductivity of electrode stack, jelly roll, and assembled cells.

Authors	Cell geometry	Electrodes	$k_{\parallel}$(W/m-K)	$k_{\perp}$(W/m-K)
Maleki *et al.* [42]	electrode stack	C/LCO	20 - 28	3.39 – 3.40
Maleki *et al.* [45]	pouch	C/LCO	32.31 – 36.96	1.19 – 1.63
Werner *et al.* [47]	jelly roll	C/LCO	24	1.4
Zhang *et al.* [44]	electrode stack	C/NMC	21	0.48
Sheng *et al.* [264]	pouch	C/NMC	-	0.66
Steinhardt *et al.* [265]	pouch	C/NMC	26.5 ± 1.6	0.878 ± 0.51
Fleckenstein *et al.* [48]	jelly roll	C/LFP	-	0.35
Drake *et al.* [43]	18650	C/LFP	30.4 ± 1.5	0.20 ± 0.01
	26650	C/LFP	32.0±1.6	0.15 ± 0.01
Bazinski *et al.* [50]	pouch	C/LFP	-	0.35 – 0.44
Bazinski *et al.* [46]	pouch	C/LFP	28.9 – 35.1	-
Sheng *et al.* [264]	pouch	C/LFP	-	0.53
Murashko *et al.* [49]	pouch	LTO/LMO	-	0.594 – 0.735

4.4. *Heat transfer enhancement inside LIBs*

Besides thermal management outside batteries, it is important to enhance heat transport inside the cell, especially as the cell is getting thicker for higher energy density and charged faster with more heat generation. To improve the thermal transport properties, we need to know the contribution of each component to the total thermal resistance. Considering the five layers in a unit cell, the thermal resistance of current collectors with high k is negligible, while that of cathode, anode, separator, and interfaces can vary with the k of the medium and cycling conditions. As an example calculation of the thermal resistance contribution by each component, we use the thermal transport properties of electrodes and interfaces by Lubner *et al.* [58] and the k of separator in Ref [55]. Fig. 15 shows the thermal resistance contribution to the total thermal resistance by the electrodes, separator, and interfaces in an example unit cell (70 μm graphite anode, 26 μm separator, and 70 μm NMC cathode). Adding electrolyte decreases the thermal resistance of the electrodes, separator, and interfaces by ~70%, ~58%, and ~51%, respectively. For the fresh unit cell with electrolyte, the thermal resistance of the electrodes, separator, and interfaces accounts for 34.9%, 27.3%, and 37.8%, respectively. After formation cycling, the total thermal resistance increases by ~60% compared to that of the fresh unit cell with electrolyte due to the increase of TCR. Specifically, the relative thermal resistance contribution by the electrodes, separator, and interfaces changes to 21.9%, 17.1%, and 61.0%, respectively. Based on this analysis, we can evaluate the improvement of the total thermal resistance by the k enhancement of each component. As the TCR dominates the total thermal resistance of a unit cell, a significant enhancement of thermal transport inside batteries relies on minimizing the TCR. Only a few related works can be found in the literature. Yang *et al*. reported a hierarchical separator with a high k ~1 W/m-K [11], which reduced the total thermal resistance by 13.7%. As a comparison, the surface treatment by Vishwakarma *et al.* decreased the TCR in a dry stack by 78.6%, and thus reduced the total thermal resistance by 47.9% [12]. In addition, the TCR model by Lubner *et al.* predicted that the TCR in a wet stack can be reduced by using a high-k electrolyte [58]. Considering the dominance of TCR, it is reasonable

to expect more works on improving the thermal interfaces inside batteries accompanied with the development of LIBs with high energy density and charge rate.

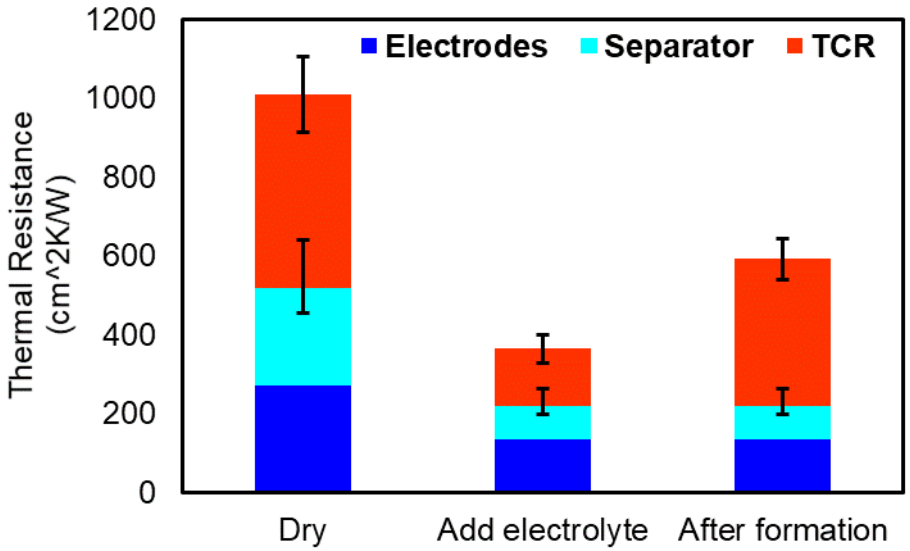

Fig. 15. Thermal resistance contribution by the electrodes, separator, and interfaces for a unit cell without electrolyte, with electrolyte, and after formation cycle.

5. Thermal management strategies

Battery thermal management (BTM) is critical for the operation of LIBs. Maintaining the optimal temperature depends on regulating external heating/cooling power and thermal conditions. Refs [5,8,26,31,86,96,266] have a systematical review of various heating and cooling methods in BTMSs. However, as discussed in Section 2, the increase of battery energy density and charge rate affects the optimal temperature and the temperature uniformity. As a result, the need of BTMSs can change as the optimal thermal conditions vary with the high energy density and charge rate. Here, we summarize and discuss recent works on thermal management of LIBs towards high energy density, XFC, and all-climate applications.

First, we discuss the need of battery thermal management for XFC based on recent works. Extremely high cooling need was identified as a thermal challenge for XFC in prior works [5,86,96]. Note that in those calculations the target charge temperature is around room temperature. As discussed in Section 2.2, the optimal temperature for XFC can shift to a temperature higher than room temperature. With an increased charge temperature, the heat generation rate reduces due to the decreased cell resistance. Further, the larger temperature difference between the battery and ambient enables more efficient heat dissipation. Thus, maintaining an increased charge temperature can dramatically reduce the cooling need during XFC. A recent work by Yang *et al.* demonstrated that no extra cooling power is needed for charging batteries at a 6C rate around 60 °C [92]. Instead of cooling the battery, the optimal thermal conditions for 6C charge described in their work consist of preheating the battery to 60 °C and maintaining the battery temperature at 60 °C. An innovative self-heating battery (see Fig. 16a), developed by Wang *et al.* [91], was used for rapid heating of the battery, *e.g.*, heating the battery from room temperature to 60 °C in 30 secs. Maintaining the high temperature during fast charging required extra thermal insulation. As a comparison, the same type of cell was charged at 6C at lower temperatures and with different levels of cooling. They found that the cycle life degraded when the battery was charged at lower temperatures with different levels of cooling (see Fig. 16b). From their study, extra heating power and thermal insulation, rather than cooling, is beneficial for XFC. The essential requirements of battery thermal management change because of the increased optimal battery temperature at XFC.

XFC at an elevated temperature requires extra heating power and /or thermal insulation, which is a matter of concern to BTM. For rapid and energy-efficient preheating, battery internal heating requiring a modification of the battery structure may be needed [91]. Further, the thermal isolation used for XFC makes cooling the battery extremely difficult, which can degrade the performance of batteries at slow and moderate charge rates and fast discharge rates. It is well known that appropriate cooling greatly extends the battery life in those conditions. Besides, it is unclear how the elevated temperature during XFC affects discharging and cycle life, especially for a prompt battery operation after XFC. Extra cooling power may be needed to cool the battery from the high charging temperature, which should be considered in the energy and cost analysis. As for the thermal safety and reliability of XFC at a high temperature like 60 °C, more experimental verifications are needed before a conclusion can be made. As discussed in Section 2.2.2, recent works demonstrated that thick SEI layers formed at high temperatures do not decrease the battery thermal safety, while plated lithium can lead to an earlier thermal runaway of cells [18,39,41,84,87–89].

In addition, all-climate applications of LIBs complicate thermal management of batteries. The role of battery heat generation can be different at various ambient temperatures, *i.e.*, whether the generated heat should be retained or dissipated to regulate the battery temperature. In general, battery heat needs to be efficiently removed to avoid overheating in hot climates, while in cold weathers the heat should be retained for elevating the battery temperature. That motivates a thermal functionality regulating the thermal boundary conditions, *i.e.*, thermal conduction at high temperatures and thermal isolation at low temperatures. Adjusting the pumping power in liquid cooling systems can somewhat change the thermal conditions. Further, Hao *et al.* designed a solid passive thermal switch to regulate the thermal conditions of LIBs according to the battery temperature (see Fig. 16c) [33]. The battery was thermally isolated from the heat sink when the battery temperature was below 15 °C. The battery heat was able to greatly elevate the battery temperature and improve the discharge performance in cold weathers (see Fig. 16d). On the other hand, the regulator was turned on as the battery temperature reached above ~30 °C, and thus extra battery heat can be efficiently removed to avoid overheating (see Fig. 16e). Without extra power and logic control, such a simple passive thermal management enabled regulating the temperature rise due to battery heat for the optimal discharge performance. However, its impact on charge performance, especially XFC, has not been investigated. Unlike discharge, existing studies demonstrated that the optimal charge temperature can vary with the charge rate, *e.g.*, 60 °C and thermal insulation was advantageous to a 6C charge. As the optimal thermal conditions vary with charge rate and energy density, smart logic control based on the ambient temperature and charge rate may be needed for the next generation BTMSs. In addition to regulating the thermal boundary conditions, Wang *et al.* proposed a self-heating battery with embedded nickel foils inside the battery as internal heaters, which enabled a rapid preheating of the battery and thus an improved cycling performance at 0 °C [91,267]. Heating inside LIBs with embedded heaters is advantageous over other heating approaches for the high heating efficiency, but the battery structure has to be modified.

Besides the temperature rise, the temperature uniformity inside a battery becomes an important issue as the heat generation rate of batteries and the power of external heating or cooling increases. As discussed in Section 2, increasing the power of heating or cooling outside batteries speeds up the process towards the target temperature, but with a larger temperature gradient. In an extreme case for the coin cell with graphite anode at 0 °C and NMC cathode at 40 °C, the temperature gradient caused an early failure due to lithium plating [268]. For cylindrical and pouch cells, surface cooling can dissipate heat along the cross-plane direction and reduce the temperature rise. Accordingly, a non-negligible temperature gradient develops across the cell given the low cross-plane k. Recently, Offer *et al*. proposed a tab cooling method, *i.e.*, using cell tabs to remove battery heat [9,93–97]. Removing heat through the tabs cooled the battery evenly and decreased the cross-plane temperature gradient as tabs were connected to each current collector with a high k. However, tab cooling typically led to a higher temperature rise than surface cooling since the cross-section area of tabs is much smaller than the battery surface area. Hunt *et al.* investigated the impact of tab and surface cooling on the lifetime of the cells with large tabs at two ends [9]. For this certain type of cell, despite the slightly higher temperature rise with tab cooling, their study demonstrated that tab cooling extended the lifetime of the battery by 3 times compared to surface cooling. But for most commercial pouch cells, tabs are too small and thin and not well distributed

for heat dissipation. As a result, the larger temperature rise in cells by tab cooling accelerates aging due to severe side reactions at high temperatures, which dominates over the aging due to non-uniform SOCs in electrodes associated with non-uniform temperature distributions. A recent work by Dondelewski *et al*. verified that surface cooling was advantageous over tab cooling for the long cycle life of common commercial pouch cells [97].

Therefore, an ideal BTMS should be able to maintain the battery temperature near the optimal temperature and with a uniform temperature distribution inside the cell. Rapid external heating/cooling typically leads to a large temperature gradient across the cell. The heating efficiency and temperature uniformity can be improved by embedding multiple heaters in the cell, but that requires a modification of the battery structure. Direct self-heating of the battery itself can provide the most uniform heating, but that requires temporarily creating thermally insulating boundary conditions. Thus, future BTMSs should be able to dynamically adjust both the heating/cooling power and thermal boundary condition in order to maintain the battery in the optimal thermal condition.

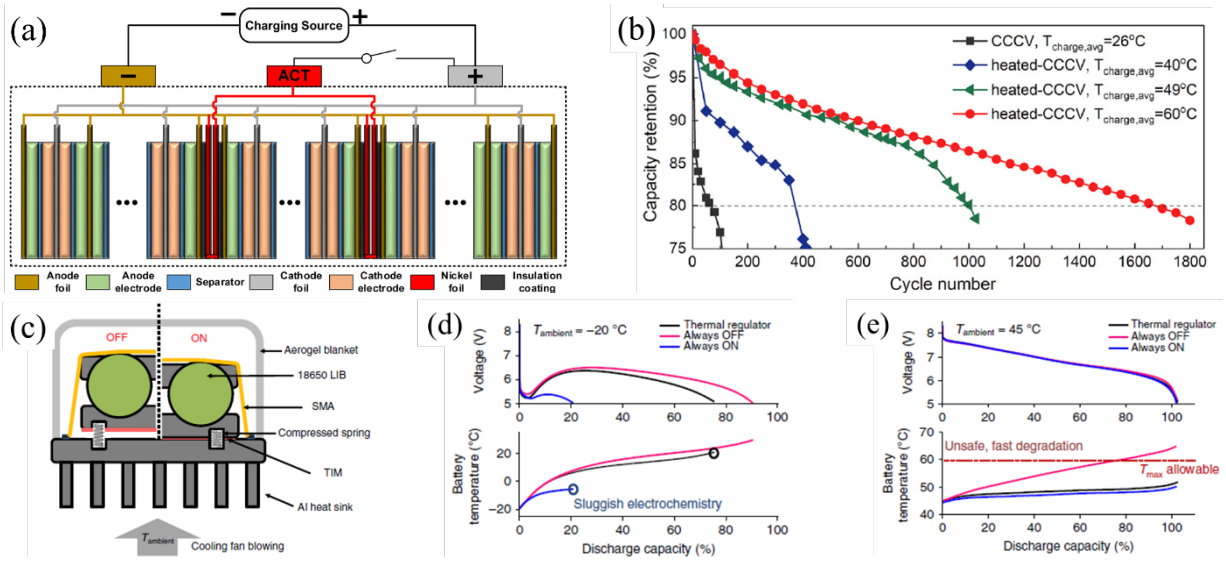

Fig. 16. (a) Schematic of the self-heating battery; (b) Capacity retention *vs.* cycle for 6C charge tests at different temperatures; (c) Schematic of the passive thermal regulator for LIBs; Battery discharge performance at (d) low and (e) high temperatures. Panels reproduced from: (a) and (b) Ref [92], Cell Press; (c-e) Ref [33], Springer Nature Ltd.

6. Conclusion and prospect

In summary, resolving battery thermal challenges requires understanding and regulating thermal phenomena inside and outside batteries. With the development of LIBs towards high energy density and fast charging, thermal issues inside the cell need to be addressed given the increased heat generation and the poor thermal transport inside the battery. In this review, we first discuss the optimal temperature for batteries as the energy density and charge rate increases. Contrary to the traditional wisdom that batteries should operate around room temperature, existing studies support that the optimal charge temperature increases as the battery's energy density and charge rate increase. This results from the competition between the two main aging mechanisms, *i.e.*, SEI formation and lithium plating. Knowing the battery temperature and the optimal temperature can provide guidance for BTMSs, *i.e.*, heating or cooling the battery when the battery temperature is lower or higher than the optimal temperature, respectively. Future BTMSs should be responsive to both the ambient temperature and operating conditions like charge rate.

The different sources of heat generation inside the battery are reviewed in detail. The heat of mixing due to lithium-ion diffusion in electrode particles increases with the charge rate and contributes significantly at higher C rates. From the understanding of heat generation by various sources, different methods to minimize heat generation are summarized and proposed. Additionally, from modeling perspective, the need for a robust electrochemical-thermal heat generation model that eliminates the prevalent inconsistencies has been identified.

As the electrode and cell is made thicker for higher energy density and capacity, the poor thermal transport inside the battery needs to be improved to avoid undesirable internal temperature rises and temperature non-uniformity. Heat transfer in batteries can be enhanced by thermally engineering the components, *e.g.*, addition of Al_2O_3 nanoparticles and interface treatments. A quantitative analysis of the thermal resistance of each component reveals that the TCR between the electrodes and separator dominates the total thermal resistance of a unit cell. Thus, it is reasonable to expect more work on reducing the TCR in batteries in addition to improving the k of individual cell components.

Finally, a summary of the latest advancements in external thermal management such as different cooling approaches (tab and surface cooling), novel heating methods, and regulation of thermal boundary conditions are summarized and evaluated for XFC and all-climate applications. The optimal battery temperature depends on charge rate and energy density, and the role of battery-generated heat toward maintaining this optimal temperature (helping *vs.* hurting) depends on the ambient temperature and the optimal temperature. Therefore, ideal BTMSs should be able to dynamically adjust the power of heating/cooling as well as the thermal conductance between the battery and its heat sink, based on the charge rate, battery temperature, and the optimal temperature. This motivates the development of smart BTMSs to go along with the development of LIBs with high energy densities, fast charging, and all-climate capabilities.

Declaration of Competing Interest

The authors declare that they have no known competing financial interests or personal relationships that could have appeared to influence the work reported in this paper.

Acknowledgement

This work was supported by Energy Efficiency and Renewable Energy, Vehicle Technologies Program, of the U.S. Department of Energy under Contract No. DEAC02-05CH11231.

References

[1] Z.P. Cano, D. Banham, S. Ye, A. Hintennach, J. Lu, M. Fowler, Z. Chen, Batteries and fuel cells for emerging electric vehicle markets, Nat. Energy. 3 (2018) 279–289. doi:10.1038/s41560-018-0108-1.

[2] B. Dunn, H. Kamath, J.M. Tarascon, Electrical energy storage for the grid: A battery of choices, Science (80-.). 334 (2011) 928–935. doi:10.1126/science.1212741.

[3] D. Howell, B. Cunningham, T. Duong, P. Faguy, Overview of the DOE VTO advanced battery R&D program, 2016. https://scholar.google.com/scholar_lookup?title=Overview of the DOE VTO Advanced Battery R%26D Pprogram&author=D. Howell&publication_year=June%2C 2016 (accessed October 2, 2020).

[4] S. Ahmed, I. Bloom, A.N. Jansen, T. Tanim, E.J. Dufek, A. Pesaran, A. Burnham, R.B. Carlson, F. Dias, K. Hardy, M. Keyser, C. Kreuzer, A. Markel, A. Meintz, C. Michelbacher, M. Mohanpurkar, P.A. Nelson, D.C. Robertson, D. Scoffield, M. Shirk, T. Stephens, R. Vijayagopal, J. Zhang, Enabling fast charging – A battery technology gap assessment, J. Power Sources. 367 (2017) 250–262. doi:10.1016/j.jpowsour.2017.06.055.

[5] M. Keyser, A. Pesaran, Q. Li, S. Santhanagopalan, K. Smith, E. Wood, S. Ahmed, I. Bloom, E. Dufek, M. Shirk, A. Meintz, C. Kreuzer, C. Michelbacher, A. Burnham, T. Stephens, J. Francfort, B. Carlson, J. Zhang, R. Vijayagopal, K. Hardy, F. Dias, M. Mohanpurkar, D. Scoffield, A.N. Jansen, T. Tanim, A. Markel, Enabling fast charging – Battery thermal considerations, J. Power Sources. 367 (2017) 228–236. doi:10.1016/j.jpowsour.2017.07.009.

[6] Q. Zhang, W. Cai, Y.X. Yao, G.L. Zhu, C. Yan, L.L. Jiang, C. He, J.Q. Huang, A review on energy chemistry of fast-charging anodes, Chem. Soc. Rev. 49 (2020) 3806–3833. doi:10.1039/c9cs00728h.

[7] R. Mathieu, O. Briat, P. Gyan, J.M. Vinassa, Comparison of the impact of fast charging on the cycle life of three lithium-ion cells under several parameters of charge protocol and temperatures, Appl. Energy. 283 (2021) 116344. doi:10.1016/j.apenergy.2020.116344.

[8] L. Ianniciello, P.H. Biwolé, P. Achard, Electric vehicles batteries thermal management systems employing phase change materials, J. Power Sources. 378 (2018) 383–403. doi:10.1016/j.jpowsour.2017.12.071.

[9] I.A. Hunt, Y. Zhao, Y. Patel, J. Offer, Surface Cooling Causes Accelerated Degradation Compared to Tab Cooling for Lithium-Ion Pouch Cells, J. Electrochem. Soc. 163 (2016) A1846–A1852. doi:10.1149/2.0361609jes.

[10] L. Song, Y. Chen, J.W. Evans, Measurements of the Thermal Conductivity of Poly (ethylene oxide) − Lithium Salt Electrolytes Measurements of the Thermal Conductivity of Poly (ethylene oxide) -Lithium Salt Electrolytes, 144 (1997) 3797–3800. doi:10.1149/1.1838094.

[11] Y. Yang, X. Huang, Z. Cao, G. Chen, Thermally conductive separator with hierarchical nano/microstructures for improving thermal management of batteries, Nano Energy. 22 (2016) 301–309. doi:10.1016/j.nanoen.2016.01.026.

[12] V. Vishwakarma, C. Waghela, Z. Wei, R. Prasher, S.C. Nagpure, J. Li, F. Liu, C. Daniel, A. Jain, Heat transfer enhancement in a lithium-ion cell through improved material-level thermal transport, J. Power Sources. 300 (2015) 123–131. doi:10.1016/j.jpowsour.2015.09.028.

[13] J. Vetter, P. Novák, M.R. Wagner, C. Veit, K.C. Möller, J.O. Besenhard, M. Winter, M. Wohlfahrt-Mehrens, C. Vogler, A. Hammouche, Ageing mechanisms in lithium-ion batteries, J. Power Sources. 147 (2005) 269–281. doi:10.1016/j.jpowsour.2005.01.006.

[14] A. Barré, B. Deguilhem, S. Grolleau, M. Gérard, F. Suard, D. Riu, A review on lithium-ion battery ageing mechanisms and estimations for automotive applications, J. Power Sources. 241 (2013) 680–689. doi:10.1016/j.jpowsour.2013.05.040.

[15] T. Waldmann, M. Wilka, M. Kasper, M. Fleischhammer, M. Wohlfahrt-Mehrens, Temperature dependent ageing mechanisms in Lithium-ion batteries - A Post-Mortem study, J. Power Sources. 262 (2014) 129–135. doi:10.1016/j.jpowsour.2014.03.112.

[16] M.-T.F. Rodrigues, G. Babu, H. Gullapalli, K. Kalaga, F.N. Sayed, K. Kato, J. Joyner, P.M. Ajayan, A materials perspective on Li-ion batteries at extreme temperatures, Nat. Energy. 2 (2017). doi:10.1038/nenergy.2017.108.

[17] B. Rieger, S.F. Schuster, S. V. Erhard, P.J. Osswald, A. Rheinfeld, C. Willmann, A. Jossen, Multi-directional laser scanning as innovative method to detect local cell damage during fast charging of lithium-ion cells, J. Energy Storage. 8 (2016) 1–5. doi:10.1016/j.est.2016.09.002.

[18] T. Waldmann, J.B. Quinn, K. Richter, M. Kasper, A. Tost, A. Klein, M. Wohlfahrt-Mehrens, Electrochemical, Post-Mortem, and ARC Analysis of Li-Ion Cell Safety in Second-Life Applications, J. Electrochem. Soc. 164 (2017) A3154–A3162. doi:10.1149/2.0961713jes.

[19] W. Diao, S. Saxena, M. Pecht, Accelerated cycle life testing and capacity degradation modeling of LiCoO2-graphite cells, J. Power Sources. 435 (2019) 226830. doi:10.1016/j.jpowsour.2019.226830.

[20] P. Ramadass, B. Haran, R. White, B.N. Popov, Capacity fade of Sony 18650 cells cycled at elevated temperatures: Part I. Cycling performance, J. Power Sources. 112 (2002) 606–613. doi:10.1016/S0378-7753(02)00474-3.

[21] J. Shim, R. Kostecki, T. Richardson, X. Song, K.A. Striebel, Electrochemical analysis for cycle performance and capacity fading of a lithium-ion battery cycled at elevated temperature, J. Power Sources. 112 (2002) 222–230. doi:10.1016/S0378-7753(02)00363-

4.

[22] M. Dubarry, B.Y. Liaw, M.S. Chen, S.S. Chyan, K.C. Han, W.T. Sie, S.H. Wu, Identifying battery aging mechanisms in large format Li ion cells, J. Power Sources. 196 (2011) 3420–3425. doi:10.1016/j.jpowsour.2010.07.029.

[23] F. Leng, C.M. Tan, M. Pecht, Effect of Temperature on the Aging rate of Li Ion Battery Operating above Room Temperature, Sci. Rep. 5 (2015) 1–12. doi:10.1038/srep12967.

[24] J. Sturm, F.B. Spingler, B. Rieger, A. Rheinfeld, A. Jossen, Non-Destructive Detection of Local Aging in Lithium-Ion Pouch Cells by Multi-Directional Laser Scanning, J. Electrochem. Soc. 164 (2017) A1342–A1351. doi:10.1149/2.0161707jes.

[25] T. Matsuda, K. Ando, M. Myojin, M. Matsumoto, T. Sanada, N. Takao, H. Imai, D. Imamura, Investigation of the influence of temperature on the degradation mechanism of commercial nickel manganese cobalt oxide-type lithium-ion cells during long-term cycle tests, J. Energy Storage. 21 (2019) 665–671. doi:10.1016/j.est.2019.01.009.

[26] H. Liu, Z. Wei, W. He, J. Zhao, Thermal issues about Li-ion batteries and recent progress in battery thermal management systems: A review, Energy Convers. Manag. 150 (2017) 304–330. doi:10.1016/j.enconman.2017.08.016.

[27] S. Ma, M. Jiang, P. Tao, C. Song, J. Wu, J. Wang, T. Deng, W. Shang, Temperature effect and thermal impact in lithium-ion batteries: A review, Prog. Nat. Sci. Mater. Int. 28 (2018) 653–666. doi:10.1016/j.pnsc.2018.11.002.

[28] X. Han, L. Lu, Y. Zheng, X. Feng, Z. Li, J. Li, M. Ouyang, A review on the key issues of the lithium ion battery degradation among the whole life cycle, ETransportation. 1 (2019) 100005. doi:10.1016/j.etran.2019.100005.

[29] S. Yang, C. Ling, Y. Fan, Y. Yang, X. Tan, H. Dong, A review of lithium-ion battery thermal management system strategies and the evaluate criteria, Int. J. Electrochem. Sci. 14 (2019) 6077–6107. doi:10.20964/2019.07.06.

[30] T. Liu, X.G. Yang, S. Ge, Y. Leng, C.Y. Wang, Ultrafast charging of energy-dense lithium-ion batteries for urban air mobility, ETransportation. 7 (2021) 100103. doi:10.1016/j.etran.2021.100103.

[31] Y. Ji, C.Y. Wang, Heating strategies for Li-ion batteries operated from subzero temperatures, Electrochim. Acta. 107 (2013) 664–674. doi:10.1016/j.electacta.2013.03.147.

[32] Y. Ji, Y. Zhang, C.-Y. Wang, Li-Ion Cell Operation at Low Temperatures, J. Electrochem. Soc. 160 (2013) A636–A649. doi:10.1149/2.047304jes.

[33] M. Hao, J. Li, S. Park, S. Moura, C. Dames, Efficient thermal management of Li-ion batteries with a passive interfacial thermal regulator based on a shape memory alloy, Nat. Energy. 3 (2018) 899–906. doi:10.1038/s41560-018-0243-8.

[34] S. Mohan, J.B. Siegel, A.G. Stefanopoulou, R. Vasudevan, An Energy-Optimal Warm-Up Strategy for Li-Ion Batteries and Its Approximations, IEEE Trans. Control Syst. Technol. 27 (2019) 1165–1180. doi:10.1109/TCST.2017.2785833.

[35] H. Ruan, J. Jiang, B. Sun, X. Su, X. He, K. Zhao, An optimal internal-heating strategy for lithium-ion batteries at low temperature considering both heating time and lifetime reduction, Appl. Energy. 256 (2019) 113797. doi:10.1016/j.apenergy.2019.113797.

[36] A. Mistry, A. Verma, P.P. Mukherjee, Controllable Electrode Stochasticity Self-Heats Lithium-Ion Batteries at Low Temperatures, ACS Appl. Mater. Interfaces. 11 (2019) 26764–26769. doi:10.1021/acsami.9b05468.

[37] C. Vidal, O. Gross, R. Gu, P. Kollmeyer, A. Emadi, XEV Li-Ion Battery Low-Temperature Effects-Review, IEEE Trans. Veh. Technol. 68 (2019) 4560–4572. doi:10.1109/TVT.2019.2906487.

[38] N.E. Galushkin, N.N. Yazvinskaya, D.N. Galushkin, Mechanism of Thermal Runaway in Lithium-Ion Cells, J. Electrochem. Soc. 165 (2018) A1303–A1308. doi:10.1149/2.0611807jes.

[39] X. Feng, M. Ouyang, X. Liu, L. Lu, Y. Xia, X. He, Thermal runaway mechanism of lithium ion battery for electric vehicles: A review, Energy Storage Mater. 10 (2018) 246–267. doi:10.1016/j.ensm.2017.05.013.

[40] X. Liu, D. Ren, H. Hsu, X. Feng, G.L. Xu, M. Zhuang, H. Gao, L. Lu, X. Han, Z. Chu, J. Li, X. He, K. Amine, M. Ouyang, Thermal Runaway of Lithium-Ion Batteries without Internal Short Circuit, Joule. 2 (2018) 2047–2064. doi:10.1016/j.joule.2018.06.015.

[41] X. Feng, D. Ren, X. He, M. Ouyang, Mitigating Thermal Runaway of Lithium-Ion Batteries, Joule. 4 (2020) 743–770. doi:10.1016/j.joule.2020.02.010.

[42] H. Maleki, S. Al Hallaj, J.R. Selman, R.B. Dinwiddie, H. Wang, Thermal Properties of Lithium-Ion Battery and Components, J. Electrochem. Soc. 146 (1999) 947–954. doi:10.1149/1.1391704.

[43] S.J. Drake, D.A. Wetz, J.K. Ostanek, S.P. Miller, J.M. Heinzel, A. Jain, Measurement of anisotropic thermophysical properties of cylindrical Li-ion cells, J. Power Sources. 252 (2014) 298–304. doi:10.1016/j.jpowsour.2013.11.107.

[44] J. Zhang, B. Wu, Z. Li, J. Huang, Simultaneous estimation of thermal parameters for large-format laminated lithium-ion batteries, J. Power Sources. 259 (2014) 106–116. doi:10.1016/j.jpowsour.2014.02.079.

[45] H. Maleki, H. Wang, W. Porter, J. Hallmark, Li-Ion polymer cells thermal property changes as a function of cycle-life, J. Power Sources. 263 (2014) 223–230. doi:10.1016/j.jpowsour.2014.04.033.

[46] S.J. Bazinski, X. Wang, B.P. Sangeorzan, L. Guessous, Measuring and assessing the effective in-plane thermal conductivity of lithium iron phosphate pouch cells, Energy. 114 (2016) 1085–1092. doi:10.1016/j.energy.2016.08.087.

[47] D. Werner, A. Loges, D.J. Becker, T. Wetzel, Thermal conductivity of Li-ion batteries and their electrode configurations – A novel combination of modelling and experimental approach, J. Power Sources. 364 (2017) 72–83. doi:10.1016/j.jpowsour.2017.07.105.

[48] M. Fleckenstein, S. Fischer, O. Bohlen, B. Bäker, Thermal Impedance Spectroscopy - A

method for the thermal characterization of high power battery cells, J. Power Sources. 223 (2013) 259–267. doi:10.1016/j.jpowsour.2012.07.144.

[49] K.A. Murashko, A. V. Mityakov, J. Pyrhönen, V.Y. Mityakov, S.S. Sapozhnikov, Thermal parameters determination of battery cells by local heat flux measurements, J. Power Sources. 271 (2014) 48–54. doi:10.1016/j.jpowsour.2014.07.117.

[50] S.J. Bazinski, X. Wang, Experimental study on the influence of temperature and state-of-charge on the thermophysical properties of an LFP pouch cell, J. Power Sources. 293 (2015) 283–291. doi:10.1016/j.jpowsour.2015.05.084.

[51] H. Maleki, J.R. Selman, R.B. Dinwiddie, H. Wang, High thermal conductivity negative electrode material for lithium-ion batteries, J. Power Sources. 94 (2001) 26–35. doi:10.1016/S0378-7753(00)00661-3.

[52] M. Khandelwal, M.M. Mench, Direct measurement of through-plane thermal conductivity and contact resistance in fuel cell materials, J. Power Sources. 161 (2006) 1106–1115. doi:10.1016/j.jpowsour.2006.06.092.

[53] T.M. Bandhauer, S. Garimella, T.F. Fuller, A Critical Review of Thermal Issues in Lithium-Ion Batteries, J. Electrochem. Soc. 158 (2011) R1. doi:10.1149/1.3515880.

[54] F. Richter, P.J.S. Vie, S. Kjelstrup, O.S. Burheim, Measurements of ageing and thermal conductivity in a secondary NMC-hard carbon Li-ion battery and the impact on internal temperature profiles, Electrochim. Acta. 250 (2017) 228–237. doi:10.1016/j.electacta.2017.07.173.

[55] F. Richter, S. Kjelstrup, P.J.S. Vie, O.S. Burheim, Thermal conductivity and internal temperature profiles of Li-ion secondary batteries, J. Power Sources. 359 (2017) 592–600. doi:10.1016/j.jpowsour.2017.05.045.

[56] A. Gaitonde, A. Nimmagadda, A. Marconnet, Measurement of interfacial thermal conductance in Lithium ion batteries, J. Power Sources. 343 (2017) 431–436. doi:10.1016/j.jpowsour.2017.01.019.

[57] R. Ponnappan, T.S. Ravigururajan, Contact thermal resistance of Li-ion cell electrode stack, J. Power Sources. 129 (2004) 7–13. doi:10.1016/j.jpowsour.2003.11.006.

[58] S.D. Lubner, S. Kaur, Y. Fu, V. Battaglia, R.S. Prasher, Identification and characterization of the dominant thermal resistance in lithium-ion batteries using operando 3-omega sensors, J. Appl. Phys. 127 (2020) 105104. doi:10.1063/1.5134459.

[59] C.-F. Chen, A. Verma, P.P. Mukherjee, Probing the Role of Electrode Microstructure in the Lithium-Ion Battery Thermal Behavior, J. Electrochem. Soc. 164 (2017) E3146–E3158. doi:10.1149/2.0161711jes.

[60] N. Damay, C. Forgez, M.P. Bichat, G. Friedrich, Thermal modeling of large prismatic LiFePO4/graphite battery. Coupled thermal and heat generation models for characterization and simulation, J. Power Sources. 283 (2015) 37–45. doi:10.1016/j.jpowsour.2015.02.091.

[61] J.C. Zhao, S.H. Liu, J.F. Zhang, Personalized distance learning system based on sequence

analysis algorithm, Int. J. Online Eng. 11 (2015) 33–36. doi:10.3991/ijoe.v11i7.4764.

[62] W.B. Gu, C.Y. Wang, Thermal-Electrochemical Modeling of Battery Systems, J. Electrochem. Soc. 147 (2000) 2910. doi:10.1149/1.1393625.

[63] D. Bernardi, E. Pawlikowski, J. Newman, A General Energy Balance for Battery Systems, J. Electrochem. Soc. 132 (1985) 5–12.

[64] M. Farag, H. Sweity, M. Fleckenstein, S. Habibi, Combined electrochemical, heat generation, and thermal model for large prismatic lithium-ion batteries in real-time applications, J. Power Sources. 360 (2017) 618–633. doi:10.1016/j.jpowsour.2017.06.031.

[65] C. Forgez, D. Vinh Do, G. Friedrich, M. Morcrette, C. Delacourt, Thermal modeling of a cylindrical LiFePO4/graphite lithium-ion battery, J. Power Sources. 195 (2010) 2961–2968. doi:10.1016/j.jpowsour.2009.10.105.

[66] X. Lin, H.E. Perez, S. Mohan, J.B. Siegel, A.G. Stefanopoulou, Y. Ding, M.P. Castanier, A lumped-parameter electro-thermal model for cylindrical batteries, J. Power Sources. 257 (2014) 12–20. doi:10.1016/j.jpowsour.2014.01.097.

[67] U.S. Kim, J. Yi, C.B. Shin, T. Han, S. Park, Modelling the thermal behaviour of a lithium-ion battery during charge, J. Power Sources. 196 (2011) 5115–5121. doi:10.1016/j.jpowsour.2011.01.103.

[68] G.H. Kim, A. Pesaran, R. Spotnitz, A three-dimensional thermal abuse model for lithium-ion cells, J. Power Sources. 170 (2007) 476–489. doi:10.1016/j.jpowsour.2007.04.018.

[69] P.M. Attia, W.C. Chueh, S.J. Harris, Revisiting the t 0.5 Dependence of SEI Growth , J. Electrochem. Soc. 167 (2020) 090535. doi:10.1149/1945-7111/ab8ce4.

[70] A. Wang, S. Kadam, H. Li, S. Shi, Y. Qi, Review on modeling of the anode solid electrolyte interphase (SEI) for lithium-ion batteries, Npj Comput. Mater. 4 (2018). doi:10.1038/s41524-018-0064-0.

[71] M. Schimpe, M.E. von Kuepach, M. Naumann, H.C. Hesse, K. Smith, A. Jossen, Comprehensive Modeling of Temperature-Dependent Degradation Mechanisms in Lithium Iron Phosphate Batteries, J. Electrochem. Soc. 165 (2018) A181–A193. doi:10.1149/2.1181714jes.

[72] L. Liu, J. Park, X. Lin, A.M. Sastry, W. Lu, A thermal-electrochemical model that gives spatial-dependent growth of solid electrolyte interphase in a Li-ion battery, J. Power Sources. 268 (2014) 482–490. doi:10.1016/j.jpowsour.2014.06.050.

[73] M.B. Pinson, M.Z. Bazant, M.B. Pinsona, M.Z. Bazant, Theory of SEI Formation in Rechargeable Batteries: Capacity Fade, Accelerated Aging and Lifetime Prediction, J. Electrochem. Soc. 160 (2013) A243–A250. doi:10.1149/2.044302jes.

[74] X.G. Yang, C.Y. Wang, Understanding the trilemma of fast charging, energy density and cycle life of lithium-ion batteries, J. Power Sources. 402 (2018) 489–498. doi:10.1016/j.jpowsour.2018.09.069.

[75] Y. Yin, S.Y. Choe, Actively temperature controlled health-aware fast charging method for

lithium-ion battery using nonlinear model predictive control, Appl. Energy. 271 (2020). doi:10.1016/j.apenergy.2020.115232.

[76] T. Wu, Z. Zhao, J. Zhang, C. Zhang, Y. Guo, Y. Cao, S. Pan, Y. Liu, P. Liu, Y. Ge, W. Liu, L. Dong, H. Lu, Thick electrode with thickness-independent capacity enabled by assembled two-dimensional porous nanosheets, Energy Storage Mater. 36 (2021) 265–271. doi:10.1016/j.ensm.2020.12.034.

[77] C. Zhang, L. Dong, N. Zheng, H. Zhu, C. Wu, F. Zhao, W. Liu, Aligned graphene array anodes with dendrite-free behavior for high-performance Li-ion batteries, Energy Storage Mater. 37 (2021) 296–305. doi:10.1016/j.ensm.2021.02.014.

[78] Y. Zhu, Z. Ju, X. Zhang, D.M. Lutz, L.M. Housel, Y. Zhou, K.J. Takeuchi, E.S. Takeuchi, A.C. Marschilok, G. Yu, Evaporation-Induced Vertical Alignment Enabling Directional Ion Transport in a 2D-Nanosheet-Based Battery Electrode, Adv. Mater. 32 (2020) 1–7. doi:10.1002/adma.201907941.

[79] J. Landesfeind, J. Hattendorff, A. Ehrl, W.A. Wall, H.A. Gasteiger, Tortuosity Determination of Battery Electrodes and Separators by Impedance Spectroscopy, J. Electrochem. Soc. 163 (2016) A1373–A1387. doi:10.1149/2.1141607jes.

[80] S. Malifarge, B. Delobel, C. Delacourt, Experimental and Modeling Analysis of Graphite Electrodes with Various Thicknesses and Porosities for High-Energy-Density Li-Ion Batteries, J. Electrochem. Soc. 165 (2018) A1275–A1287. doi:10.1149/2.0301807jes.

[81] Z. Du, D.L. Wood, C. Daniel, S. Kalnaus, J. Li, Understanding limiting factors in thick electrode performance as applied to high energy density Li-ion batteries, J. Appl. Electrochem. 47 (2017) 405–415. doi:10.1007/s10800-017-1047-4.

[82] K.G. Gallagher, S.E. Trask, C. Bauer, T. Woehrle, S.F. Lux, M. Tschech, P. Lamp, B.J. Polzin, S. Ha, B. Long, Q. Wu, W. Lu, D.W. Dees, A.N. Jansen, Optimizing Areal Capacities through Understanding the Limitations of Lithium-Ion Electrodes, J. Electrochem. Soc. 163 (2016) A138–A149. doi:10.1149/2.0321602jes.

[83] F.B. Spingler, W. Wittmann, J. Sturm, B. Rieger, A. Jossen, Optimum fast charging of lithium-ion pouch cells based on local volume expansion criteria, J. Power Sources. 393 (2018) 152–160. doi:10.1016/j.jpowsour.2018.04.095.

[84] A. Friesen, X. Mönnighoff, M. Börner, J. Haetge, F.M. Schappacher, M. Winter, Influence of temperature on the aging behavior of 18650-type lithium ion cells: A comprehensive approach combining electrochemical characterization and post-mortem analysis, J. Power Sources. 342 (2017) 88–97. doi:10.1016/j.jpowsour.2016.12.040.

[85] A. Tomaszewska, Z. Chu, X. Feng, S. O'Kane, X. Liu, J. Chen, C. Ji, E. Endler, R. Li, L. Liu, Y. Li, S. Zheng, S. Vetterlein, M. Gao, J. Du, M. Parkes, M. Ouyang, M. Marinescu, G. Offer, B. Wu, Lithium-ion battery fast charging: A review, ETransportation. 1 (2019) 100011. doi:10.1016/j.etran.2019.100011.

[86] Y. Liu, Y. Zhu, Y. Cui, Challenges and opportunities towards fast-charging battery materials, Nat. Energy. 4 (2019) 540–550. doi:10.1038/s41560-019-0405-3.

[87] M. Börner, A. Friesen, M. Grützke, Y.P. Stenzel, G. Brunklaus, J. Haetge, S. Nowak,

F.M. Schappacher, M. Winter, Correlation of aging and thermal stability of commercial 18650-type lithium ion batteries, J. Power Sources. 342 (2017) 382–392. doi:10.1016/j.jpowsour.2016.12.041.

[88] Y. Li, X. Feng, D. Ren, M. Ouyang, L. Lu, X. Han, Thermal Runaway Triggered by Plated Lithium on the Anode after Fast Charging, ACS Appl. Mater. Interfaces. 11 (2019) 46839–46850. doi:10.1021/acsami.9b16589.

[89] P. Lyu, X. Liu, J. Qu, J. Zhao, Y. Huo, Z. Qu, Z. Rao, Recent advances of thermal safety of lithium ion battery for energy storage, Elsevier B.V., 2020. doi:10.1016/j.ensm.2020.06.042.

[90] T. Matsuda, M. Myojin, K. Ando, D. Imamura, Degradation Analyses of Commercial Lithium-Ion Cells by Temperature/C-rate Controlled Cycle Test, ECS Trans. 64 (2015) 69–75. doi:10.1149/06422.0069ecst.

[91] C.Y. Wang, G. Zhang, S. Ge, T. Xu, Y. Ji, X.G. Yang, Y. Leng, Lithium-ion battery structure that self-heats at low temperatures, Nature. 529 (2016) 515–518. doi:10.1038/nature16502.

[92] X.G. Yang, T. Liu, Y. Gao, S. Ge, Y. Leng, D. Wang, C.Y. Wang, Asymmetric Temperature Modulation for Extreme Fast Charging of Lithium-Ion Batteries, Joule. 3 (2019) 3002–3019. doi:10.1016/j.joule.2019.09.021.

[93] Y. Zhao, Y. Patel, T. Zhang, G.J. Offer, Modeling the Effects of Thermal Gradients Induced by Tab and Surface Cooling on Lithium Ion Cell Performance, J. Electrochem. Soc. 165 (2018) A3169–A3178. doi:10.1149/2.0901813jes.

[94] A. Hales, L.B. Diaz, M.W. Marzook, Y. Zhao, Y. Patel, G. Offer, The Cell Cooling Coefficient: A Standard to Define Heat Rejection from Lithium-Ion Batteries, J. Electrochem. Soc. 166 (2019) A2383–A2395. doi:10.1149/2.0191912jes.

[95] A. Hales, M.W. Marzook, L. Bravo Diaz, Y. Patel, G. Offer, The Surface Cell Cooling Coefficient: A Standard to Define Heat Rejection from Lithium Ion Battery Pouch Cells, J. Electrochem. Soc. 167 (2020) 020524. doi:10.1149/1945-7111/ab6985.

[96] G. Offer, Y. Patel, A. Hales, L. Bravo Diaz, M. Marzook, Cool metric for lithium-ion batteries could spur progress, Nature. 582 (2020) 485–487. doi:10.1038/d41586-020-01813-8.

[97] O. Dondelewski, T. Szemberg O'Connor, Y. Zhao, I.A. Hunt, A. Holland, A. Hales, G.J. Offer, Y. Patel, The role of cell geometry when selecting tab or surface cooling to minimise cell degradation, ETransportation. 5 (2020) 100073. doi:10.1016/j.etran.2020.100073.

[98] L.H.J. Raijmakers, D.L. Danilov, R.-A. Eichel, P.H.L. Notten, A review on various temperature-indication methods for Li-ion batteries, Appl. Energy. 240 (2019) 918–945. doi:10.1016/j.apenergy.2019.02.078.

[99] L. Raijmakers, Sensorless Temperature Measurements for Advanced Battery Management Systems, Delft University of Technology Sensorless, 2018. doi:10.4233/uuid:73aa76cf-d38a-49b0-b363-3a7c5ab9dc9b.

[100] J.B. Robinson, P.R. Shearing, D.J.L. Brett, Thermal Imaging of Electrochemical Power Systems : A Review, J. Imaging. 2 (2016). doi:10.3390/jimaging2010002.

[101] P.M. Sarro, a. W. Van Herwaarden, Thermal sensors based on the seebeck effect, Sensors and Actuators. 10 (1986) 321–346.

[102] D. Chalise, K. Shah, T. Halama, L. Komsiyska, A. Jain, An experimentally validated method for temperature prediction during cyclic operation of a Li-ion cell, Int. J. Heat Mass Transf. 112 (2017) 89–96. doi:10.1016/j.ijheatmasstransfer.2017.04.115.

[103] H.E. Perez, X. Hu, S. Dey, S.J. Moura, Optimal Charging of Li-Ion Batteries with Coupled Electro-Thermal-Aging Dynamics, IEEE Trans. Veh. Technol. 66 (2017) 7761–7770. doi:10.1109/TVT.2017.2676044.

[104] T. Waldmann, M. Wohlfahrt-Mehrens, In-Operando measurement of temperature gradients in cylindrical lithium-ion cells during high-current discharge, ECS Electrochem. Lett. 4 (2015) A1–A3. doi:10.1149/2.0031501eel.

[105] R.R. Richardson, P.T. Ireland, D.A. Howey, Battery internal temperature estimation by combined impedance and surface temperature measurement, J. Power Sources. 265 (2014) 254–261. doi:10.1016/j.jpowsour.2014.04.129.

[106] M. Debert, G. Colin, G. Bloch, Y. Chamaillard, An observer looks at the cell temperature in automotive battery packs, Control Eng. Pract. 21 (2013) 1035–1042. doi:10.1016/j.conengprac.2013.03.001.

[107] J. Sun, G. Wei, L. Pei, R. Lu, K. Song, C. Wu, C. Zhu, Online internal temperature estimation for lithium-ion batteries based on Kalman filter, Energies. 8 (2015) 4400–4415. doi:10.3390/en8054400.

[108] M. Parhizi, M.B. Ahmed, A. Jain, Determination of the core temperature of a Li-ion cell during thermal runaway, J. Power Sources. 370 (2017) 27–35. doi:10.1016/j.jpowsour.2017.09.086.

[109] C. Heubner, M. Schneider, A. Michaelis, Detailed study of heat generation in porous LiCoO 2 electrodes, J. Power Sources. 307 (2016) 199–207. doi:10.1016/j.jpowsour.2015.12.096.

[110] C. Heubner, M. Schneider, C. Lämmel, A. Michaelis, Local heat generation in a single stack lithium ion battery cell, Electrochim. Acta. 186 (2015) 404–412. doi:10.1016/j.electacta.2015.10.182.

[111] Z. Li, J. Zhang, B. Wu, J. Huang, Z. Nie, Y. Sun, F. An, N. Wu, Examining temporal and spatial variations of internal temperature in large-format laminated battery with embedded thermocouples, J. Power Sources. 241 (2013) 536–553. doi:10.1016/j.jpowsour.2013.04.117.

[112] C. Heubner, M. Schneider, C. Lämmel, U. Langklotz, A. Michaelis, In-operando temperature measurement across the interfaces of a lithium-ion battery cell, Electrochim. Acta. 113 (2013) 730–734. doi:10.1016/j.electacta.2013.08.091.

[113] M. Nascimento, M.S. Ferreira, J.L. Pinto, Real time thermal monitoring of lithium

batteries with fiber sensors and thermocouples: A comparative study, Meas. J. Int. Meas. Confed. 111 (2017) 260–263. doi:10.1016/j.measurement.2017.07.049.

[114] R. Srinivasan, B.G. Carkhuff, M.H. Butler, A.C. Baisden, Instantaneous measurement of the internal temperature in lithium-ion rechargeable cells, Electrochim. Acta. 56 (2011) 6198–6204. doi:10.1016/j.electacta.2011.03.136.

[115] S. Novais, M. Nascimento, L. Grande, M.F. Domingues, P. Antunes, N. Alberto, C. Leitão, R. Oliveira, S. Koch, G.T. Kim, S. Passerini, J. Pinto, Internal and external temperature monitoring of a li-ion battery with fiber bragg grating sensors, Sensors (Switzerland). 16 (2016) 1–9. doi:10.3390/s16091394.

[116] J. Huang, L. Albero Blanquer, J. Bonefacino, E.R. Logan, D. Alves Dalla Corte, C. Delacourt, B.M. Gallant, S.T. Boles, J.R. Dahn, H.Y. Tam, J.M. Tarascon, Operando decoding of chemical and thermal events in commercial Na(Li)-ion cells via optical sensors, Nat. Energy. 5 (2020) 674–683. doi:10.1038/s41560-020-0665-y.

[117] M.S. Rad, D.L. Danilov, M. Baghalha, M. Kazemeini, P.H.L. Notten, Thermal Modeling of Cylindrical LiFePO4 Batteries, J. Mod. Phys. 04 (2013) 1–7. doi:10.4236/jmp.2013.47a2001.

[118] C.Y. Lee, S.J. Lee, M.S. Tang, P.C. Chen, In situ monitoring of temperature inside lithium-ion batteries by flexible micro temperature sensors, Sensors. 11 (2011) 9942–9950. doi:10.3390/s111009942.

[119] R.P. Day, J. Xia, R. Petibon, J. Rucska, H. Wang, A.T.B. Wright, J.R. Dahn, Differential Thermal Analysis of Li-Ion Cells as an Effective Probe of Liquid Electrolyte Evolution during Aging, J. Electrochem. Soc. 162 (2015) A2577–A2581. doi:10.1149/2.0181514jes.

[120] T. Waldmann, G. Bisle, B.-I. Hogg, S. Stumpp, M.A. Danzer, M. Kasper, P. Axmann, M. Wohlfahrt-Mehrens, Influence of Cell Design on Temperatures and Temperature Gradients in Lithium-Ion Cells: An In Operando Study, J. Electrochem. Soc. 162 (2015) A921–A927. doi:10.1149/2.0561506jes.

[121] S. Goutam, J.M. Timmermans, N. Omar, P. Van den Bossche, J. Van Mierlo, Comparative study of surface temperature behavior of commercial li-ion pouch cells of different chemistries and capacities by infrared thermography, Energies. 8 (2015) 8175–8192. doi:10.3390/en8088175.

[122] J. Christensen, D. Cook, P. Albertus, An Efficient Parallelizable 3D Thermoelectrochemical Model of a Li-Ion Cell, J. Electrochem. Soc. 160 (2013) A2258–A2267. doi:10.1149/2.086311jes.

[123] D. Anthony, D. Sarkar, A. Jain, Contactless, non-intrusive core temperature measurement of a solid body in steady-state, Int. J. Heat Mass Transf. 101 (2016) 779–788. doi:10.1016/j.ijheatmasstransfer.2016.05.073.

[124] F. Bahiraei, M. Ghalkhani, A. Fartaj, G.A. Nazri, A pseudo 3D electrochemical-thermal modeling and analysis of a lithium-ion battery for electric vehicle thermal management applications, Appl. Therm. Eng. 125 (2017) 904–918. doi:10.1016/j.applthermaleng.2017.07.060.

[125] J.B. Robinson, E.C.S. Electrochem, A. Lett, J.B. Robinson, E. Engebretsen, D.P. Finegan, J. Darr, G. Hinds, P.R. Shearing, D.J.L. Brett, Detection of Internal Defects in Lithium-Ion Batteries Using Lock-in Thermography Detection of Internal Defects in Lithium-Ion Batteries Using Lock-in Thermography, (2015). doi:10.1149/2.0071509eel.

[126] J. Sturm, A. Rheinfeld, I. Zilberman, F.B. Spingler, S. Kosch, F. Frie, A. Jossen, Modeling and simulation of inhomogeneities in a 18650 nickel-rich, silicon-graphite lithium-ion cell during fast charging, J. Power Sources. 412 (2019) 204–223. doi:10.1016/j.jpowsour.2018.11.043.

[127] S. Kosch, A. Rheinfeld, S. V. Erhard, A. Jossen, An extended polarization model to study the influence of current collector geometry of large-format lithium-ion pouch cells, J. Power Sources. 342 (2017) 666–676. doi:10.1016/j.jpowsour.2016.12.110.

[128] D. Anthony, D. Wong, D. Wetz, A. Jain, International Journal of Heat and Mass Transfer Non-invasive measurement of internal temperature of a cylindrical Li-ion cell during high-rate discharge, Int. J. Heat Mass Transf. 111 (2017) 223–231. doi:10.1016/j.ijheatmasstransfer.2017.03.095.

[129] A. Gaitonde, Thermal Transport In Lithium Ion Batteries: An Experimental Investigation Of Interfaces And Granular Materials, Purdue University, 2016.

[130] K. Smith, C.Y. Wang, Power and thermal characterization of a lithium-ion battery pack for hybrid-electric vehicles, J. Power Sources. 160 (2006) 662–673. doi:10.1016/j.jpowsour.2006.01.038.

[131] C.Y. Wang, V. Srinivasan, Computational battery dynamics (CBD) - Electrochemical/thermal coupled modeling and multi-scale modeling, J. Power Sources. 110 (2002) 364–376. doi:10.1016/S0378-7753(02)00199-4.

[132] I. Esho, K. Shah, A. Jain, Measurements and modeling to determine the critical temperature for preventing thermal runaway in Li-ion cells, Appl. Therm. Eng. 145 (2018) 287–294. doi:10.1016/j.applthermaleng.2018.09.016.

[133] M.R. Giuliano, S.G. Advani, A.K. Prasad, Thermal analysis and management of lithium-titanate batteries, J. Power Sources. 196 (2011) 6517–6524. doi:10.1016/j.jpowsour.2011.03.099.

[134] A. Fernicola, F. Croce, B. Scrosati, T. Watanabe, H. Ohno, LiTFSI-BEPyTFSI as an improved ionic liquid electrolyte for rechargeable lithium batteries, J. Power Sources. 174 (2007) 342–348. doi:10.1016/j.jpowsour.2007.09.013.

[135] M.R. Busche, T. Drossel, T. Leichtweiss, D.A. Weber, M. Falk, M. Schneider, M.L. Reich, H. Sommer, P. Adelhelm, J. Janek, Dynamic formation of a solid-liquid electrolyte interphase and its consequences for hybrid-battery concepts, Nat. Chem. 8 (2016) 426–434. doi:10.1038/nchem.2470.

[136] A.J. Bard, L.R. Faulkner, Electrochemical Methods: Fundamentals and Applications, Second, John Wiley & Sons, Inc., 2001. doi:10.1038/s41929-019-0277-8.

[137] H.P.G.J. Beelen, L.H.J. Raijmakers, M.C.F. Donkers, P.H.L. Notten, H.J. Bergveld, An improved impedance-based temperature estimation method for li-ion batteries, IFAC-

PapersOnLine. 28 (2015) 383–388. doi:10.1016/j.ifacol.2015.10.055.

[138] H. Beelen, K. Mundaragi Shivakumar, L. Raijmakers, M.C.F. Donkers, H.J. Bergveld, Towards impedance-based temperature estimation for Li-ion battery packs, Int. J. Energy Res. 44 (2020) 2889–2908. doi:10.1002/er.5107.

[139] P. Haussmann, J. Melbert, Internal Cell Temperature Measurement and Thermal Modeling of Lithium Ion Cells for Automotive Applications by Means of Electrochemical Impedance Spectroscopy, SAE Int. J. Altern. Powertrains. 6 (2017). doi:10.4271/2017-01-1215.

[140] L.H.J. Raijmakers, D.L. Danilov, J.P.M. Van Lammeren, M.J.G. Lammers, P.H.L. Notten, Sensorless battery temperature measurements based on electrochemical impedance spectroscopy, J. Power Sources. 247 (2014) 539–544. doi:10.1016/j.jpowsour.2013.09.005.

[141] R.R. Richardson, S. Zhao, D.A. Howey, On-board monitoring of 2-D spatially-resolved temperatures in cylindrical lithium-ion batteries: Part II. State estimation via impedance-based temperature sensing, J. Power Sources. 327 (2016) 726–735. doi:10.1016/j.jpowsour.2016.06.104.

[142] R.R. Richardson, D.A. Howey, Sensorless Battery Internal Temperature Estimation Using a Kalman Filter with Impedance Measurement, IEEE Trans. Sustain. Energy. 6 (2015) 1190–1199. doi:10.1109/TSTE.2015.2420375.

[143] N.S. Spinner, C.T. Love, S.L. Rose-Pehrsson, S.G. Tuttle, Expanding the operational limits of the single-point impedance diagnostic for internal temperature monitoring of lithium-ion batteries, Electrochim. Acta. 174 (2015) 488–493. doi:10.1016/j.electacta.2015.06.003.

[144] R. Schwarz, K. Semmler, M. Wenger, V.R.H. Lorentz, M. Marz, Sensorless battery cell temperature estimation circuit for enhanced safety in battery systems, IECON 2015 - 41st Annu. Conf. IEEE Ind. Electron. Soc. (2015) 1536–1541. doi:10.1109/IECON.2015.7392319.

[145] L.H.J. Raijmakers, K.M. Shivakumar, M.C.F. Donkers, M.J.G. Lammers, H.J. Bergveld, Crosstalk Interferences on Impedance Measurements in Battery Packs, IFAC-PapersOnLine. 49 (2016) 42–47. doi:10.1016/j.ifacol.2016.08.007.

[146] D. Chalise, W. Lu, V. Srinivasan, R. Prasher, Heat of Mixing During Fast Charge/Discharge of a Li-Ion Cell : A Study on NMC523 Cathode Heat of Mixing During Fast Charge / Discharge of a Li-Ion Cell : A Study on NMC523 Cathode, J. Electrochem. Soc. 167 (2020). doi:10.1149/1945-7111/abaf71.

[147] K.E.T.-A. John Newman, J. Newman, K.E. Thomas, Electrochemical systems, 3rd ed., John Wiley & Sons, Inc., 2004.

[148] M. Doyle, T.F. Fuller, J. Newman, Modeling of Galvanostatic Charge and Discharge of the Lithium/Polymer/Insertion Cell, J. Electrochem. Soc. 140 (1993) 1526–1533. doi:10.1149/1.2221597.

[149] T.F. Fuller, M. Doyle, J. Newman, Simulation and Optimization of the Dual Lithium Ion

Insertion Cell, J. Electrochem. Soc. 141 (1994) 1. doi:10.1149/1.2054684.

[150] V. Srinivasan, C.Y. Wang, Analysis of Electrochemical and Thermal Behavior of Li-Ion Cells, J. Electrochem. Soc. 150 (n.d.) A98. doi:10.1149/1.1526512.

[151] S. Panchal, M. Mathew, R. Fraser, M. Fowler, Electrochemical thermal modeling and experimental measurements of 18650 cylindrical lithium-ion battery during discharge cycle for an EV, Appl. Therm. Eng. 135 (2018) 123–132. doi:10.1016/j.applthermaleng.2018.02.046.

[152] K.M. Diederichsen, E.J. McShane, B.D. McCloskey, Promising Routes to a High Li+ Transference Number Electrolyte for Lithium Ion Batteries, ACS Energy Lett. 2 (2017) 2563–2575. doi:10.1021/acsenergylett.7b00792.

[153] L. Rao, J. Newman, Heat-Generation Rate and General Energy Balance for Insertion Battery Systems, J. Electrochem. Soc. 144 (1997) 2697–2704.

[154] W. Lu, H. Yang, J. Prakash, Determination of the reversible and irreversible heats of LiNi 0.8Co0.2O2/mesocarbon microbead Li-ion cell reactions using isothermal microcalorimetery, Electrochim. Acta. 51 (2006) 1322–1329. doi:10.1016/j.electacta.2005.06.028.

[155] K.E. Thomas, Lithium-Ion Batteries: Thermal and Interfacial Phenomena, University of California at Berkeley, 2002.

[156] K.E. Thomas, J. Newman, Thermal Modeling of Porous Insertion Electrodes, J. Electrochem. Soc. 150 (2003) A176. doi:10.1149/1.1531194.

[157] K.E. Thomas, J. Newman, Heats of mixing and of entropy in porous insertion electrodes, J. Power Sources. 119–121 (2003) 844–849. doi:10.1016/S0378-7753(03)00283-0.

[158] W. Kong, H. Li, X. Huang, L. Chen, Gas evolution behaviors for several cathode materials in lithium-ion batteries, J. Power Sources. 142 (2005) 285–291. doi:10.1016/j.jpowsour.2004.10.008.

[159] D. Goers, M. Holzapfel, W. Scheifele, E. Lehmann, P. Vontobel, P. Novák, In situ neutron radiography of lithium-ion batteries: The gas evolution on graphite electrodes during the charging, J. Power Sources. 130 (2004) 221–226. doi:10.1016/j.jpowsour.2003.11.065.

[160] J. Hou, L. Lu, L. Wang, A. Ohma, D. Ren, X. Feng, Y. Li, Y. Li, I. Ootani, X. Han, W. Ren, X. He, Y. Nitta, M. Ouyang, Thermal runaway of Lithium-ion batteries employing LiN(SO2F)2-based concentrated electrolytes, Nat. Commun. 11 (2020) 5100. doi:10.1038/s41467-020-18868-w.

[161] J. Hou, X. Feng, L. Wang, X. Liu, A. Ohma, L. Lu, D. Ren, W. Huang, Y. Li, M. Yi, Y. Wang, J. Ren, Z. Meng, Z. Chu, G.L. Xu, K. Amine, X. He, H. Wang, Y. Nitta, M. Ouyang, Unlocking the self-supported thermal runaway of high-energy lithium-ion batteries, Energy Storage Mater. 39 (2021) 395–402. doi:10.1016/j.ensm.2021.04.035.

[162] R. Chen, A.M. Nolan, J. Lu, J. Wang, X. Yu, Y. Mo, L. Chen, X. Huang, H. Li, The Thermal Stability of Lithium Solid Electrolytes with Metallic Lithium, Joule. 4 (2020) 812–821. doi:10.1016/j.joule.2020.03.012.

[163] T. Waldmann, B.I. Hogg, M. Wohlfahrt-Mehrens, Li plating as unwanted side reaction in commercial Li-ion cells – A review, J. Power Sources. 384 (2018) 107–124. doi:10.1016/j.jpowsour.2018.02.063.

[164] Q. Wang, P. Ping, X. Zhao, G. Chu, J. Sun, C. Chen, Thermal runaway caused fire and explosion of lithium ion battery, J. Power Sources. 208 (2012) 210–224. doi:10.1016/j.jpowsour.2012.02.038.

[165] Y. Lai, S. Du, L.L. Ai, L.L. Ai, Y. Cheng, Y. Tang, M. Jia, Insight into heat generation of lithium ion batteries based on the electrochemical-thermal model at high discharge rates, Int. J. Hydrogen Energy. 40 (2015) 13039–13049. doi:10.1016/j.ijhydene.2015.07.079.

[166] K. Shah, A. Jain, Prediction of thermal runaway and thermal management requirements in cylindrical Li-ion cells in realistic scenarios, Int. J. Energy Res. 43 (2019) 1827–1838. doi:10.1002/er.4411.

[167] R. Zhu, C. Liu, J. Feng, Z. Guo, In Situ Observation of Lithium Dendrite of Different Graphite Electrodes, ECS Trans. 85 (2018) 347–356. doi:10.1149/08513.0347ecst.

[168] C. Zhao, T. Wang, Z. Huang, J. Wu, H. Zhou, M. Ma, J. Xu, Z. Wang, H. Li, J. Sun, Q. Wang, Experimental study on thermal runaway of fully charged and overcharged lithium-ion batteries under adiabatic and side-heating test, J. Energy Storage. 38 (2021) 102519. doi:10.1016/j.est.2021.102519.

[169] X. Feng, M. Fang, X. He, M. Ouyang, L. Lu, H. Wang, M. Zhang, Thermal runaway features of large format prismatic lithium ion battery using extended volume accelerating rate calorimetry, J. Power Sources. 255 (2014) 294–301. doi:10.1016/j.jpowsour.2014.01.005.

[170] Z. Tang, S. Wang, J. Liao, S. Wang, X. He, B. Pan, H. He, C. Chen, Facilitating Lithium-Ion Diffusion in Layered Cathode Materials by Introducing Li + /Ni 2+ Antisite Defects for High-Rate Li-Ion Batteries , Research. 2019 (2019) 1–10. doi:10.34133/2019/2198906.

[171] J. Xu, C. Lan, Y. Qiao, Y. Ma, Prevent thermal runaway of lithium-ion batteries with minichannel cooling, Appl. Therm. Eng. 110 (2017) 883–890. doi:10.1016/j.applthermaleng.2016.08.151.

[172] K. Shah, D. Chalise, A. Jain, Experimental and theoretical analysis of a method to predict thermal runaway in Li-ion cells, J. Power Sources. 330 (2016) 167–174. doi:10.1016/j.jpowsour.2016.08.133.

[173] R. Malik, Safety First, Joule. 2 (2018) 1923–1924. doi:10.1016/j.joule.2018.10.002.

[174] B. Liu, J.G. Zhang, W. Xu, Advancing Lithium Metal Batteries, Joule. 2 (2018) 833–845. doi:10.1016/j.joule.2018.03.008.

[175] S. Wang, K. Rafiz, J. Liu, Y. Jin, J.Y.S. Lin, Effects of lithium dendrites on thermal runaway and gassing of LiFePO4batteries, Sustain. Energy Fuels. 4 (2020) 2342–2351. doi:10.1039/d0se00027b.

[176] X. Yang, Y. Duan, X. Feng, T. Chen, C. Xu, X. Rui, M. Ouyang, L. Lu, X. Han, D. Ren,

Z. Zhang, C. Li, S. Gao, An Experimental Study on Preventing Thermal Runaway Propagation in Lithium-Ion Battery Module Using Aerogel and Liquid Cooling Plate Together, Fire Technol. 56 (2020) 2579–2602. doi:10.1007/s10694-020-00995-x.

[177] W. Cai, C. Yan, Y.X. Yao, L. Xu, X.R. Chen, J.Q. Huang, Q. Zhang, The Boundary of Lithium Plating in Graphite Electrode for Safe Lithium-Ion Batteries, Angew. Chemie - Int. Ed. 100081 (2021) 13007–13012. doi:10.1002/anie.202102593.

[178] X. Huang, J. Xue, M. Xiao, S. Wang, Y. Li, S. Zhang, Y. Meng, Comprehensive evaluation of safety performance and failure mechanism analysis for lithium sulfur pouch cells, Energy Storage Mater. 30 (2020) 87–97. doi:10.1016/j.ensm.2020.04.035.

[179] Y. Chen, Y. Kang, Y. Zhao, L. Wang, J. Liu, Y. Li, Z. Liang, X. He, X. Li, N. Tavajohi, B. Li, A review of lithium-ion battery safety concerns: The issues, strategies, and testing standards, J. Energy Chem. 59 (2021) 83–99. doi:10.1016/j.jechem.2020.10.017.

[180] H. Yang, H. Bang, K. Amine, J. Prakash, Investigations of the Exothermic Reactions of Natural Graphite Anode for Li-Ion Batteries during Thermal Runaway, J. Electrochem. Soc. 152 (2005) A73. doi:10.1149/1.1836126.

[181] J. ichi Yamaki, H. Takatsuji, T. Kawamura, M. Egashira, Thermal stability of graphite anode with electrolyte in lithium-ion cells, Solid State Ionics. 148 (2002) 241–245. doi:10.1016/S0167-2738(02)00060-7.

[182] K. Kumaresan, G. Sikha, R.E. White, Thermal Model for a Li-Ion Cell, J. Electrochem. Soc. 155 (2008) A164. doi:10.1149/1.2817888.

[183] C.R. Pals, J. Newman, Thermal Modeling of the Lithium/Polymer Battery II. Temperature Profiles in a Cell Stack, J. Electrochem. Soc. 142 (1995) 3282–3288.

[184] T. Bandhauer, S. Garimella, T.F. Fuller, Electrochemical-Thermal Modeling to Evaluate Battery Thermal Management Strategies: II. Edge and Internal Cooling, J. Electrochem. Soc. 162 (2014) A137–A148. doi:10.1149/2.0581501jes.

[185] K. An, P. Barai, K. Smith, P.P. Mukherjee, Probing the Thermal Implications in Mechanical Degradation of Lithium-Ion Battery Electrodes, J. Electrochem. Soc. 161 (2014) A1058–A1070. doi:10.1149/2.069406jes.

[186] G. Zhang, C.E. Shaffer, C.-Y. Wang, C.D. Rahn, In-Situ Measurement of Current Distribution in a Li-Ion Cell, J. Electrochem. Soc. 160 (2013) A610–A615. doi:10.1149/2.046304jes.

[187] W. Huo, H. He, F. Sun, Electrochemical-thermal modeling for a ternary lithium ion battery during discharging and driving cycle testing, RSC Adv. 5 (2015) 57599–57607. doi:10.1039/c5ra09018k.

[188] B. Wu, V. Yufit, M. Marinescu, G.J. Offer, R.F. Martinez-Botas, N.P. Brandon, Coupled thermal-electrochemical modelling of uneven heat generation in lithium-ion battery packs, J. Power Sources. 243 (2013) 544–554. doi:10.1016/j.jpowsour.2013.05.164.

[189] B. Yan, C. Lim, L. Yin, L. Zhu, Simulation of heat generation in a reconstructed LiCoO2 cathode during galvanostatic discharge, Electrochim. Acta. 100 (2013) 171–179.

doi:10.1016/j.electacta.2013.03.132.

[190] X. Zhang, Multiscale Modeling of Li-ion Cells: Mechanics, Heat Generation and Electrochemical Kinetics, University of Michigan, 2009.

[191] X. Zhang, A.M. Sastry, W. Shyy, Intercalation-Induced Stress and Heat Generation within Single Lithium-Ion Battery Cathode Particles, J. Electrochem. Soc. 155 (2008) A542. doi:10.1149/1.2926617.

[192] J. Li, Y. Cheng, M. Jia, Y. Tang, Y. Lin, Z. Zhang, Y. Liu, An electrochemical-thermal model based on dynamic responses for lithium iron phosphate battery, J. Power Sources. 255 (2014) 130–143. doi:10.1016/j.jpowsour.2014.01.007.

[193] S.J. Bazinski, X. Wang, The Influence of Cell Temperature on the Entropic Coefficient of a Lithium Iron Phosphate (LFP) Pouch Cell, J. OfThe Electrochem. Soc. 161 (2014) A168–A175. doi:10.1149/2.082401jes.

[194] P. Jindal, J. Bhattacharya, Criticality of incorporating explicit in-situ measurement of temperature-dependent heat generation for accurate design of thermal management system for Li-ion battery pack, Int. J. Energy Res. 44 (2020) 6023–6034. doi:10.1002/er.5303.

[195] S. Basu, R.S. Patil, S. Ramachandran, K.S. Hariharan, S.M. Kolake, T. Song, D. Oh, T. Yeo, S. Doo, Non-isothermal electrochemical model for lithium-ion cells with composite cathodes, J. Power Sources. 283 (2015) 132–150. doi:10.1016/j.jpowsour.2015.02.127.

[196] M. Yazdanpour, P. Taheri, A. Mansouri, M. Bahrami, A Distributed Analytical Electro-Thermal Model for Pouch-Type Lithium-Ion Batteries, J. Electrochem. Soc. 161 (2014) A1953–A1963. doi:10.1149/2.1191412jes.

[197] M. Chen, F. Bai, W. Song, J. Lv, S. Lin, Z. Feng, Y. Li, Y. Ding, A multilayer electro-thermal model of pouch battery during normal discharge and internal short circuit process, Appl. Therm. Eng. 120 (2017) 506–516. doi:10.1016/j.applthermaleng.2017.03.135.

[198] P. Amiribavandpour, Modelling of Batteries in Electric Vehicles, Swinburne University of Technology, 2017.

[199] K. Shah, C. McKee, D. Chalise, A. Jain, Experimental and numerical investigation of core cooling of Li-ion cells using heat pipes, Energy. 113 (2016) 852–860. doi:10.1016/j.energy.2016.07.076.

[200] G. Xia, L. Cao, G. Bi, A review on battery thermal management in electric vehicle application, J. Power Sources. 367 (2017) 90–105. doi:10.1016/j.jpowsour.2017.09.046.

[201] A. Mills, S. Al-Hallaj, Simulation of passive thermal management system for lithium-ion battery packs, J. Power Sources. 141 (2005) 307–315. doi:10.1016/j.jpowsour.2004.09.025.

[202] C. Zhao, A.C.M. Sousa, F. Jiang, Minimization of thermal non-uniformity in lithium-ion battery pack cooled by channeled liquid flow, Int. J. Heat Mass Transf. 129 (2019) 660–670. doi:10.1016/j.ijheatmasstransfer.2018.10.017.

[203] V. Vishwakarma, A. Jain, Enhancement of thermal transport in Gel Polymer Electrolytes

with embedded BN / Al 2 O 3 nano- and micro-particles, J. Power Sources. 362 (2017) 219–227. doi:10.1016/j.jpowsour.2017.07.035.

[204] S. Kuroda, N. Tobori, M. Sakuraba, Y. Sato, Charge-discharge properties of a cathode prepared with ketjen black as the electro-conductive additive in lithium ion batteries, J. Power Sources. 119–121 (2003) 924–928. doi:10.1016/S0378-7753(03)00230-1.

[205] A. Nyman, M. Behm, G. Lindbergh, Electrochemical characterisation and modelling of the mass transport phenomena in LiPF6-EC-EMC electrolyte, Electrochim. Acta. 53 (2008) 6356–6365. doi:10.1016/j.electacta.2008.04.023.

[206] M.Z. Kufian, S.R. Majid, Performance of lithium-ion cells using 1 M LiPF6 in EC/DEC (v/v = 1/2) electrolyte with ethyl propionate additive, Ionics (Kiel). 16 (2010) 409–416. doi:10.1007/s11581-009-0413-6.

[207] A. Guerfi, M. Dontigny, P. Charest, M. Petitclerc, M. Lagacé, A. Vijh, K. Zaghib, Improved electrolytes for Li-ion batteries: Mixtures of ionic liquid and organic electrolyte with enhanced safety and electrochemical performance, J. Power Sources. 195 (2010) 845–852. doi:10.1016/j.jpowsour.2009.08.056.

[208] S.K. Das, S.S. Mandal, A.J. Bhattacharyya, Ionic conductivity, mechanical strength and Li-ion battery performance of mono-functional and bi-functional (“Janus”) “soggy sand” electrolytes, Energy Environ. Sci. 4 (2011) 1391–1399. doi:10.1039/c0ee00566e.

[209] Y. Tominaga, K. Yamazaki, Fast Li-ion conduction in poly(ethylene carbonate)-based electrolytes and composites filled with TiO2 nanoparticles, Chem. Commun. 50 (2014) 4448–4450. doi:10.1039/c3cc49588d.

[210] I. V. Thorat, D.E. Stephenson, N.A. Zacharias, K. Zaghib, J.N. Harb, D.R. Wheeler, Quantifying tortuosity in porous Li-ion battery materials, J. Power Sources. 188 (2009) 592–600. doi:10.1016/j.jpowsour.2008.12.032.

[211] L. Shen, Z. Chen, Critical review of the impact of tortuosity on diffusion, Chem. Eng. Sci. 62 (2007) 3748–3755. doi:10.1016/j.ces.2007.03.041.

[212] Y. Zhai, N. Wang, X. Mao, Y. Si, J. Yu, S.S. Al-Deyab, M. El-Newehy, B. Ding, Sandwich-structured PVdF/PMIA/PVdF nanofibrous separators with robust mechanical strength and thermal stability for lithium ion batteries, J. Mater. Chem. A. 2 (2014) 14511–14518. doi:10.1039/c4ta02151g.

[213] R. Zahn, M.F. Lagadec, M. Hess, V. Wood, Improving Ionic Conductivity and Lithium-Ion Transference Number in Lithium-Ion Battery Separators, ACS Appl. Mater. Interfaces. 8 (2016) 32637–32642. doi:10.1021/acsami.6b12085.

[214] X. Mao, L. Shi, H. Zhang, Z. Wang, J. Zhu, Z. Qiu, Y. Zhao, M. Zhang, S. Yuan, Polyethylene separator activated by hybrid coating improving Li+ ion transference number and ionic conductivity for Li-metal battery, J. Power Sources. 342 (2017) 816–824. doi:10.1016/j.jpowsour.2017.01.006.

[215] S.H. Choi, H.J. Kang, E.N. Ryu, K.P. Lee, Electrochemical properties of polyolefin nonwoven fabric modified with carboxylic acid group for battery separator, Radiat. Phys. Chem. 60 (2001) 495–502. doi:10.1016/S0969-806X(00)00396-0.

[216] K. Hayamizu, Temperature dependence of self-diffusion coefficients of ions and solvents in ethylene carbonate, propylene carbonate, and diethyl carbonate single solutions and ethylene carbonate + diethyl carbonate binary solutions of LiPF 6 studied by NMR, J. Chem. Eng. Data. 57 (2012) 2012–2017. doi:10.1021/je3003089.

[217] M.T. Ong, O. Verners, E.W. Draeger, A.C.T. Van Duin, V. Lordi, J.E. Pask, Lithium Ion Solvation and Di ff usion in Bulk Organic Electrolytes from First-Principles and Classical Reactive Molecular Dynamics, J. Phys. Chem. B. 119 (2015) 1535–1545. doi:10.1021/jp508184f.

[218] P.M. Bayley, G.H. Lane, N.M. Rocher, B.R. Clare, A.S. Best, D.R. MacFarlane, M. Forsyth, Transport properties of ionic liquid electrolytes with organic diluents, Phys. Chem. Chem. Phys. 11 (2009) 7202–7208. doi:10.1039/b902200g.

[219] A. Deshpande, L. Kariyawasam, P. Dutta, S. Banerjee, Enhancement of lithium ion mobility in ionic liquid electrolytes in presence of additives, J. Phys. Chem. C. 117 (2013) 25343–25351. doi:10.1021/jp409498w.

[220] Y. Lu, M. Tikekar, R. Mohanty, K. Hendrickson, L. Ma, L.A. Archer, Stable cycling of lithium metal batteries using high transference number electrolytes, Adv. Energy Mater. 5 (2015) 1–7. doi:10.1002/aenm.201402073.

[221] T. Frömling, M. Kunze, M. Schönhoff, J. Sundermeyer, B. Roling, Enhanced lithium transference numbers in ionic liquid electrolytes, J. Phys. Chem. B. 112 (2008) 12985–12990. doi:10.1021/jp804097j.

[222] E.R. Logan, J.R. Dahn, Electrolyte Design for Fast-Charging Li-Ion Batteries, Trends Chem. 2 (2020) 354–366. doi:10.1016/j.trechm.2020.01.011.

[223] K.D. Fong, J. Self, K.M. Diederichsen, B.M. Wood, B.D. McCloskey, K.A. Persson, Ion Transport and the True Transference Number in Nonaqueous Polyelectrolyte Solutions for Lithium Ion Batteries, ACS Cent. Sci. 5 (2019) 1250–1260. doi:10.1021/acscentsci.9b00406.

[224] H.G. Buss, S.Y. Chan, N.A. Lynd, B.D. McCloskey, Nonaqueous Polyelectrolyte Solutions as Liquid Electrolytes with High Lithium Ion Transference Number and Conductivity, ACS Energy Lett. 2 (2017) 481–487. doi:10.1021/acsenergylett.6b00724.

[225] M.Z. Bazant, Theory of chemical kinetics and charge transfer based on nonequilibrium thermodynamics, Acc. Chem. Res. 46 (2013) 1144–1160. doi:10.1021/ar300145c.

[226] N. Yabuuchi, K. Kubota, Y. Aoki, S. Komaba, Understanding Particle-Size-Dependent Electrochemical Properties of Li2MnO3-Based Positive Electrode Materials for Rechargeable Lithium Batteries, J. Phys. Chem. C. 120 (2016) 875–885. doi:10.1021/acs.jpcc.5b10517.

[227] Z. Ogumi, Interfacial Reactions of Lithium-ion Batteries, Electrochemistry. 5 (2010).

[228] Y. Yamada, Y. Iriyama, T. Abe, Z. Ogumi, Kinetics of lithium ion transfer at the interface between graphite and liquid electrolytes: effects of solvent and surface film, Langmuir. 25 (2009) 12766–12770. doi:10.1021/la901829v.

[229] T. Abe, F. Sagane, M. Ohtsuka, Y. Iriyama, Z. Ogumi, Lithium-Ion Transfer at the Interface Between Lithium-Ion Conductive Ceramic Electrolyte and Liquid Electrolyte-A Key to Enhancing the Rate Capability of Lithium-Ion Batteries, J. Electrochem. Soc. 152 (2005) A2151. doi:10.1149/1.2042907.

[230] T.R. Jow, S.A. Delp, J.L. Allen, J.-P. Jones, M.C. Smart, Factors Limiting Li + Charge Transfer Kinetics in Li-Ion Batteries , J. Electrochem. Soc. 165 (2018) A361–A367. doi:10.1149/2.1221802jes.

[231] T. Abe, H. Fukuda, Y. Iriyama, Z. Ogumi, Solvated Li-Ion Transfer at Interface Between Graphite and Electrolyte, J. Electrochem. Soc. 151 (2004) A1120. doi:10.1149/1.1763141.

[232] Y. Ishihara, K. Miyazaki, T. Fukutsuka, T. Abe, Kinetics of lithium-ion transfer at the interface between Li4Ti5O12 thin films and organic electrolytes, ECS Electrochem. Lett. 3 (2014) A83–A86. doi:10.1149/2.0011408eel.

[233] J.-P. Jones, M.C. Smart, F.C. Krause, R. V. Bugga, The Effect of Electrolyte Additives upon Lithium Plating during Low Temperature Charging of Graphite-LiNiCoAlO 2 Lithium-Ion Three Electrode Cells , J. Electrochem. Soc. 167 (2020) 020536. doi:10.1149/1945-7111/ab6bc2.

[234] K.S. Park, P. Xiao, S.Y. Kim, A. Dylla, Y.M. Choi, G. Henkelman, K.J. Stevenson, J.B. Goodenough, Enhanced charge-transfer kinetics by anion surface modification of LiFePO4, Chem. Mater. 24 (2012) 3212–3218. doi:10.1021/cm301569m.

[235] C. Li, H.P. Zhang, L.J. Fu, H. Liu, Y.P. Wu, E. Rahm, R. Holze, H.Q. Wu, Cathode materials modified by surface coating for lithium ion batteries, Electrochim. Acta. 51 (2006) 3872–3883. doi:10.1016/j.electacta.2005.11.015.

[236] F. Zhou, X. Zhao, J. Jiang, J.R. Dahn, Advantages of simultaneous substitution of Co in Li[Ni1/3Mn 13Co1/3]O2 by Ni and Al, Electrochem. Solid-State Lett. 12 (2009) 81–83. doi:10.1149/1.3072759.

[237] Y.S. Jung, A.S. Cavanagh, L.A. Riley, S.H. Kang, A.C. Dillon, M.D. Groner, S.M. George, S.H. Lee, Ultrathin direct atomic layer deposition on composite electrodes for highly durable and safe Li-Ion batteries, Adv. Mater. 22 (2010) 2172–2176. doi:10.1002/adma.200903951.

[238] S.S. Zhang, A review on electrolyte additives for lithium-ion batteries, J. Power Sources. 162 (2006) 1379–1394. doi:10.1016/j.jpowsour.2006.07.074.

[239] C. Shi, J. Dai, C. Li, X. Shen, L. Peng, P. Zhang, D. Wu, D. Sun, J. Zhao, A modified ceramic-coating separator with high-temperature stability for lithium-ion battery, Polymers (Basel). 9 (2017) 10–14. doi:10.3390/polym9050159.

[240] C. Shi, P. Zhang, S. Huang, X. He, P. Yang, D. Wu, D. Sun, J. Zhao, Functional separator consisted of polyimide nonwoven fabrics and polyethylene coating layer for lithium-ion batteries, J. Power Sources. 298 (2015) 158–165. doi:10.1016/j.jpowsour.2015.08.008.

[241] H.F. Xiang, B. Yin, H. Wang, H.W. Lin, X.W. Ge, S. Xie, C.H. Chen, Improving electrochemical properties of room temperature ionic liquid (RTIL) based electrolyte for Li-ion batteries, Electrochim. Acta. 55 (2010) 5204–5209.

doi:10.1016/j.electacta.2010.04.041.

[242] X. Guan, A. Wang, S. Liu, G. Li, F. Liang, Y.W. Yang, X. Liu, J. Luo, Controlling Nucleation in Lithium Metal Anodes, Small. 14 (2018). doi:10.1002/smll.201801423.

[243] M. Bakierska, M. Świętosławski, K. Chudzik, M. Lis, M. Molenda, Enhancing the lithium ion diffusivity in LiMn2O4−ySy cathode materials through potassium doping, Solid State Ionics. 317 (2018) 190–193. doi:10.1016/j.ssi.2018.01.014.

[244] J. Tian, Y. Su, F. Wu, S. Xu, F. Chen, R. Chen, Q. Li, J. Li, F. Sun, S. Chen, High-Rate and Cycling-Stable Nickel-Rich Cathode Materials with Enhanced Li+ Diffusion Pathway, ACS Appl. Mater. Interfaces. 8 (2016) 582–587. doi:10.1021/acsami.5b09641.

[245] W. Liu, Q. Shi, Q. Qu, T. Gao, G. Zhu, J. Shao, H. Zheng, Improved Li-ion diffusion and stability of a LiNi0.5Mn1.5O4 cathode through in situ co-doping with dual-metal cations and incorporation of a superionic conductor, J. Mater. Chem. A. 5 (2017) 145–154. doi:10.1039/c6ta08891k.

[246] G. Sikha, B.N. Popov, R.E. White, Effect of Porosity on the Capacity Fade of a Lithium-Ion Battery, J. Electrochem. Soc. 151 (2004) A1104. doi:10.1149/1.1759972.

[247] M. Broussely, P. Biensan, F. Bonhomme, P. Blanchard, S. Herreyre, K. Nechev, R.J. Staniewicz, Main aging mechanisms in Li ion batteries, J. Power Sources. 146 (2005) 90–96. doi:10.1016/j.jpowsour.2005.03.172.

[248] E. Sarasketa-Zabala, F. Aguesse, I. Villarreal, L.M. Rodriguez-Martinez, C.M. López, P. Kubiak, Understanding lithium inventory loss and sudden performance fade in cylindrical cells during cycling with deep-discharge steps, J. Phys. Chem. C. 119 (2015) 896–906. doi:10.1021/jp510071d.

[249] M. Klett, P. Svens, C. Tengstedt, A. Seyeux, J. ̄wiatowska, G. Lindbergh, R.W. Lindström, Uneven film formation across depth of porous graphite electrodes in cycled commercial li-ion batteries, J. Phys. Chem. C. 119 (2015) 90–100. doi:10.1021/jp509665e.

[250] S. Frisco, A. Kumar, J.F. Whitacre, S. Litster, Understanding Li-Ion Battery Anode Degradation and Pore Morphological Changes through Nano-Resolution X-ray Computed Tomography, J. Electrochem. Soc. 163 (2016) A2636–A2640. doi:10.1149/2.0681613jes.

[251] X.G. Yang, Y. Leng, G. Zhang, S. Ge, C.Y. Wang, Modeling of lithium plating induced aging of lithium-ion batteries: Transition from linear to nonlinear aging, J. Power Sources. 360 (2017) 28–40. doi:10.1016/j.jpowsour.2017.05.110.

[252] W. Huang, P.M. Attia, H. Wang, S.E. Renfrew, N. Jin, S. Das, Z. Zhang, D.T. Boyle, Y. Li, M.Z. Bazant, B.D. McCloskey, W.C. Chueh, Y. Cui, Evolution of the Solid-Electrolyte Interphase on Carbonaceous Anodes Visualized by Atomic-Resolution Cryogenic Electron Microscopy, Nano Lett. 19 (2019) 5140–5148. doi:10.1021/acs.nanolett.9b01515.

[253] C. Hou, J. Han, P. Liu, C. Yang, G. Huang, T. Fujita, A. Hirata, M. Chen, Operando Observations of SEI Film Evolution by Mass-Sensitive Scanning Transmission Electron Microscopy, Adv. Energy Mater. 9 (2019) 1–9. doi:10.1002/aenm.201902675.

[254] J. Cho, M.D. Losego, H.G. Zhang, H. Kim, J. Zuo, I. Petrov, D.G. Cahill, P. V. Braun, Electrochemically tunable thermal conductivity of lithium cobalt oxide, Nat. Commun. 5 (2014) 2–7. doi:10.1038/ncomms5035.

[255] Z. Wei, F. Yang, K. Bi, J. Yang, Y. Chen, Tunable Anisotropic Thermal Conductivity and Elastic Properties in Intercalated Graphite via Lithium Ions, J. Phys. Chem. C. 122 (2018) 1447–1455. doi:10.1021/acs.jpcc.7b09717.

[256] X. Qian, X. Gu, M.S. Dresselhaus, R. Yang, Anisotropic Tuning of Graphite Thermal Conductivity by Lithium Intercalation, J. Phys. Chem. Lett. 7 (2016) 4744–4750. doi:10.1021/acs.jpclett.6b02295.

[257] R. Matsumoto, Y. Okabe, N. Akuzawa, Thermoelectric Properties and Performance of n-Type and p-Type Graphite Intercalation Compounds, J. Electron. Mater. 44 (2015) 399–406. doi:10.1007/s11664-014-3409-6.

[258] V. Vishwakarma, A. Jain, Measurement of in-plane thermal conductivity and heat capacity of separator in Li-ion cells using a transient DC heating method, J. Power Sources. 272 (2014) 378–385. doi:10.1016/j.jpowsour.2014.08.066.

[259] D.G. Cahill, Thermal conductivity measurement from 30 to 750 K: The 3ω method, Rev. Sci. Instrum. 61 (1990) 802–808. doi:10.1063/1.1141498.

[260] T. Borca-Tasciuc, A.R. Kumar, G. Chen, Data reduction in 3ω method for thin-film thermal conductivity determination, Rev. Sci. Instrum. 72 (2001) 2139–2147. doi:10.1063/1.1353189.

[261] C. Dames, G. Chen, 1Ω, 2Ω, and 3Ω Methods for Measurements of Thermal Properties, Rev. Sci. Instrum. 76 (2005) 1–14. doi:10.1063/1.2130718.

[262] T. Tong, A. Majumdar, Reexamining the 3-omega technique for thin film thermal characterization, Rev. Sci. Instrum. 77 (2006). doi:10.1063/1.2349601.

[263] R. Prasher, Ultralow thermal conductivity of a packed bed of crystalline nanoparticles: A theoretical study, Phys. Rev. B - Condens. Matter Mater. Phys. 74 (2006) 1–5. doi:10.1103/PhysRevB.74.165413.

[264] L. Sheng, L. Su, H. Zhang, Experimental determination on thermal parameters of prismatic lithium ion battery cells, Int. J. Heat Mass Transf. 139 (2019) 231–239. doi:10.1016/j.ijheatmasstransfer.2019.04.143.

[265] M. Steinhardt, E.I. Gillich, M. Stiegler, A. Jossen, Thermal conductivity inside prismatic lithium-ion cells with dependencies on temperature and external compression pressure, J. Energy Storage. 32 (2020) 101680. doi:10.1016/j.est.2020.101680.

[266] M. Al-Zareer, I. Dincer, M.A. Rosen, A review of novel thermal management systems for batteries, Int. J. Energy Res. 42 (2018) 3182–3205. doi:10.1002/er.4095.

[267] X.G. Yang, G. Zhang, S. Ge, C.Y. Wang, Fast charging of lithium-ion batteries at all temperatures, Proc. Natl. Acad. Sci. U. S. A. 115 (2018) 7266–7271. doi:10.1073/pnas.1807115115.

[268] R. Carter, C.T. Love, Modulation of Lithium Plating in Li-Ion Batteries with External Thermal Gradient, ACS Appl. Mater. Interfaces. 10 (2018) 26328–26334. doi:10.1021/acsami.8b09131.